The PHILOSOPHICAL MAGAZINE

FIRST PUBLISHED IN 1798

L. 43 SEVENTH SERIES No. 341 June, 1952

A Journal of Theoretical Experimental and Applied Physics

PRICE 15s. 0d.
Annual Subscription £8 0s. 0d. payable in advance

D AND PUBLISHED BY TAYLOR & FRANCIS LTD., RED LION COURT, FLEET ST., LONDON, E.C.4.

ADVANCES IN PHYSICS

A QUARTERLY SUPPLEMENT OF THE PHILOSOPHICAL MAGAZINE

On 1st January, 1952, the first number of this new Quarterly Supplement to the Philosophical Magazine was published. The aim of this Supplement will be to give those interested in physics comprehensive and authoritative accounts of recent important developments. It is felt by the Editor that in view of the rapid advances in many branches of physics, scientists will welcome a journal devoted to articles of this type.

VOLUME 1 JULY 1952 NUMBER 3

The whole part is devoted to one paper:

THE MATHEMATICAL THEORY OF STATIONARY DISLOCATIONS

By

Dr. F. R. N. NABARRO
Department of Metallurgy, The University of Birmingham

PRICE *per part* 15/- *plus postage* **PRICE** *per annum* £2 15s. 0d. *post free*

Printed and Published by
TAYLOR & FRANCIS, LTD., RED LION COURT, FLEET ST., LONDON, E.C.4

LVI. *The Properties of Charged V-particles*

By
R. Armenteros, K. H. Barker, C. C. Butler, A. Cachon and C. M. York
The Physical Laboratories, University of Manchester*

[Received March 11, 1952]

Abstract

Twenty-one examples of the decay of charged V-particles have been found among 25 000 counter-controlled cloud-chamber photographs obtained on the Pic-du-Midi (2 867 m). These events have been analysed and compared with the data obtained by other groups. The measurements show that, if the majority of the $V^{\pm}$-tracks are produced by one type of particle having a single mode of decay, there must be at least two neutral secondary particles, in addition to the charged secondary particle. The latter is probably a μ- or a π-meson and the combined mass of the neutral particles must be less than 1 000 m_e. Since the κ-particles, of mass about 1 200 m_e, which were discovered in photographic emulsions, also decay into a charged meson and at least two neutral particles, it is plausible to assume, provisionally, that the $V^{\pm}$-particles and the κ-particles are the same. On this assumption most of the available data concerning $V^{\pm}$- and κ-particles can be explained if the unstable particle has a mass of about 1 200 m_e and decays into a charged μ-meson, a π°-meson and a neutrino, or alternatively into a charged μ-meson and two neutrinos. As yet no direct evidence has been found for the existence of a π°-meson in the decay scheme. One negatively charged V-particle probably produced a neutral V-track and a charged meson.

§ 1. Introduction

The cloud-chamber work on the Pic-du-Midi (2 867 m), described by Armenteros *et al.* (1951 a and b), has been continued and a special study made of the charged V-particles. These particles have been found in small numbers in many cloud-chamber experiments, for example, by Rochester and Butler (1947), Seriff *et al.* (1951), Bridge and Annis (1951), Fretter (1951), Thompson *et al.* (1951), Leighton *et al.* (1951) and Astbury *et al.* (1951). Nearly all these workers have found a smaller number of charged than neutral V-tracks ; in most cases the $V^{\pm}$-tracks number about 15% of the V°-tracks. A tentative explanation of the phenomena observed on the Pic-du-Midi is given below, where the cloud-chamber

* Communicated by Professor P. M. S. Blackett, F.R.S.

events are compared with the decay process of κ-particles, discovered in photographic emulsions by O'Ceallaigh (1951). The lifetime and frequency of production of $V^{\pm}$-particles will be discussed in a later paper.

§2. Experimental Data

(i) *The Classification of the Data*

Twenty-five thousand pictures, obtained with the cloud chamber and electromagnet described by Armenteros *et al.* (1951 a and b), have been examined and forty-five examples of the sudden deflection of tracks in the gas of the cloud chamber, without the production of visible recoil tracks, have been found. It has already been shown by Armenteros *et al.* (1951 a) and by Butler (1951) that this type of track is only very rarely due to the production of a two-pronged star in the cloud-chamber gas or to the large-angle scattering of particles with momenta greater than 500 Mev/c. The tracks may, however, be divided into two categories, those due to (*a*) the large-angle elastic scattering of low-energy particles making nuclear collisions and (*b*) the decay-in-flight of π-mesons and particles heavier than the π-meson, known as charged V-particles.

The events of type (*a*) have been identified by using the momentum and ionization measurements ; two were slow mesons, one was a slow proton and eight were electrons. An argon recoil with a momentum of 75 Mev/c would be just visible in the chamber ; for each of the events of type (*a*) the recoil was too short to be visible. The decay of a slow, that is heavily-ionizing, π-meson can easily be identified but it is sometimes difficult to distinguish the decay of a fast π-meson from that of a $V^{\pm}$-particle, because both types of particle frequently produce minimum ionization tracks. However, the dynamics of the π-meson decay process can be used to ascertain which of these events can be interpreted by means of the scheme : $\pi \rightarrow \mu +$ neutrino.

The momentum component of the μ-meson transverse to the direction of the π-meson, namely p_T, cannot be greater than the momentum p^* of the μ-meson in the rest system of the π-meson. The value of p^* can be obtained, in terms of m_1 and m_2, the masses (in energy units) of the π- and μ-mesons respectively, by using the relativistic energy equation, $m_1=(m_2^2+p^{*2})^{\frac{1}{2}}+p^*$. Since $m_1=275\, m_e$ and $m_2=210\, m_e$, $p^*=29$ Mev/c. In addition to this condition, the momentum P (in Mev/c) of the π-meson and the maximum permissible angle, $\phi_{\max}$, between the directions of the π- and μ-mesons are related by an equation which reduces to $\sin \phi_{\max}=40/P$. The majority of the values of ϕ will be close to $\phi_{\max}$; if a particular track has a value of ϕ greater than the appropriate $\phi_{\max}$, then it cannot be due to the decay of a π-meson. If P cannot be measured, then the first condition alone is used. These two tests, based on the dynamics of the π-meson decay scheme, have been used to classify the 35 events in category (*b*) ; 14 can be explained as $\pi \rightarrow \mu$ decays leaving the remaining 21 to be explained as the decay of $V^{\pm}$-particles. Following this procedure, it is possible that a small number of decays due to $V^{\pm}$-particles may be interpreted as π-meson

decays. In addition, a few tracks of type (*a*) may be classified as $\pi \rightarrow \mu$-decays, but probably not as $V^{\pm}$-decays since the transverse momenta of all but one of the $V^{\pm}$-particles are greater than 75 Mev/c, the minimum momentum for a visible recoil. The exceptional case (track 2) cannot be classified in category (*a*).

(ii) *Measurements on the Charged V-particle Tracks*

The data for the twenty-one charged V-tracks and the original one found by Rochester and Butler (1947) are given in table 1. The errors given in table 1 and throughout this paper are the probable errors of measurement. Only six of the events can be measured completely ; the remainder have at least one track which is too short for measurement. It will be seen, however, that the primary momenta of these six events have large errors, and, therefore, they are not very valuable in a detailed analysis of the nature of the decay process.

Table 1. Measurements on 22 $V^{\pm}$-particles

(1) Sign of V	(2) Primary momentum (100 Mev/c)	(3) $I/I_{\min}$ of Primary	(4) Angle† ϕ (deg)	(5) Sign and momentum of secondary (100 Mev/c)	(6) Transverse momentum p_T (100 Mev/c)
1* +	—	1	18·9	$+7{\cdot}7 \pm 1{\cdot}0$	$2{\cdot}5 \pm 0{\cdot}3$
2** −	15 ± 5	1	24·5	$-0{\cdot}73 \pm 0{\cdot}20$	$0{\cdot}30 \pm 0{\cdot}10$
3 −	—	4–8	103	$-1{\cdot}85 \pm 0{\cdot}20$	$1{\cdot}80 \pm 0{\cdot}20$
4 ?	—	1	43	—	—
5 ?	—	1	11	>5	$>0{\cdot}95$
6 −	11 ± 4	1	12·5	$-5{\cdot}5 \pm 0{\cdot}8$	$1{\cdot}19 \pm 0{\cdot}17$
7 +	—	1	9·5	$+8{\cdot}3 \pm 1{\cdot}2$	$1{\cdot}37 \pm 0{\cdot}20$
8 ?	—	4–6	68·5	—	—
9 −	$8{\cdot}0 \pm 2{\cdot}6$	1	15	$-5{\cdot}3 \pm 0{\cdot}8$	$1{\cdot}38 \pm 0{\cdot}20$
10 −	—	1	34	$-2{\cdot}9 \pm 0{\cdot}60$	$1{\cdot}62 \pm 0{\cdot}32$
11 +	$6{\cdot}0 \pm 0{\cdot}6$	1	22	—	—
12 −	15 ± 3	1	27·5	$-4{\cdot}4 \pm 1{\cdot}1$	$2{\cdot}04 \pm 0{\cdot}50$
13 +	50 ± 20	1	15	$+6{\cdot}2 \pm 1{\cdot}2$	$1{\cdot}62 \pm 0{\cdot}35$
14 +	—	1	20	—	—
15 −	$6{\cdot}0 \pm 1{\cdot}5$	1	9·5	$+5{\cdot}4 \pm 1{\cdot}8$	$0{\cdot}89 \pm 0{\cdot}30$
16 −	—	1	25	$-6{\cdot}5 \pm 1{\cdot}3$	$2{\cdot}50 \pm 0{\cdot}40$
17 −	—	1	20·5	$-6{\cdot}7 \pm 0{\cdot}7$	$2{\cdot}40 \pm 0{\cdot}20$
18 ?	>40	1	7	—	—
19 −	>40	1	21·5	$-4{\cdot}0 \pm 1{\cdot}0$	$1{\cdot}47 \pm 0{\cdot}40$
20 +	—	1	34	$+5{\cdot}1 \pm 1{\cdot}0$	$2{\cdot}85 \pm 0{\cdot}57$
21 ?	>40	1	5	—	—
22 +	$4{\cdot}1 \pm 0{\cdot}4$	1–3	60	—	—

* discovered by Rochester and Butler 1947.

** associated with V°-track.

† angle between direction of $V^{\pm}$-particle and direction of charged secondary particle.

Unfortunately, the masses of two of the heavily-ionizing V-particles (3 and 8) cannot be estimated directly, because the tracks are too short for their momenta to be measured. The estimated ionization of track 22, which is reproduced in Plate XXX,* is about twice minimum; using the measured momentum, the mass of the unstable particle is thus about 1 100 m_e. It is unlikely that the ionization exceeds three times the minimum value; therefore an upper limit to the mass is (1 580$\pm$160) m_e, where the probable error is due to the uncertainty in the momentum measurement. The estimated ionization of track 11 (Plate XXXI) lies between the minimum value and an upper limit of twice the minimum ionization, which is consistent with an upper limit of (1 630$\pm$160) m_e for the mass of the unstable particle. Similarly the ionization of track 15 lies between minimum and twice minimum but, owing to the large error in the momentum of the primary, no reliable estimate of the upper limit to the mass can be made. The ionization estimates and momentum measurements for the remaining measurable primary tracks give considerably higher upper limits for the mass of the $V^{\pm}$-particles. Thus the preliminary measurements show that, if the $V^{\pm}$-particles are all of the same type, the smallest observed upper limit for their mass is 1 600 m_e. Therefore, the $V^{\pm}$-particle cannot be the charged counterpart of the $V^{\circ}{}_1$-particle of mass 2 200 m_e, found by Armenteros *et al.* (1951 b). In the discussion of the decay process of $V^{\pm}$-particles in § 3, section (i), an upper limit for their mass is required; this is taken to be 1 900 m_e, which is about two probable errors above the value of 1 600 m_e.

It is impossible to determine the mass of any of the 14 charged secondary particles whose momenta have been measured, because their tracks are all approximately at minimum ionization. An ionization of twice the minimum value may be regarded as an upper limit for all of the secondaries; considering this value in conjunction with the momenta, it will be seen that the masses of the negatively-charged secondaries of tracks 2 and 3 were less than 500 m_e. If all the ionizations are close to the upper limit, then several of the positive secondaries could have been protons.

The secondary particle of event 1 penetrated 3·4 cm of lead and was certainly heavier than an electron. Seriff *et al.* (1950) observed a similar charged secondary particle; it penetrated their 2 cm lead plate without producing an interaction. Assuming that electrons and negative protons are not produced and that the charged secondary particles are all of the same type then, in terms of well-known particles, they are probably either μ- or π-mesons. Bridge and Annis (1951) have described an event in which a slow secondary particle from the decay of a charged V-particle was scattered through a large angle in an aluminium plate and subsequently behaved as a meson; they consider that this secondary was a π-meson.

Event 2 is of particular interest since it represents, either the chance occurrence of both a charged and a neutral decay on the same photograph, or the decay of a charged V-particle with the production of a secondary

* For plates see end of issue.

neutral V-particle. This photograph is described in detail in § 4 ; meanwhile the possibility that neutral V-particles may be produced by the decay of charged V-particles must be kept in mind.

(iii) *Non-decaying Particles with Mass about* 1 000 m_e

Since the decays of several heavily-ionizing charged V-particles have been observed in the cloud chamber, their mean range for decay cannot be very much shorter than the average chamber dimensions. Therefore, it is expected that some of these particles will cross the chamber without decaying. About 900 heavily-ionizing particles which did not decay have been examined ; they were associated with nuclear interactions immediately above the chamber or in the lead plate. The great majority are protons, but some are mesons with estimated masses less than 350 m_e. Two particles, however, have estimated masses between those of the π-meson and the proton ; the data are given in rows (1) and (2) of table 2. Butler *et al.* (1950) found two similar events, the data for which are given in rows (3) and (4) of table 2.

Table 2. Measurements on Four Slow Non-decaying Particles of Mass about 1 000 m_e

Sign	Measured momentum (Mev/c)	Estimated ionization (min.)	Mass range (m_e)
(1) −	160(±10%)	6—10	900—1 500
(2) +	170(± 7%)	4— 6	800—1 000
(3) +	170(±10%)	5— 7	900—1 140
(4) −	170(±10%)	4— 6	800—1 020

Butler *et al.* (1950) discussed the problem of the detection of positive particles of mass about 1 000 m_e when they are associated with a very much larger number of protons. They showed that the error in the momentum measurements combined with the uncertainty of the ionization estimates makes it possible to separate these particles from protons only if they have momenta within the narrow band (100–200) Mev/c. This difficulty does not apply to the negative particles, providing it is assumed that there are no slow negative protons present. The measured momenta of the two negative particles (1) and (4) would have to be reduced by a factor of about four before they could be interpreted as π-mesons, this possibility is clearly very remote, because the errors in the momenta are only 10% of the measured values. Therefore, particles (1) and (4) are more massive than the π-meson ; their average mass is approximately 1 000 m_e. Similarly the positive particles (2) and (3) cannot be π-mesons. If, however, their actual momenta are each about twice the measured values and the ionizations are close to the upper limits, they could be protons. Again the observed errors are 10% of the measured momenta so that this possibility is remote, but it cannot be excluded completely.

Some of these non-decaying 1 000 m_e particles are probably identical with the $V^{\pm}$- and κ-particles, but they may possibly be the same as the τ-particles, found in photographic emulsions. The latter particles can be identified unambiguously by their decay into three charged π-mesons (Fowler *et al.* (1951)).

§3. Interpretation of the Charged V-Tracks

The available data on charged V-tracks, given in table 1, can be used for a study of the dynamics of their decay process. For this purpose it is reasonable to assume that all the events, with the possible exception of event 2, can be explained in terms of a single process.

Fig. 1

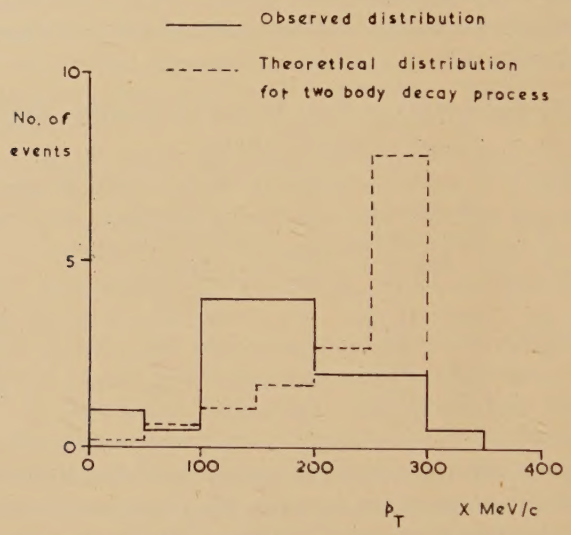

The distributions of the transverse momentum components (p^*=300 MeV/c for theoretical distribution)

(i) *The Number and Nature of the Secondary Particles*

The momenta of fourteen of the charged secondary particles are given in column (5) of table 1, and the momentum component of each secondary transverse to the direction of the V-particle is given in column (6). The observed distribution of the transverse momenta, shown in fig. 1, can be compared with the expected distribution on the assumption that all the $V^{\pm}$-particles are of the same kind and that they decay into only two secondary particles. Assuming that the secondary particles are emitted isotropically in the rest system, it has been shown by Armenteros *et al.* (1951 b) that the distribution of transverse momenta, p_T, has the form :

$$\mathscr{P}(p_T)\,dp_T = \frac{p_T}{p^*(p^{*2}-p_T^{\,2})^{\frac{1}{2}}}\,dp_T, \qquad \ldots\ldots (1)$$

where p^* is the momentum of the secondary particles in the rest system and so is a constant for all the events. The value of p^* depends only on the mass of the unstable particle and the masses of the two secondary particles. These quantities, however, are unknown and so a value must be deduced indirectly from the relation $p_T = p^* \sin \theta^*$, where θ^* is the angle of emission of the two secondaries in the rest system with respect to the direction of the $V^{\pm}$-particle. Thus the maximum value of p_T is equal to p^*. Since the largest observed value of p_T is 285 Mev/c, p^* is assumed to have this value in the theoretical distribution (1). This is also shown in fig. 1, in the form of a histogram (dotted) normalized to the total number of events. The estimated errors in the values of p_T, given in table 1, are too small to reconcile the observations with the theoretical distribution, although the observed number of events in each range of p_T is small. Hence it is concluded that the assumption of a unique two-body decay scheme is probably false. It is necessary to assume, therefore, that either the $V^{\pm}$-particles have two or more modes of decay, each giving two secondary particles, or that there is a single decay process involving three or more secondary particles.

Assuming that at least three secondary particles are produced by the decay of $V^{\pm}$-particles, then the data given in table 1 can be used in a discussion of the nature of the secondary particles. It was shown in § 2, section (ii), that, if all the $V^{\pm}$-particles are of the same kind, the single charged secondary is probably either a μ- or a π-meson. It was also shown that 1 900 m_e is the upper limit to the mass of the $V^{\pm}$-particles. Therefore, neutrons, or $V^{\circ}{}_1$-particles of mass 2 200 m_e, cannot be produced.

Owing to the limited data available, the momentum distribution of the charged secondary in the rest system cannot be found. However, it is reasonable to assume, as previously, that the largest observed transverse momentum, p_T, is approximately the maximum possible value of the momentum of the charged meson in the rest system, namely $p^*_{\max}$. Assuming this value, the maximum energy, $E_{\max}$, of the charged μ- or π-meson in the rest system can be calculated. If a three-body process is considered, then the conditions that hold when the energy of the charged meson is $E_{\max}$ can be obtained. Assuming that M is the mass of the unstable particle, m_1, the mass of the charged meson, and m_2 and m_3, the masses of the neutral secondary particles, expressed in energy units, it can be shown that when the charged secondary is emitted with energy $E_{\max}$ the neutral secondaries move parallel to each other and with equal velocities in the opposite direction to the charged secondary. Using these conditions, it follows that the combined mass of the neutral particles is given by:

$$(m_2+m_3)^2 = M^2 + m_1{}^2 - 2ME_{\max}. \quad . \quad . \quad . \quad . \quad . \quad . \quad (2)$$

A proof of this formula, which remains valid if either m_2 or m_3, or both, is zero, is given in the appendix. Values of (m_2+m_3) can be calculated, as a function of M, for various values of $p^*_{\max}$; they are shown graphically in fig. 2, where the charged secondary is assumed to be a μ-meson.

The observed upper limit of the p_T distribution is between 250 MeV/c and 300 MeV/c. The precise form of this distribution is unknown owing to the limited data available, and it is possible that the upper limit may be as high as 350 MeV/c. Using these values and the upper limit of 1 900 m_e for M, values of (m_2+m_3) can be obtained. They are summarized in table 3 ; those in column (2) are obtained if the charged secondary is a μ-meson while those in column (3) are obtained if it is a π-meson.

Fig. 2

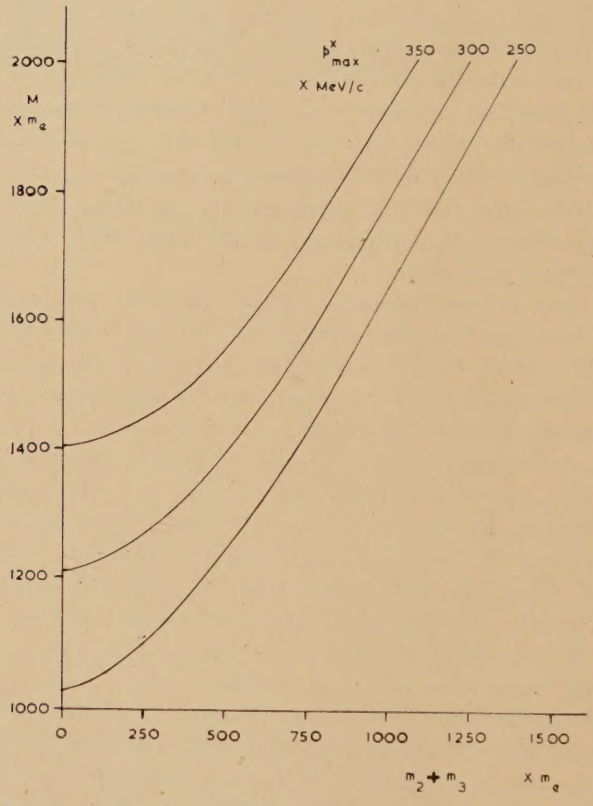

Relationships between M and (m_2+m_3) for $m_1=210\ m_e$

Table 3. The Values of (m_2+m_3), for $M=1\,900\ m_e$

(1) p^*_{max} (MeV/c)	(2) (m_2+m_3) for charged μ-meson (m_e)	(3) (m_2+m_3) for charged π-meson (m_e)
250	1 280	1 245
300	1 130	1 105
350	960	940

The calculated values of (m_2+m_3) show that a $V^\circ{}_2$-particle of mass about 800 m_e, described by Armenteros *et al.* (1951 b), may be produced by the decay of a $V^\pm$-particle, if the value of $p^*_{\max}$ lies in the range (250–350) MeV/c, but only if the value of M is close to the upper limit.

The above arguments, based on all the data at present available, show that no definite decay scheme for $V^\pm$-particles can be obtained. It is possible, however, to compare the properties of the $V^\pm$-particle with those of the $\kappa^\pm$-particles and to discuss possible decay schemes which may be used for the interpretation of both types of event.

(ii) *Possible Decay Schemes for $V^\pm$-particles*

Unstable charged particles, known as κ-particles, which decay into at least three secondary particles, only one of which is charged, have been found in photographic emulsions by O'Ceallaigh (1951), Menon (1951) and Trembley (1951). Bridge and Annis (1951) have observed the decay of several particles each into a single charged particle, one of which was heavier than the electron. These decays occurred when the particles were brought to rest in thin lead plates. These unstable particles are probably the same as the κ-particles. It is important to consider if the $V^\pm$-particles and these $\kappa^\pm$-particles are of the same type.

The masses of several κ-particles have been measured by O'Ceallaigh and Menon; the average is about 1 200 m_e. In two cases, the charged secondary has been identified. The first came to the end of its range in the emulsion and produced an electron, a characteristic of the μ-meson; the track of the second was very long and the particle was identified as a μ-meson from measurements of its grain density and scattering. Other κ-particles had charged secondaries with masses less than 400 m_e. The momenta of four of the secondary particles found at Bristol have been measured; assuming they were μ-mesons, the values range from 35 MeV/c to 268 MeV/c. Since the κ-particles decayed at rest, it is impossible to explain the momentum distribution of the charged secondary particles by means of a unique two-body decay process. It is plausible to assume, however, that the κ-particles have a single decay process because their mass values are the same, within experimental error; this decay process must have at least three secondary particles, the charged one being a μ-meson.

Several heavily-ionizing particles of mass about 1 000 m_e, which did not decay in the chamber, were described in § 2, section (iii). If these are the same as the $V^\pm$-particles, then the mass of the latter must be appreciably smaller than the upper limit of 1 900 m_e. Their mass could well be the same as the average mass of the κ-particles. In addition, the charged particles produced by the decay of $V^\pm$-particles could be μ-mesons. It is, therefore, plausible to assume, provisionally, that the κ- and $V^\pm$-particles are the same.

The highest observed momentum of the μ-meson in the rest system of a κ-particle is 268 MeV/c. This value is consistent with the range of values of $p^*_{\max}$ for the charged secondaries from the decay of $V^\pm$-particles, namely

(250–300) MeV/c. Using this result, values of (m_2+m_3) can be obtained from fig. 2 for values of M between 1 000 m_e and 1 400 m_e, which cover the range of the individual measurements of the masses of the κ-particles; the values of (m_2+m_3) are given in table 4.

Table 4. Possible Values of (m_2+m_3) for κ- and $V^{\pm}$-particles

	$(m_1=210\ m_e)$				
M (m_e)	1 000	1 100	1 200	1 300	1 400
(m_2+m_3) if p^*_{max} is 250 MeV/c (m_e)	—	245	425	570	700
(m_2+m_3) if p^*_{max} is 300 MeV/c (m_e)	—	—	—	330	506

A dash in table 4 indicates that the particular set of conditions is not possible. A value of p^*_{max} of 350 MeV/c is inconsistent with the observed range of values of M. Thus, if the values of M are correct, a κ-particle cannot produce a $V^{\circ}{}_2$-particle. In § 2, section (ii), it was suggested that track 2, in which a V^--particle is associated with a V°-particle, may be unique and, since it cannot be interpreted with the κ-particles, if this association is real, it will be omitted from the analysis; a possible interpretation is given in § 4. Should the mass of the κ-particles and the remaining $V^{\pm}$-particles lie between 1 000 m_e and 1 400 m_e then, if p^*_{max} is (250–300) MeV/c, the maximum mass of the neutral particle is about 500 m_e. The most likely combinations of neutral particles are therefore a π°-meson and a neutrino or alternatively two neutrinos.

If π°-mesons are produced they will decay into γ-rays which might be detected by their interaction in thin lead plates. Unfortunately very few of the cloud-chamber photographs of $V^{\pm}$-particles were taken with a suitable lead plate and so no direct evidence for the production of π°-mesons by $V^{\pm}$-particles has been obtained. O'Ceallaigh (1951) suggested a scheme for κ-particles involving a π°-meson in order to give them integral spin. This scheme is:

$$\kappa^{\pm}\rightarrow\mu^{\pm}+\pi^{\circ}+\text{neutrino}. \qquad (3)$$

Now the $V^{\pm}$-particles are nearly always observed in high-energy penetrating showers and, if they are not produced in pairs, they probably have integral spin and may possibly decay according to scheme (3). If p^*_{max} for the μ-meson is (250–300) MeV/c then, assuming scheme (3), the mass of the $V^{\pm}$-particles is about (1 100–1 260) m_e, which is consistent with the direct mass measurement on the tracks of κ-particles.

The only other plausible scheme for $V^{\pm}$-particles and κ-particles is:

$$V^{\pm} \text{ or } \kappa^{\pm}\rightarrow\mu^{\pm}+2 \text{ neutrinos}. \qquad (4)$$

Assuming this scheme and the same range for p^*_{max} as before, the mass of the unstable particles is within the range (1 025–1 225) m_e. If (m_2+m_3) $<300\ m_e$, the curves in fig. 2 show that the value of M is not strongly

dependent on the precise value of (m_2+m_3). Thus the range of values of M for schemes (3) and (4) is about the same; this is only the case if $p^*_{max} \gtrsim 250$ MeV/c.

§4. Description of Track 2 (Plate XXVIII)

Track 2, reproduced in Plate XXVIII, is so far unique because a V°-track is apparently associated with the charged decay. The spatial orientation of all the tracks on the photograph has been examined by reprojection. Two orthogonal projections are shown in fig. 3. The negative particle

Fig. 3

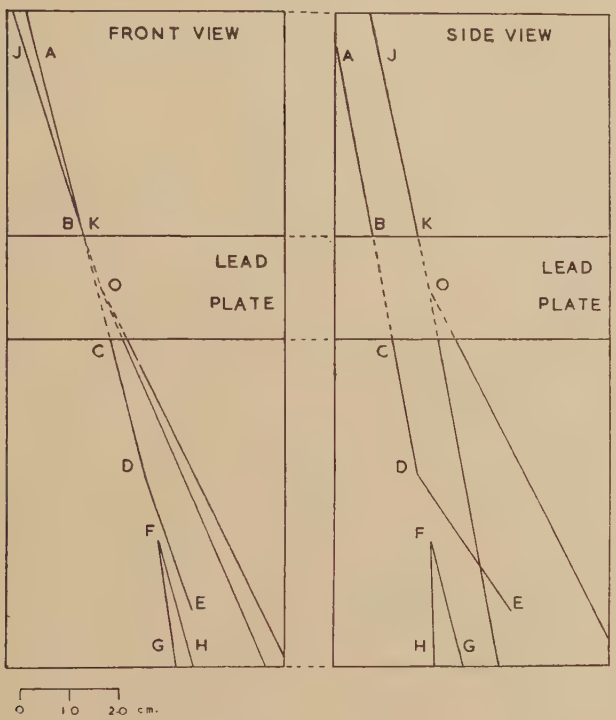

Projections of track 2

AB penetrated the lead plate with an angle of scattering $\leqslant 1^\circ$ and emerged as track CD. The particle decayed at D and the secondary particle DE was emitted at an angle of $(24{\cdot}5 \pm 2)^\circ$ to the direction CD. It can be shown from the ionization of this particle, which is between minimum and twice minimum, and the momentum of (73 ± 20) MeV/c, that the mass is less than $(200 \pm 50)\, m_e$. A V°-track was produced about 1·25 cm from D; point D lies in the plane of the V°-track within experimental error. A second incident particle JK interacted at O in the lead and produced two charged secondary particles. The plane of the V°-track

almost passes through the point O, in addition to point D. The line OF makes an angle of $(3{\cdot}5 \pm 2)^\circ$ with the plane of the V°-track GFH. It is, therefore, just possible that the V°-particle was produced at O and is only fortuitously related to the decay of the V^--particle. The first interpretation namely that the V^--particle produced the V°-particle, must, however, be given serious consideration.

The momenta of the primary and secondary tracks of the V^--particle 2 are given in columns (2) and (5) of table 1. No useful measurements can be made on the short secondary tracks of the V°-particle. FG makes an angle of 4° with the line of flight DF of the V°-particle. With this very limited data it is impossible to decide whether the fork was due to a V°_1- or to a V°_2-particle.

If it is assumed that the V^--particle of track 2 decayed into a meson and V°-particle, it cannot be interpreted by schemes (3) and (4). It is possible that track 2 and also the particle discovered by Bridge and Annis (§ 2, section (ii)) which decayed into a charged π-meson may be different from the κ-particles and the majority of the $V^\pm$-particles. A large fraction of the primary momentum of track 2, namely about (1–2) Bev/c, was given up to the neutral particles and, consequently, if the decay scheme involves only two secondaries, the neutral secondary was probably more massive than the charged one. A simple interpretation may be according to the scheme :

$$V^- \rightarrow V^\circ_{1 \text{ or } 2} + \text{meson}^-. \qquad (5)$$

If the event observed by Bridge and Annis is similar to track 2, the meson is a π-meson. Assuming that the neutral secondary is a V°_1-particle of mass 2 200 m_e, then the mass of the V^--particle (track 2) lies between 2 500 m_e and 2 800 m_e and the Q-value is about 60 Mev. For decay into a V°_2-particle, the mass would be between 1 100 m_e and 1 500 m_e.

If V°-particles were produced when the remaining twenty-one $V^\pm$-particles decayed in the chamber then, after correction for the relativistic dilatation factors and geometrical factors, the total path length of the V°-particles inside the chamber is greater than 50 cm. No V°-tracks were found, however, so that the lifetime of these V°-particles can hardly be less than 10^{-9} sec, which is longer than the lifetime of about 3×10^{-10} sec obtained from an examination of V°-tracks found in penetrating showers (Seriff *et al.* 1950). It is, therefore, unlikely that every $V^\pm$-particle produces a V°-particle.

§5. Conclusions

The decays of twenty-two $V^\pm$-particles have been examined. Each particle produces a charged secondary, which is probably a meson, and at least two neutral particles ; the combined mass of the latter particles is less than 1 000 m_e. Additional information can be obtained from a comparison of the $V^\pm$-tracks with those of κ-particles. It is concluded, provisionally, that both particles are of the same type ; each produces a

charged μ-meson and at least two neutral particles whose combined mass is less than 500 m_e. Two possible schemes are :

$$V^{\pm} \text{ or } \kappa^{\pm} \rightarrow \mu^{\pm} + \pi^{\circ} + \text{ neutrino}, \quad . \quad . \quad . \quad . \quad . \quad (6)$$

$$V^{\pm} \text{ or } \kappa^{\pm} \rightarrow \mu^{\pm} + 2 \text{ neutrinos}. \quad . \quad . \quad . \quad . \quad . \quad (7)$$

Both schemes are consistent with a mass of about 1 200 m_e for the unstable particle.

One photograph (track 2, Plate XXVIII) shows the apparent association of a V°-track with a V^{-}-track. This may be fortuitous, but, if it is assumed that the V^{-}-particle did produce a V°-secondary, a possible explanation of the double-decay process is :

$$V^{-} \rightarrow V^{\circ}_{1 \text{ or } 2} + \pi^{-}. \quad . \quad . \quad . \quad . \quad . \quad . \quad . \quad . \quad (8)$$

If a V°_1-particle was produced, the mass of the V^{-}-particle is about 2 600 m_e ; if a V°_2-particle was produced, then the mass is about 1 300 m_e.

Acknowledgments

It is with pleasure that we express our thanks to Professor P. M. S. Blackett for the excellent facilities he has given us and for the great interest he has taken in the analysis of the results. We are very much indebted to Dr. J. Rösch, the Director of the Observatoire du Pic-du-Midi, for his help during the experimental work and to Mr. A. H. Chapman who helped both with the work on the Pic-du-Midi and with the measurement of the tracks. Mr. M. G. Sowerby has been of great assistance during the measurement and analysis of the data. We also wish to thank Dr. J. Podolanski, Dr. G. D. Rochester, Prof. R. D. Sard, and Dr. J. G. Wilson for many helpful discussions. Financial assistance, which is very much appreciated, has been received from the Department of Scientific and Industrial Research, which has also given a grant to R. Armenteros. A. Cachon and C. M. York have received grants from the Centre National de la Recherche Scientifique and the United States Education Commission in the United Kingdom, respectively.

APPENDIX

When an unstable particle, of mass M, decays into three secondary particles, the relativistic energy equation, referring to conditions in the rest system of the unstable particle, may be written :

$$M = E_1 + E_2 + E_3 , \quad . \quad . \quad . \quad . \quad . \quad . \quad . \quad . \quad (9)$$

where E_1, E_2 and E_3 are the total energies of the three secondary particles in the rest system and M is expressed in energy units. If one of the secondaries, of mass m_1, has its maximum energy, $E_{\max}$, in the rest system, then it will be shown that $E_{\max}$ can be expressed simply in terms of M,

m_1 and (m_2+m_3), where m_2 and m_3 are the masses of the remaining secondary particles, and, for convenience, all the masses are expressed in energy units.

For the special conditions under consideration, eqn. (9) may be written :

$$M-E_{\max}=E_2+E_3\,, \qquad \ldots\ldots \quad (10)$$

where the term (E_2+E_3) takes a minimum value. The two conditions that hold when this occurs will now be obtained.

The conservation of momentum in the decay process imposes the condition :

$$\overrightarrow{p^*_{\max}}+\overrightarrow{p_2{}^*}+\overrightarrow{p_3{}^*}=0, \qquad \ldots\ldots \quad (11)$$

where $\overrightarrow{p^*_{\max}}$ is the maximum momentum of the charged secondary in the rest system and $\overrightarrow{p_2{}^*}$ and $\overrightarrow{p_3{}^*}$ are the momenta of the remaining secondaries in the rest system. The vector eqn. (11) shows that the three vectors are coplanar. If the direction of $p^*_{\max}$ is along the x axis, then $\overrightarrow{p_2{}^*}$ may be resolved into two orthogonal components p^*_{2x} and p^*_{2y}. Similarly, the components of $\overrightarrow{p_3{}^*}$ are p^*_{3x} and p^*_{3y}. Now momentum is conserved in the y direction, so that

$$p^*_{2y}=-p^*_{3y}=p_t{}^*. \qquad \ldots\ldots \quad (12)$$

Substituting these momentum components in eqn. (10), we obtain :

$$M-E_{\max}=(m_2{}^2+p^{*2}_{2x}+p_t{}^{*2})^{\frac{1}{2}}+(m_3{}^2+p^{*2}_{3x}+p_t{}^{*2})^{\frac{1}{2}}. \qquad \ldots \quad (13)$$

The two right-hand terms of this equation take a minimum value if $p_t=0$; consequently, the first condition is that particles 2 and 3 move parallel to one another in the opposite direction to particle 1. Thus the vector eqn. (11) may be re-written as a scalar equation :

$$p^*_{\max}=p_2{}^*+p_3{}^* \qquad \ldots\ldots \quad (14)$$

and eqn. (13) may be re-written in the form

$$M-E_{\max}=(m_2{}^2+p_2{}^{*2})^{\frac{1}{2}}+(m_3{}^2+p_3{}^{*2})^{\frac{1}{2}}. \qquad \ldots \quad (15)$$

The second condition that holds, if the right-hand side of eqn. (10) has a minimum value, can be obtained by eliminating $p_3{}^*$ from eqn. (15) by means of eqn. (14) and differentiating with respect to the variable momentum, $p_2{}^*$. It will then be seen that the second condition may be written in the form :

$$p_2{}^*(m_2{}^2+p_2{}^{*2})^{-\frac{1}{2}}=p_3{}^*(m_3{}^2+p_3{}^{*2})^{-\frac{1}{2}}. \qquad \ldots \quad (16)$$

Therefore particles 2 and 3 have equal velocities in the rest system of the unstable particle.

The unknown momenta $p_2{}^*$ and $p_3{}^*$ can now be eliminated from eqns. (14), (15) and (16) and the following value of (m_2+m_3) is obtained :

$$(m_2+m_3)^2=M^2+m_1{}^2-2ME_{\max}. \qquad \ldots\ldots \quad (17)$$

This equation, which remains valid if either m_2 or m_3, or both, is zero, has been used in a β-decay problem by Kofoed-Hansen (1951).

References

Armenteros, R., Barker, K. H., Butler, C. C., Cachon, A., and Chapman, A. H., 1951, *Nature, Lond.*, **167**, 501.

Armenteros, R., Barker, K. H., Butler, C. C., and Cachon, A., 1951, *Phil. Mag.*, **42**, 1113.

Astbury, P., Chippindale, P., Newth, J. A., Page, D. I., Rytz, A., and Sahiar, A. B., 1951, *Report given at Bristol Conference in December.*

Bridge, H. S., and Annis, M., 1951, *Phys. Rev.*, **82**, 445.

Butler, C. C., 1951, *Progress in Cosmic Ray Physics*, (North Holland Publishing Co.), 110.

Butler, C. C., Rosser, W. G. V., and Barker, K. H., 1950, *Proc. Phys. Soc.* A, **63**, 145.

Fowler, P. H., Menon, M. G. K., Powell, C. F., and Rochat, O., 1951, *Phil. Mag.*, **42**, 1040.

Fretter, W. B., 1951, *Phys. Rev.*, **83**, 1053.

Kofoed-Hansen, O., 1951, *Phil. Mag.*, **42**, 1411.

Leighton, R. B., Wanlass, S. D., and Alford, W. L., 1951, *Phys. Rev.*, **83**, 843.

Menon, M. G. K., 1951, *Report given at Bristol Conference in December.*

O'Ceallaigh, C., 1951, *Phil. Mag.*, **42**, 1032.

Rochester, G. D., and Butler, C. C., 1947, *Nature, Lond.*, **160**, 855.

Seriff, A. J., Leighton, R. B., Hsiao, C., Cowan, E. W., and Anderson, C. D., 1950, *Phys. Rev.*, **78**, 290.

Thompson, R. W., Cohn, H. O., and Flum, R. S., 1951, *Phys. Rev.*, **83**, 175.

Trembley, J., 1951, *Report given at Bristol Conference in December.*

DESCRIPTION OF THE PLATES

Plate XXVIII

(Track number 2)

This photograph is described in detail in § 4 and two projections are given in fig. 3. The unstable charged particle entered the chamber at (1) and decayed at level *D* into the charged particle (2) and probably a V°-particle which decayed at level *F* and produced tracks (3) and (4).

Plate XXIX

(Track number 6)

A high-energy negatively-charged particle (1), associated with a penetrating shower, decayed in the chamber producing one charged secondary particle, track (2). The measurements on the tracks are given in table 1. This photograph is a typical example of the decay of a high-energy charged *V*-particle.

Plate XXX

(Track number 22)

The data obtained from this photograph are discussed in § 2, section (ii). The unstable particle entered the chamber at (1) and produced a single charged secondary (2). The track of this secondary is too short for measurement. The momentum of the positively-charged primary is (400 ± 40) Mev/c and the estimated ionization is about twice the minimum value. The

measurements are consistent with a value of 1 100 m_e for the mass of the particle. The ionization may be compared with that of the neighbouring track (3) which was produced by a proton with a measured momentum of (400±40) Mev/c. The momentum of the proton is the same as that of the V^+-particle but there is no doubt that it is more heavily ionizing. The estimated ionization for particle (3) is (3–5) minimum : assuming it to be a proton, the expected ionization, allowing for the error in the momentum, is within the range (3·5–5·0) minimum. This comparison of the proton track (3) with that of the V^+-particle track (1) shows that an ionization of three times minimum is an upper limit for the ionization of the latter particle. This ionization is consistent with an upper limit of (1580±160) m_e for the mass of the V^+-particle ; the error in this mass arises from the error in the momentum measurement.

Track (4) is produced by a second proton, the measured momentum is (210±20) Mev/c and the estimated ionization within the range (8–10) minimum ; the calculated ionization for a proton is (9–12) minimum, this range of values arises from the error in the momentum measurement.

Plate XXXI

(Track number 11)

The data obtained from this photograph are discussed in § 2, section (ii). The positively-charged particle entered the chamber at (1) and produced a charged secondary track (2) which is too short for measurement. The measured momentum of the primary particle is (600±60) Mev c and the ionization is between the minimum value and an upper limit of twice the minimum value. This range of values for the ionization is obtained by comparing the ionization of track (1) with the ionizations of the electrons and other fast particles in the photograph. If the upper value of twice the minimum is assumed for the ionization, then the upper limit for the mass of the unstable particle is (1660±160) m_e ; the error arises from the uncertainty in the momentum. It will be noticed that the V^+-particle is associated with a high-energy penetrating shower.

LVII. *The Effect of Four Transition Metals on the α/β Brass Type of Equilibrium*

By J. B. Haworth*
and
W. Hume-Rothery, F.R.S.
Inorganic Chemistry Laboratory, Oxford†

[Received March 5, 1952]

Synopsis

Copper is able to dissolve both zinc and aluminium, and in the binary systems Cu–Zn and Cu–Al there are typical primary (α) face-centred-cubic solid solutions, and body-centred-cubic (β) phases, which are 3/2 electron compounds. In these and other similar alloys of copper, the equilibrium between the α and β phases is determined mainly by the electron concentration, provided that the size-factors are favourable and the electrochemical factors are small. The present paper describes an experimental investigation of the effect of manganese, iron, cobalt and nickel on the α/β equilibrium in Cu–Zn and Cu–Al alloys at 672° C. For this purpose the isothermal sections of the ternary systems in the regions concerned have been determined by the method of annealing and microscopical examination. If it is assumed that the α/α+β and α+β/β solubility curves in the ternary isothermal sections are lines of constant electron concentration, the results show that, when present in small quantities, Ni, Co, Fe and Mn act as though they possessed valencies of about 0·6, 0·8, 1·0 and 1·9 respectively, in the systems Cu–Zn–Ni, Cu–Zn–Co, Cu–Zn–Fe, Cu–Zn–Mn, Cu–Al–Co, Cu–Al–Fe and Cu–Al–Mn. If the simple collective electron theory is assumed, the apparent valencies for nickel, cobalt and iron are approximately equal to the numbers of *s*-electrons per atom in the crystals of the metallic elements concerned. For manganese the apparent valency agrees with the divalent state previously proposed for this element. The results for the system Cu–Al–Ni are anomalous. The bearing of these results on the theory of the transition metals and their alloys is discussed.

§1. Introductory

It is well known that in alloy systems where the atomic size-factors are favourable and the electrochemical factors are small, the α/β brass type of equilibrium is determined mainly by the electron concentration, although to a higher degree of accuracy the exact positions of the phase-boundaries are affected by the lattice distortion (Andrews and Hume-Rothery 1941).

* Now Research Metallurgist with Murex Limited, Rainham, Essex.
† Communicated by the Authors.

In a previous communication (Hume-Rothery 1948) it was shown that the addition of the elements manganese, iron or nickel to $\alpha\beta$ brasses or $\alpha\beta$ copper-aluminium alloys affected the $\alpha/(\alpha+\beta)$ and $(\alpha+\beta)/\beta$ solubility curves in a way directly related to the position of the added element in the Periodic Table. It was also shown that on the assumption that the effects were due to electron concentration alone, manganese and iron appeared to act as though they possessed valencies of 2 and 1 respectively, whilst nickel appeared to exert a valency of 0·6, equal to the number of holes per atom in the 3*d* shell of pure nickel ; on the simple collective electron model this number is equal to the number of electrons in the 4*s* band. The experimental data were not, however, sufficiently accurate to establish these apparent valencies conclusively, and the present paper describes an experimental investigation of the 672° C isothermal sections of the ternary systems Cu–Zn–(Mn, Fe, Co or Ni) and Cu–Al–(Mn, Fe, Co or Ni) in the α/β region, together with a discussion of the results obtained. The temperature 672° C was chosen because it was used in the work of Andrews and Hume-Rothery (*loc. cit*). For abbreviation we shall use the term 'apparent valency' to denote the valency deduced from the initial slopes of the $\alpha/\alpha+\beta$ and $\alpha+\beta/\beta$ boundaries in the ternary isothermal sections on the assumption that the slopes are determined by a constant electron concentration alone.

§2. Experimental

(a) *Metals Used*

The British Non-Ferrous Metals Research Association kindly presented some specially pure 99·99+% electrolytic copper, and also a 60 : 40 brass master alloy prepared from electrolytic zinc and electrolytic copper. Use was also made of some specially pure copper obtained from Messrs. Johnson, Matthey & Co., Ltd. Crown Special Zinc of 99·99+% purity was obtained from the Imperial Smelting Corporation, and the aluminium was super-purity metal from the British Aluminium Company. The manganese used was pure electrolytic metal which was heat treated in hydrogen at 900° C. From this metal, one copper-manganese master alloy was prepared in an alumina-fluorspar lined crucible, using a low pressure of hydrogen in a vacuum induction furnace. The master alloy contained 35% manganese by weight, which corresponds to the lowest freezing point in the Cu–Mn system. A second master alloy was made in a recrystallized alumina crucible under a low pressure of purified argon. For the Cu–Zn–Mn alloys, this master alloy and the 60 : 40 brass were melted together with excess of copper or zinc, using alumina-fluorspar lined crucibles ; a flux of 'Analar' potassium chloride was used for this and all other alloys. Under these conditions the loss of zinc was not excessive. The corresponding Cu–Mn–Al alloys were made by melting Cu–Mn and Cu–Al master alloys with excess of copper or aluminium, and here the composition could be controlled accurately.

For the iron and cobalt alloys, use was made of pressed compacts of pure powders of copper and iron, and of copper and cobalt. These were obtained from Messrs. Johnson, Matthey & Co., Ltd., and provided a satisfactory method of introducing the high melting transition metals, although appreciable loss of zinc occurred when the compacts were melted with the 60 : 40 brass. For the nickel alloys a 50 : 50 copper–nickel master alloy was first used. The analysis of this indicated a satisfactory degree of purity, but as the work proceeded, evidence of slight contamination was obtained and this was traced to the master alloy. All the alloys prepared from this master alloy were therefore discarded for the final diagram (see page 621), and a new master alloy was prepared in this laboratory from high purity copper and Mond-nickel shot of 99·96% purity kindly presented by the Mond Nickel Company.

(b) *Preparation and Heat Treatment of Alloys*

After melting and thorough stirring, the alloys were cast into heavy copper moulds to give ingots of about $\frac{1}{4}''$ diameter. Portions of these were enclosed in sealed evacuated hard glass tubes which were annealed in electric resistance furnaces controlled by Foster Temperature Regulators. All alloys which were sufficiently ductile were hammered before annealing in order to promote recrystallization. The times of annealing are summarized in the later sections, and in each alloy system representative alloys were hammered and reannealed for further periods in order to ensure that equilibrium had been obtained. A few anneals were interfered with by power cuts, and in such cases a prolonged further anneal at 672° C was always given. At the end of an anneal the specimen tubes were quenched in iced brine, and the specimens used for microscopical examination.

(c) *Modification of the Composition of Alloys*

The volatility of zinc made it difficult to obtain exactly the desired composition in the alloys concerned, and the original ingots did not always give sufficiently close composition brackets. It was found that by annealing small portions of the alloys with weighed amounts of zinc in small sealed evacuated tubes, the zinc gradually volatilized and was absorbed by the alloy, and a completely uniform microstructure was obtained if the annealing were continued for a sufficient time. In this way homogeneous α-phase alloys whose compositions were near to the edge of the solubility curve could be converted into 2-phase (α+β) alloys with very small quantities of the β-phase, and close composition brackets could be obtained. In the same way (α+β) alloys could be converted into β-phase alloys. For abbreviation this process will be called modification of the alloys.

(d) *Microscopical Examination*

The alloys were prepared for microscopical examination by conventional methods, using hand-grinding followed by polishing with a liquid polish of the Brasso type. The distinction between the α- and β-phases was readily made with the etching reagents customary for this type of alloy.

Feathery decomposition of the β-phase was sometimes observed in the Cu–Zn ternary alloys, and acicular structures in the Cu–Al ternary alloys, but these did not prevent the detection of the small particles of the α-phase which had been present at the quenching temperature. In the ternary alloys with cobalt or iron, the iron-rich and cobalt-rich phases were visible in the unetched state, as well as after etching. In many of the critical alloys these particles were very small, and careful searching with systematic traverses across the section was undertaken. The relative amounts of the phases were estimated, using oculars with squared graticules in which the field of view was covered by 70–100 squares.

(e) *Chemical Analyses*

The compositions of all the alloys included in the present diagrams were determined by chemical analysis after at least two sections had been prepared and examined microscopically to ensure that the structure was uniform. In each ternary system at least one alloy was analysed so that all of the three constituent metals were determined. The results indicated that the alloys were satisfactorily pure, and once this was established the remaining alloys were analysed for two metals only, and the percentage of the third metal taken by difference. In this work the copper was always determined electrolytically, and the choice of the second metal to be determined varied according to the system and the composition concerned.* The analyses were carried out by Johnson, Matthey & Co., Ltd., and the authors must express their thanks to Mr. A. R. Powell for his continual help and interest.

§3. Experimental Results

(a) *The Binary System Copper–Zinc*

The $\alpha/\alpha+\beta$ and $\alpha+\beta/\beta$ points at 672° C were found to lie at 35·90 and 41·35 atomic % zinc respectively. In this work 9 alloys were prepared and annealed to equilibrium at temperatures between 619° C and 730° C, and the 12 most critical specimens were analysed. The values at 672° C agree to within 0·05% with those obtained from the annoted equilibrium diagrams of Raynor (1944), and may thus be regarded as established conclusively.

(b) *The Binary System Copper–Aluminium*

For this system 6 alloys were prepared whose nominal compositions differed by 0·1% in the region of the $\alpha/\alpha+\beta$ boundary, and these were annealed to equilibrium at 672° C; a corresponding set of six alloys was used to determine the $\alpha+\beta/\beta$ boundary. The analyses of the critical alloys showed that composition brackets differing by only 0·04% and 0·12% Al, by weight respectively had been obtained, and by considering the

* In all, 21 of the alloys in the following diagrams were analysed for all three metals, and the sums of the percentages lay between 99·90 and 100·04. The low figure 99·90 was obtained for only one alloy, and the lowest total in the remainder was 99·93.

proportions of the two phases in the critical alloys, the values deduced for the $\alpha/\alpha+\beta$ and $\alpha+\beta/\beta$ boundaries at 672° C were 18·94 atomic % and 22·66 atomic % aluminium respectively; these values are about 0·4% greater and 0·3% less than those read from Raynor's annoted diagram (1945).

(c) *The Ternary System Copper–Zinc–Manganese*

For this system 56 alloys were prepared in order to cover the field systematically, and to ensure that no unsuspected phases were present. The alloys reached equilibrium in 17 days at 672° C, and no change resulted on reannealing for a further 7 days. Eleven of the most critical alloys were analysed. and the results obtained are summarized in fig. 1,

Fig. 1

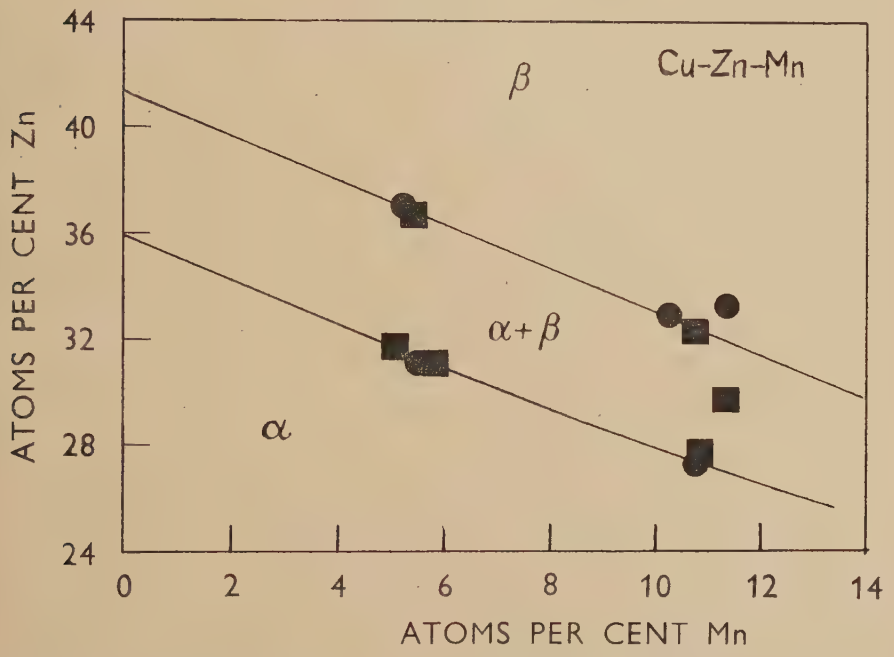

and are in good agreement with the curves of Graham, Long, Armantrout and Roberson (1949), which were published after the present work had been started. The first additions of manganese affect both the $\alpha/\alpha+\beta$ and $\alpha+\beta/\beta$ boundaries as though the apparent valency of manganese were 1·83. The $\alpha+\beta/\beta$ boundary is a straight line, but the $\alpha/\alpha+\beta$ boundary shows a slight curvature, and at 10 atomic % manganese the slope is equivalent to a valency of 1·77 for this element. In fig. 1 and all later diagrams, circles, squares and triangles are used to denote homogeneous. 2-phase and 3-phase alloys respectively.

(d) *The Ternary System Copper–Zinc–Iron*

In the system Cu–Zn–Fe the solubility of iron in the α and β phases is very small, and a direct determination of the $\alpha/\alpha+\beta$ and $\alpha+\beta/\beta$ boundaries

could not give the gradients to the desired degree of accuracy. The general form of the diagram has been determined by Bauer and Hansen (1934) and is such that the α and β phases are in equilibrium with a very dilute solid solution of copper in iron, with the formation of binary (α+Fe) and (β+Fe) fields separated by a ternary (α+β+Fe) triangle. The sides of this triangle must be straight lines, and the policy adopted was, therefore, to determine the sides of this triangle to the highest degree of accuracy in the part of the diagram concerned. In view of the small solubility of iron it appears reasonable to draw the $\alpha/\alpha+\beta$ and $\alpha+\beta/\beta$ boundaries as straight lines from the corners of the 3-phase triangle to the known values on the copper–zinc base line. For this purpose 64 ternary alloys were cast and annealed, and of these 14 were further modified by cold-work followed by annealing with zinc. Thirty of the more critical alloys were analysed and the results obtained are shown in fig. 2. The solubility of iron in copper has been taken as 0·20% from the magnetic work of Tammann and Oelsen (1930); a higher solubility has been given by Andersen and Kingsbury (1943), but the lattice spacing/composition curves given by these workers are unfortunately inconclusive in the region concerned. In the present work, primary dendrites of iron were found in the alloys containing more than about 1% of this element. In the more dilute alloys the iron was present in the form of very small particles which could be seen in the polished and unetched sections. The present work shows that the $(\alpha+\beta)/(\alpha+\beta+\text{Fe})$ boundary lies at slightly more than 0·2 atomic % zinc. The $\alpha/\alpha+\beta$ and $\alpha+\beta/\beta$ boundaries are horizontal in fig. 2, so that the apparent valency of iron is 1·0.

(e) *The Ternary System Copper–Zinc–Cobalt*

The ternary system Cu–Zn–Co has been examined by Iitsuka (1929), but the absence of detail makes this work useless for the present purpose, and some of the diagrams published by Iitsuka as vertical sections through the ternary model are clearly wrong. No other work on the ternary system appears to have been published, although C. S. Smith in a patent application (1936) states that the solubility of cobalt in copper is increased by the addition of zinc, and at 850° C and 600° C the solubility limits are stated to be 4% and 2% cobalt by weight, respectively, in a 30% zinc alloy. The binary system Cu–Co has been studied by Haschimoto (1937), and the solubility of cobalt in copper has been determined by the magnetic methods of Tammann and Oelsen (*loc. cit.*) as 0·86 weight % at 672° C, the phase in equilibrium with the copper-rich solid solution being a solid solution in the face-centred cubic β-cobalt, containing 11·2 weight % copper.

In the present work 124 ternary alloys were prepared for annealing, and a number of these were modified by annealing with zinc. The times of annealing varied between 5 and 55 days, and the time necessary to reach equilibrium was greatly influenced by the composition. In some alloys the cored structure of the cast ingot was remarkably persistent, and with 3% cobalt and 10% or 20% of zinc the cored structure was still present after

55 days at 672° C (these alloys are not critical for the equilibrium diagram). In the annealed alloys the cobalt was present in the form of small round globules which were visible in the unetched, polished surface.

The results obtained are shown in fig. 3 and enable the boundaries to be placed accurately. The diagram is of the same general form as that of the system Cu–Zn–Fe, except that the solubility of cobalt in the α- and β-phases is greater. An attempt was made to determine the composition of the cobalt-rich phase present in the 3-phase ($\alpha+\beta+$Co) alloys. For this purpose one of these alloys was reduced to powder by filing, and the ferromagnetic particles removed by a magnet. The magnetic filings were then further ground in a mortar, and were shaken with alcohol in a tap

Fig. 2

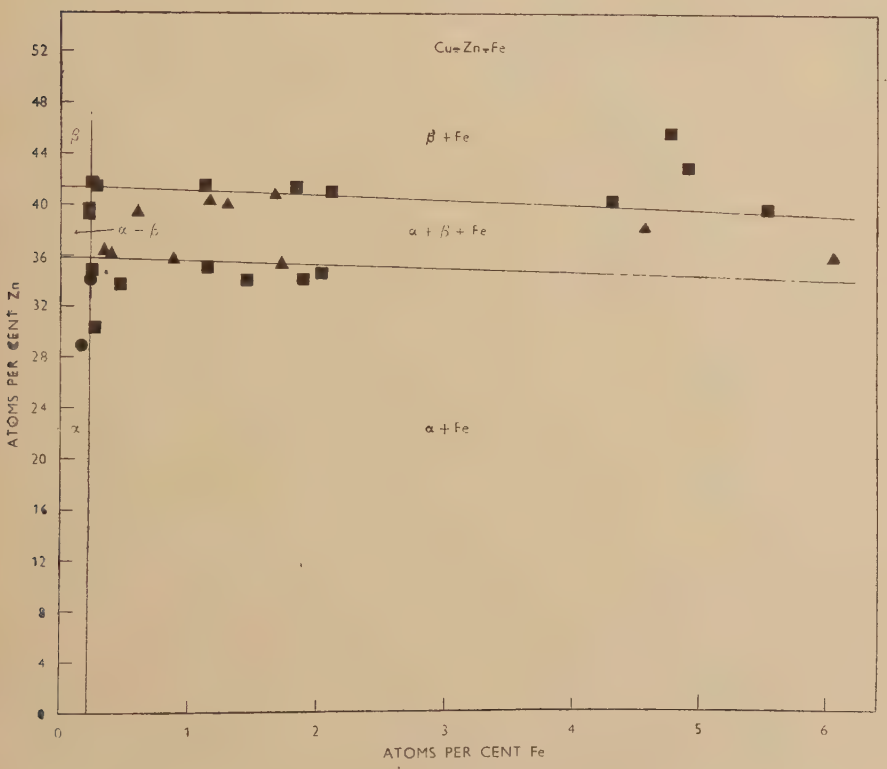

funnel surrounded by a powerful horseshoe magnet of the ' magnetron ' type. A portion of the filings adhered to the walls of the funnel nearest the pole-pieces of the magnet, and after decanting the remaining suspension, the experiment was repeated twice, after which the magnetic filings were separated, washed and dried. An x-ray powder photograph of the final product showed only the lines of a face-centred cubic structure, and the composition by analysis was Co 63·1 ; Zn 26·4 ; Cu 10·5 atomic %. This composition agrees with the phase-boundaries of fig. 3,

but the possible adhesion of particles of the α- and β-phases prevents it from being more than a tentative estimate of the cobalt-rich corner of the 3-phase triangle.

In fig. 3 the $\alpha/\alpha+\beta$ and $\alpha+\beta/\beta$ boundaries are almost exactly parallel and indicate an apparent valency of 0·8 for cobalt.

Fig. 3.

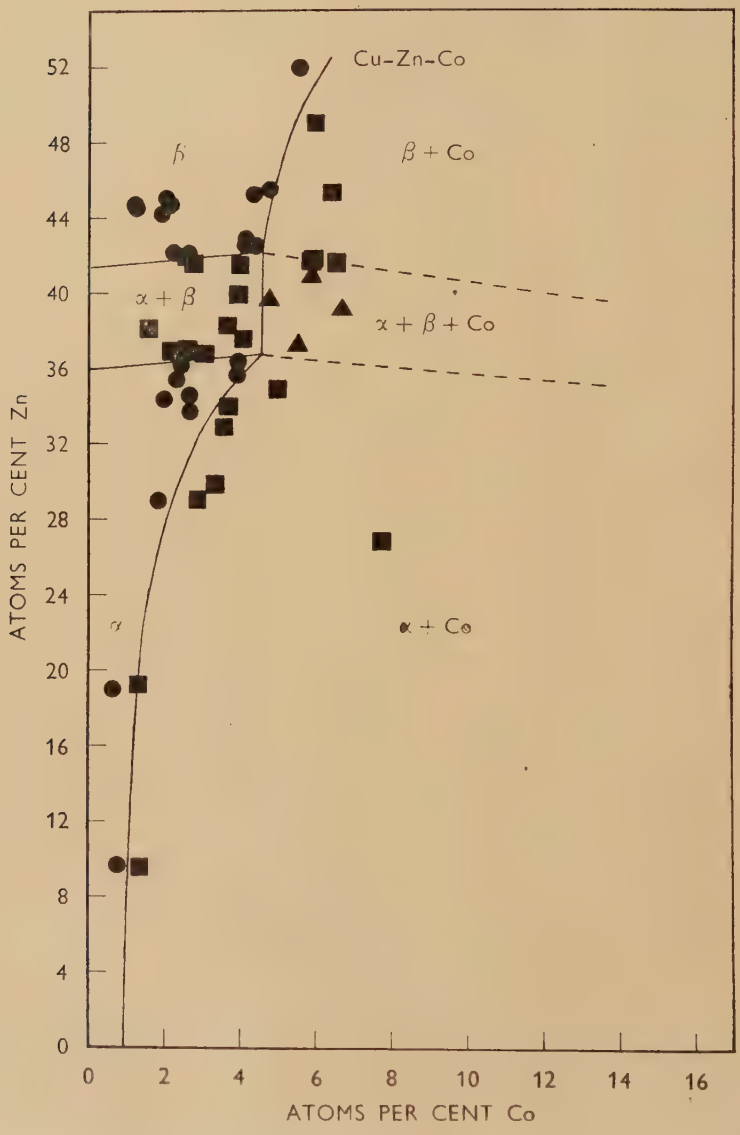

(f) *The Ternary System Copper–Zinc–Nickel*

In this system, copper and nickel form a continuous series of solid solutions, and nickel dissolves freely in both the α- and β-phases of the

system copper–zinc. The ternary system has been examined by Bauer and Hansen (1929) and by Schramm (1935), but neither investigation was in sufficient detail for the present purpose.

In the present work the approximate position of the phase-boundaries was found by preliminary work on 42 alloys, some of which were subsequently found to be slightly contaminated with iron, carbon and silicon from the impure master alloy (see page 615). The work was repeated with 24 alloys of high purity, and two of these were modified by annealing with zinc. The annealing periods used were of the order 14–28 days, and the microstructures were of the simple α, α+β, or β types. The results for

Fig. 4

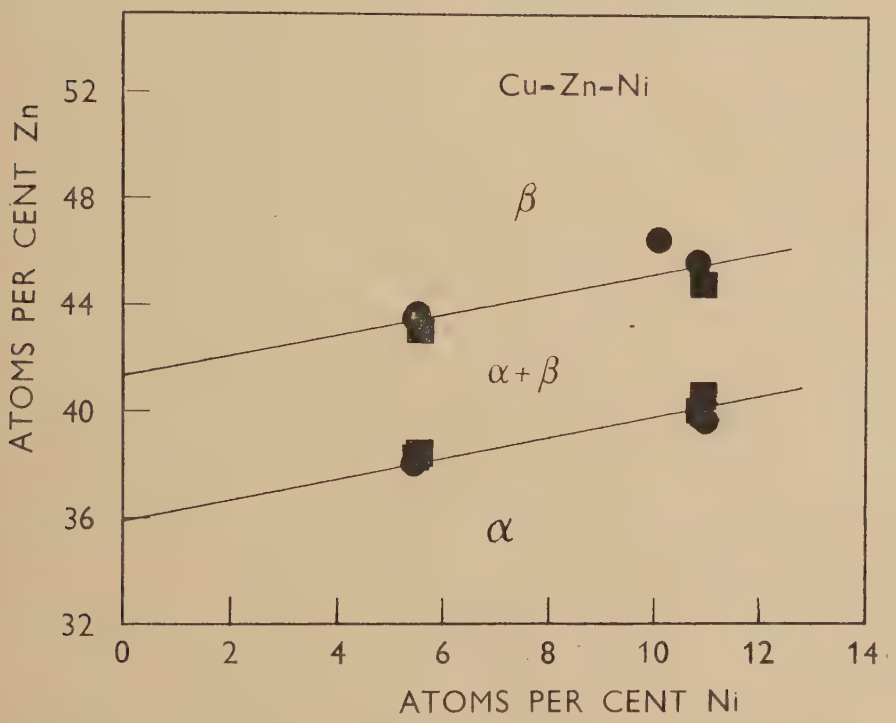

the most critical alloys are shown in fig. 4, and show that the α/α+β and α+β/β boundaries are parallel, and indicate an apparent valency of 0·61 for nickel, in contrast to the value 0·7 indicated by the work of Schramm (*loc. cit.*).

(g) *The Ternary System Copper–Aluminium–Manganese*

As in the system Cu–Zn–Mn, the complete miscibility of copper and manganese results in a wide range of ternary solid solutions, and in the present work only the α- and β-phases are concerned. The solubility limits of these phases at different temperatures have been determined by Dean, Long, Graham, Roberson and Armantrout (1946), and with their data as a guide, 24 alloys were cast and annealed for times varying from

17 to 32 days. The 8 most critical alloys were analysed, and the results are shown in fig. 5 and are in good agreement with those of Dean *et al.*, except that the two boundaries are not exactly parallel. From this diagram the apparent valencies of manganese are 1·91 and 1·93 for the $\alpha/\alpha+\beta$ and $\alpha+\beta/\beta$ boundaries respectively.

(h) *The Ternary System Copper–Aluminium–Iron*

Most of the previous work on this diagram was carried out with relatively impure materials, but Yutaka (1941) studied the system in the range 0–20% iron, and 0–20% aluminium by thermal, dilatometric, x-ray and

Fig. 5

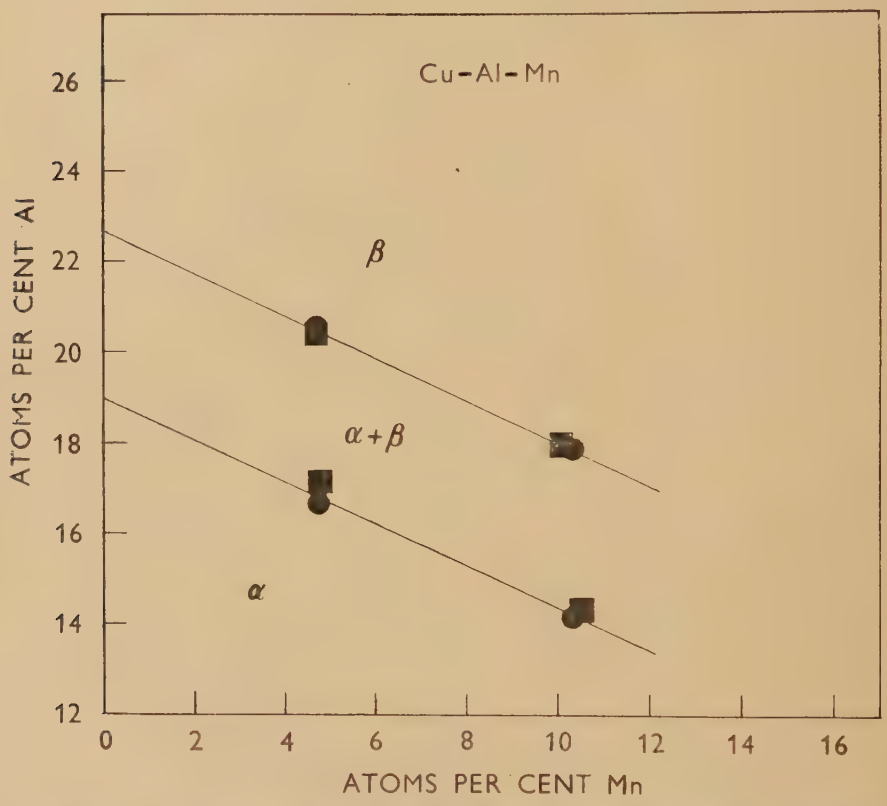

micrographic methods, and obtained results which are in good agreement with those of the present authors. In the present work 80 alloys were prepared, and annealed for periods of 27–35 days; these times were more than sufficient to produce equilibrium, and the additional time was given in an attempt to produce agglomeration of the small crystals of iron-rich phase which were difficult to detect. In alloys containing appreciable amounts of iron, the iron-rich phase was present in the form of dendritic crystals, generally in clusters, with a uniformly distributed precipitate of much smaller particles. As the limit of solubility was approached, the

dendrites disappeared, and the small particles were usually in the grain boundaries. Twenty-six of the most critical alloys were submitted to chemical analysis, and the results are shown in fig. 6, according to which the apparent valencies of iron are 1·1 and 0·9 for the $\alpha/\alpha+\beta$ and $\alpha+\beta/\beta$ boundaries respectively.

(j) *The Ternary System Copper–Aluminium–Cobalt*

No previous work appears to have been carried out on this ternary system in the range of composition concerned. In the present work, it has been possible only to determine the $\alpha/\alpha+\beta$ boundary, the data for

Fig. 6

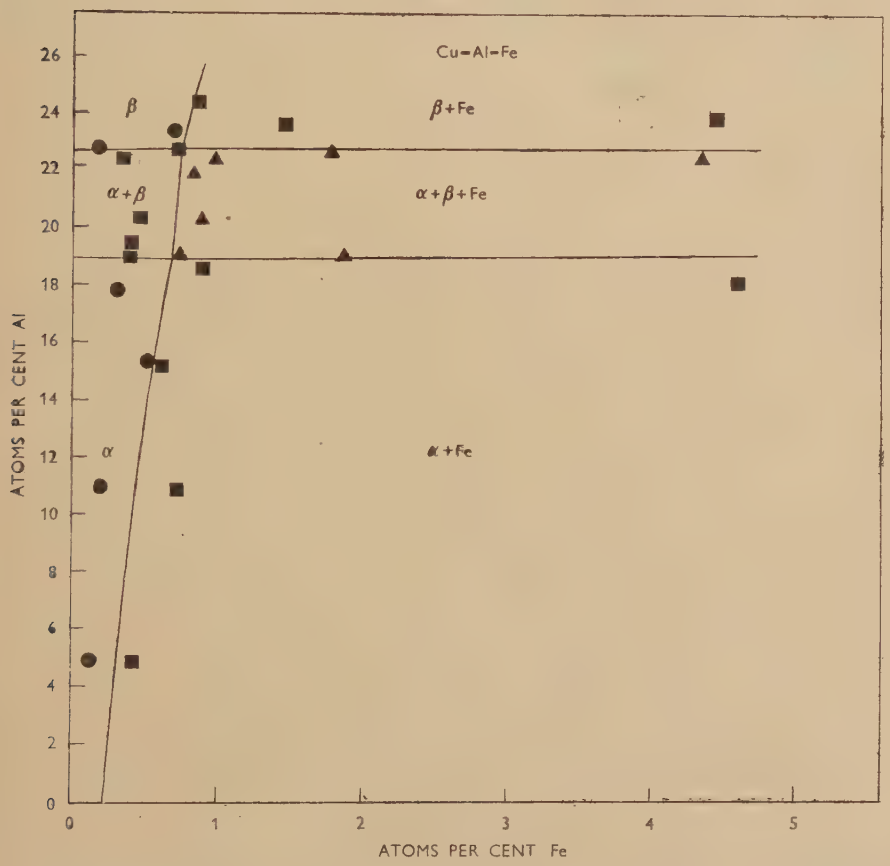

which are shown in fig. 7. This is based on the annealing of a number of alloys in the range concerned for periods of 21–29 days. The microstructures showed that the equilibrium diagram was of a type quite different from the remainder of those studied. As the cobalt content was increased from 0·3 to 2·0% there was a rapid increase in the proportion of a phase relatively rich in cobalt, suggesting the presence of either a new ternary phase, or of a very wide solid solution in cobalt. It was not

possible to study the system further, but fig. 7 shows that the apparent valency of cobalt for the $\alpha/\alpha+\beta$ boundary is $0{\cdot}9 \pm 0{\cdot}1$, and is thus nearly the same as that for the corresponding boundary in the system Cu–Zn–Co.

Fig. 7

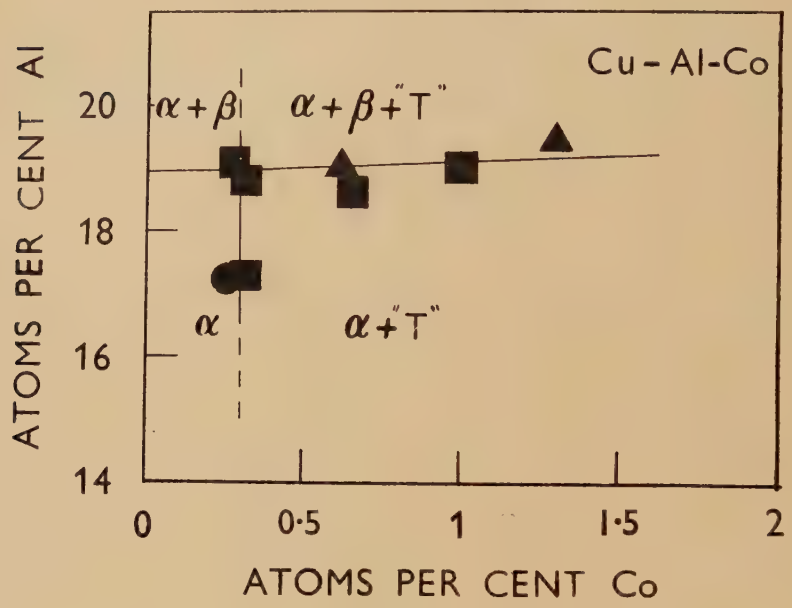

Fig. 8

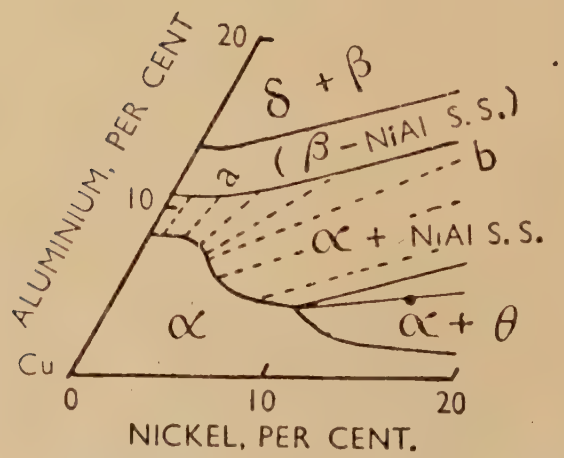

This figure is in weight percentages.

(k) *The Ternary System Copper–Aluminium–Nickel*

The general form of the Cu–Al–Ni equilibrium diagram has been established by the extensive work of Alexander and Hanson (1937), Bradley and Lipson (1938), Alexander (1939), and of Koster, Zwicker and Moeller (1948).

The system is characterized by the existence of an $\alpha/\alpha+\beta$ solubility curve with a bend in the region where the atomic ratio Al : Ni$\sim$1 (see fig. 8). This is undoubtedly connected with the development of order in the β-phase, and since the present work is concerned with the α/β equilibrium of the random solid solutions, we have concerned ourselves only with the alloys of low nickel content, for which the previous results were not sufficiently accurate. For this purpose 64 alloys were prepared and annealed for periods of 14 to 35 days. Seventeen of the most critical alloys were analysed, and the results obtained are shown in fig. 9. In this diagram the $\alpha/\alpha+\beta$ and $\alpha+\beta/\beta$

Fig. 9

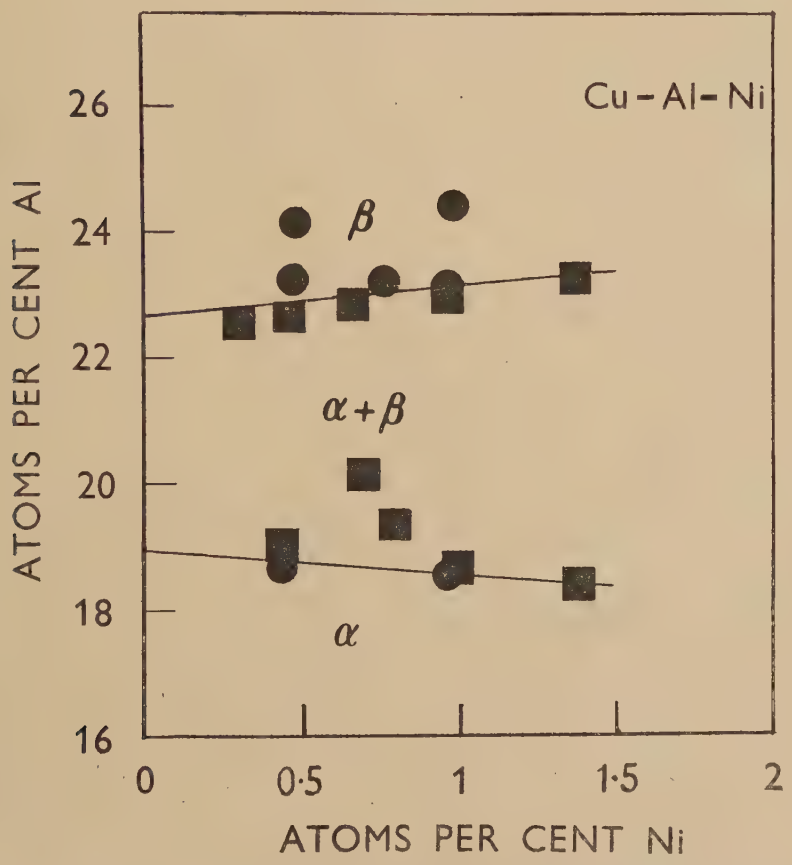

boundaries indicate apparent valencies of 1·75 and 0·02 respectively, and the boundaries are clearly not parallel. Within the narrow range of composition concerned the present results agree with those of Koster, Zwicker and Moeller (*loc. cit.*).

§4. Discussion

Table 1 shows the apparent valencies of Mn, Fe, Co and Ni deduced from the slopes of the $\alpha/\alpha+\beta$ and $\alpha+\beta/\beta$ boundaries. In discussing these, it must be admitted that the assumption of phase-boundaries determined by

electron concentration alone is to some extent arbitrary. There is, however, so much evidence that the α/β brass type of equilibrium is determined mainly by electron concentration when the size factors are favourable, and the electrochemical factors small, that it appears reasonable to make this assumption. If this is not accepted, the above table shows that in the Cu–Zn alloys the slopes of the phase boundaries are affected by amounts which increase almost uniformly on passing from Ni–Co–Fe, with a very much greater change on proceeding to Mn. In the Cu–Al alloys, in spite of the much more electropositive nature of aluminium, the effects of Mn, Fe and Co are almost exactly the same as in the Cu–Zn series, and it is only in the Cu–Al–Ni alloys that a difference occurs.

Table 1

System	Apparent Valency of Transition Element deduced from : $\alpha/\alpha+\beta$ Boundary	$\alpha+\beta/\beta$ Boundary
Cu–Zn–Mn	1·83	1·83
Cu–Al–Mn	1·91	1·93
Cu–Zn–Fe	1·0	1·0
Cu–Al–Fe	1·1	0·9
Cu–Zn–Co	0·8	0·8
Cu–Al–Co	0·9	—
Cu–Zn–Ni	0·61	0·61
Cu–Al–Ni	1·75	0·02

If the assumption of a constant electron concentration is accepted, the values in table 1 show that in spite of the preponderance of copper and zinc atoms, the ' holes ' in the $3d$ shells of the transition metal atoms are not filled in the Cu–Zn–X alloys. If the holes in the $3d$ shells were completely filled, we should expect iron, cobalt and nickel to show apparent valencies of the order -2, -1 and 0 respectively. It is only for the $\alpha+\beta/\beta$ boundary of the system Cu–Al–Ni that this expectation is fulfilled, and this is the system in which the filling of $3d$ holes is most probable, because aluminium is more electropositive than zinc, whilst nickel as the last transition element has the greatest tendency to complete the $(3d)^{10}$ sub-group.

It is now interesting to note that for nickel, cobalt and iron, the apparent valencies in table 1 are, according to the collective electron theories, approximately equal to the number of electrons/atom in s states in the crystals of the elements. In metallic nickel with saturation moment $0{\cdot}6\,\mu_B$, the number of holes in the $3d$-band is equal to, or very slightly greater than 0·6/atom, and this is equal to the number of s electrons. For cobalt the number of s-electrons is usually taken to be 0·7/atom, on the assumption that the saturation moment of $1{\cdot}7\,\mu_B$ corresponds to a completely filled half band of five d electrons with + spin, together with 3·3

electron of opposite spin. If there are any paired d holes, the number of s electrons will be slightly greater, and this is probably the case, because even for nickel the ferromagnetic forces are barely sufficient completely to fill the one half band. For iron, the saturation moment is $2{\cdot}2\,\mu_B$, but according to the analysis of Stoner (1938) and others, there are both paired and unpaired holes in the d-band. Coles (1951) has recently made a study of the magnetic properties of iron alloys, and concludes that for pure iron there are about $7{\cdot}1d$ and $0{\cdot}9s$ electrons/atom.

Comparison with table 1 shows that for all except the system Cu–Al–Ni, the apparent valencies of nickel, cobalt and iron in the alloys are equal to the number of s electrons in the metal. Manganese is not ferromagnetic, and the complicated α and β modifications probably contain atoms in more than one state. According to Hume-Rothery, Irving and Williams (1951), the γ (face-centred cubic*) and δ modifications are probably divalent, owing to the great stability of the Mn^{2+} ions which correspond to an exactly half-filled $3d$ sub group. If this view is accepted, divalent metallic manganese will involve two $4s$ electrons/atom, and this number is nearly equal to the apparent valencies in table 1.

The above results were unexpected and are difficult to understand, but the following interpretation is suggested, and for the sake of brevity is described rather dogmatically. For the earlier elements in the Long Periods, such as titanium, the electrons outside the inert gas shell are in hybrid ($s\,p\,d$) orbitals, and all of them take part in the cohesive process, and the resonance picture of Pauling (1938, 1949) is essentially correct. For the elements at the ends of the Long Periods, such as nickel, there are three kinds of electron outside the inert gas shell: (1) non-bonding d electrons, (2) bonding d electrons and (3) s electrons. It is uncertain to what extent hybridization occurs between (2) and (3), but for some purposes, such as electrical conductivity, it appears profitable to regard the s electrons as forming a separate band as in the early theory of Mott and Jones. The present results suggest that in iron, cobalt and nickel, the numbers of s electrons/atom are constants of a more fundamental nature than has previously been imagined, and that, when atoms of these elements are dissolved in copper–zinc alloys where the bonding is of an s (and partly p) type, only the s electrons of the transition element enter the conductivity band of the copper and zinc atoms, whose electron concentration determines the α/β brass equilibrium.

It is not, however, easy to see how this conclusion can be reconciled with the fact that, when copper or zinc is dissolved in pure nickel, the saturation moment is reduced by $v\,\mu_B$, where v is the valency of the solute (1 for copper, and 2 for zinc), since this indicates that the d holes are being filled. A comparison between the electronic configuration in the free atoms and in the metals is of interest. In solid nickel there are $0{\cdot}6d$ holes/atom,

* γ-manganese is usually described as face-centred tetragonal, but recent work by Z. Basinski and J. W. Christian (1952) makes it almost certain that the true structure at high temperatures is face-centred cubic.

whereas in the free atom the configuration is $(3d)^8\ (4s)^2$ with 2 holes in the d shell. From this we may conclude that increasing freedom of the nickel atom will favour the formation of holes in the d band. When compared with its state in solid nickel, an atom of nickel dissolved in copper, or in a copper–zinc alloy, is more nearly 'free', because (1) the lattice spacing is greater than that of nickel, and (2) the ions in copper or zinc are smaller than those in nickel, and interaction between d electrons of nearest neighbours is presumably less, and (3) if any effects are due to Ni–Ni interaction, the distances are considerably greater than in pure nickel. We can thus understand why when nickel is dissolved in copper or in a copper–zinc alloy, the normal tendency to fill the d-shell is counteracted by the effect of the greater freedom of the nickel atom. It is interesting to note that with palladium dissolved in silver, the effect is in the opposite direction, because the configuration of the free atom is $(4d)^{10}\ (5s)^0$ with no holes in the d-shell, whilst in the solid metal there are 0·6 holes. This may explain the fact that, as emphasized by Coles (1952), dilute solutions of palladium in silver are diamagnetic with no holes in the d band, whilst dilute solutions of nickel in copper are paramagnetic,* with holes in the d-band.

If the above view is correct, there is a distinction between the nature of the d-bands in nickel-rich and copper-rich alloys. In the nickel-rich alloys, a solute copper atom finds itself in a nickel framework whose dimensions are smaller than the lattice of copper, and whose ions have larger d-electron clouds than have the ions of copper. Under these conditions, the d electrons of the copper interact with adjacent nickel atoms, with the formation of a common d-band, and since each copper atom contains one electron more than a nickel atom, the additional electrons fill the $3d$ and $4s$ bands; the much higher N(E) curve for the former means that nearly all of the excess electrons enter the d band. A similar condition of affairs exists when silver is dissolved in palladium. In contrast to this, in copper-rich alloys, a solute nickel atom finds itself more nearly free than in solid nickel, and its d electrons do not form a common band with those of copper, although its s electrons do so. In copper zinc alloys this tendency will be increased because (1) the lattice spacing is greater than in copper, and (2) the d shells of the zinc ions are relatively smaller, and so have less tendency to form a common d band. We can thus understand why only the s electrons in nickel might be effective in determining the α/β brass solubility curves, and also why the d-shell of nickel might not be filled in these alloys. Similar considerations apply to cobalt and iron, and we can understand why in the equilibrium diagrams of these elements, the apparent valencies of the transition metal may vary. Thus, in the system Ni–Zn, the addition of zinc to nickel undoubtedly results in a filling of about two d holes per atom of zinc, whilst in the region of the γ-phase, Ni_5Zn_{21}, the apparent valency of nickel is zero, and in the β-phase its apparent valency is approximately 1. We cannot, however, understand why in the α/β brass alloys the apparent valencies of nickel,

* Coles has shown that the paramagnetism is not likely to be due to small 'islands' of ferromagnetic nickel atoms, resulting from lack of homogenity.

cobalt and iron are equal to the number of s electrons/atom in the pure metals.

The apparent valency of 2 for manganese can be understood in view of the great stability of the Mn^{2+} salts, and it is possible that the complete miscibility of copper and γ-manganese is connected with the fact that the Mn^{2+} ion, with five electrons of parallel spin in the d shell, will have its two valency electrons in $4s$ states which are similar to those in copper. Even with manganese, however, variable valency occurs, and an apparent valency of zero is shown in the γ-phase Mn_5Zn_{21}.

On passing from manganese to chromium, a complete change takes place in the nature of the alloys with copper, and the two metals are not only almost immiscible in the solid state, but also form immiscible liquids. The ground state of the free chromium atom is $(3d)^5\,(4s)^1$, but there are no stable univalent chromium compounds, and it seems that in compounds of chromium, the $3d$ and $4s$ bands overlap so completely that the single $(4s)$ electron of the free atom cannot function by itself, and so exists in alloys in a hybrid of which the $(3d)$ fraction is so pronounced that it cannot unite with that of the predominantly s-type of electron in copper. This interpretation would agree with the fact that vanadium, which resembles chromium in many ways, is also sparingly soluble in copper.

References

Alexander, W. O., 1939, *J. Inst. Metals*, **65**, 217.

Alexander, W. O., and Hanson, D., 1937, *J. Inst. Metals*, **61**, 83.

Andrews, K. W., and Hume-Rothery, W., 1941, *Proc. Roy. Soc.* A, **178**, 464.

Andersen, A. G. H., and Kingsbury, A. W., 1943, *Trans. Amer. Inst. Min. Met. Eng.*, **152**, 38.

Basinski, Z., and Christian, J. W. In the press.

Bauer, O., and Hansen, M., 1929, *Zeit. Metallkunde*, **21**, 357, 406; 1933, *Ibid.*, **25**, 17.

Bradley, A. J., and Lipson, H., 1938, *Proc. Roy. Soc.* A, **167**, 421.

Coles, B. R., 1951, *D. Phil. Thesis*, Oxford; 1952, *Proc. Phys. Soc.* B, **65**, 221.

Dean, R. S., Long, J. R., Graham, T. R., Roberson, A. H., and Armantrout, C. E., 1946, *Trans. Amer. Inst. Min. Met. Eng. Tech. Publ. No.* 2099.

Graham, T. R., Long, J. R., Armantrout, C. E., and Roberson, A. H., 1949, *Trans. Amer. Inst. Min. Met. Eng.*, **185**, 675.

Haschimoto, M., 1937, *Nippon Kinzoku Gakkai-Si.*, **1**, 5, 19.

Hume-Rothery, W., 1948, *Phil. Mag.*, [7], **39**, 89.

Hume-Rothery, W., Irving, H. M., and Williams, R. J. P., 1951, *Proc. Roy. Soc.* A, **208**, 431.

Iitsuka, D., 1929, *Mem. Coll. Sci. Kyoto Imp. Univ.*, **12**, 179.

Koster, W., Zwicker, U., and Moeller, K., 1948, *Zeit. Metallkunde*, **39**, 225.

Mott, N. F., and Jones, H., *The Theory of the Properties of Metals and Alloys.*

Pauling, L., 1938, *Phys. Rev.*, **54**, 889; 1949, *Proc. Roy. Soc.* A, **196**, 343.

Raynor, G. V., 1944, *Annoted Equilibrium Diagram Series No.* 3. Cu–Zn. Institute of Metals; 1944, *Annoted Equilibrium Diagram Series No.* 4. Cu–Al. Institute of Metals.

Schramm, J., 1935, *Cu–Ni–Zn Legierungen.* Würzburg.

Smith, C. S., 1936, *U. S. Patent No.* 2. 126, 827.

Stoner, E. C., 1938, *Proc. Roy. Soc.* A, **165**, 372.

Tammann, G., and Oelsen, W., 1930, *Zeit. anorg. Chem.*, **186**, 257.

Yutaka, A., 1941, *Nippon Kinzoku Gakkai-Si*, **5**, 136.

LVIII. *The Angular Distributions of the Gamma Rays in the Reaction* $^{19}F(p, \alpha\gamma)^{16}O$

By J. E. Sanders
Cavendish Laboratory, Cambridge*

[Received March 23, 1952]

The angular distributions of the 6·14 Mev (γ_1) radiation and the combined 6·91 and 7·11 Mev ($\gamma_2+\gamma_3$) radiations from the 874 kev resonance in the reaction $^{19}F(p, \alpha\gamma)^{16}O$ have been measured using a deuterium-filled ionization chamber as a gamma ray spectrometer. After amplification the photo-proton pulses were analysed on a 60-channel kicksorter (Hutchinson

Fig. 1

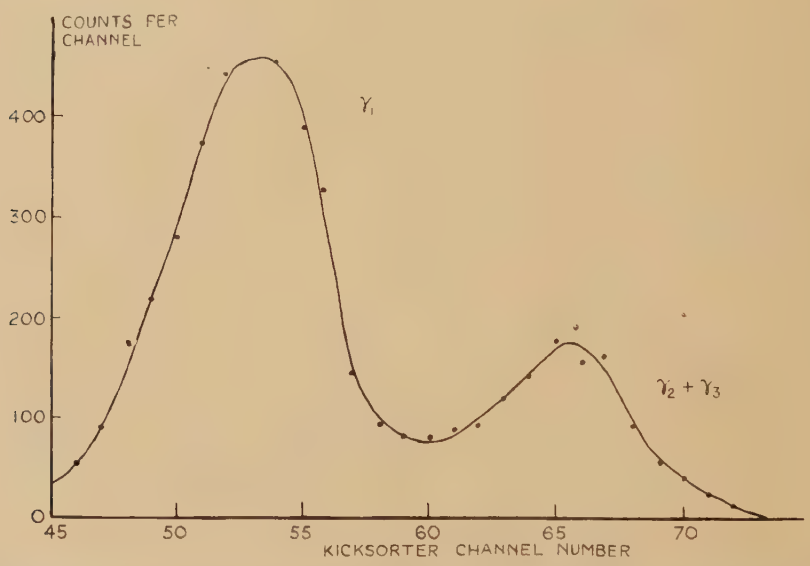

Photo-proton pulse height distribution for $\theta=0°$, showing the groups from the γ_1 and $(\gamma_2+\gamma_3)$ radiations.

and Scarrott 1951). With a 5 μ-amp proton beam from the Cavendish Electrostatic Generator and 10 kev thick CaF_2 targets, counting rates of the order of 20 per minute were obtained. Measurements of the photo-proton spectra were made at angles (θ) of 0°, 30°, 60°, 90° and 120° between the incident proton beam and the direction of observation of the gamma rays. Geiger counters were used to monitor the total gamma radiation from the reaction.

---

* Communicated by Mr. E. S. Shire.

A typical photo-proton pulse height distribution (that for $\theta=0°$) is shown in fig. 1, and this indicates the degree of resolution attained in these experiments. Within the statistical accuracy of the measurements, the intensities of the γ_1 and $(\gamma_2+\gamma_3)$ radiations derived from such photo-proton spectra at various angles can be expressed in the form $I(\theta)=1+a\cos^2\theta$, where for the γ_1 radiation $a=0{\cdot}01\pm0{\cdot}04$, and for the $(\gamma_2+\gamma_3)$ radiations $a=0{\cdot}33\pm0{\cdot}06$. Using the value of 3·0 for the intensity ratio $\gamma_1/(\gamma_2+\gamma_3)$ at 90° found in these experiments, the angular distribution of the total gamma radiation is given by $1+0{\cdot}09\cos^2\theta$, in satisfactory agreement with direct measurements of this distribution (Devons and Hine 1949; Chao 1950). Since it is difficult to correlate the experimental results with the theoretical predictions of the angular distributions given by Chao (1950), these calculations have been extended to include the effects of mixtures of the two lowest permitted values of the orbital angular momentum quantum number (l), both for the incident protons and the emitted alpha particles. It is then found possible to fit the observed distributions to those expected from the assumption that the level in ^{20}Ne formed at the 874 kev resonance is of spin 2 units and odd parity (2^-), and that the α_1, α_2, α_3 levels in ^{16}O are 3^-, 2^+ and 2^- respectively. These assignments are suggested by recent work in this laboratory on the angular correlation between the alpha particles and the gamma radiations. (Private communication from Mr. J. Seed.)

References

Chao, C. Y., 1950, *Phys. Rev.*, **80**, 1035.
Devons, S., and Hine, M. G. N., 1949, *Proc. Roy. Soc.* A, **199**, 56.
Hutchinson, G. W., and Scarrott, G. G., 1951, *Phil. Mag.*, **42**, 792.

LIX. *Elementary Structure and Slip Band Formation in Aluminium*

By D. Kuhlmann-Wilsdorf
Department of Physics, University of the Witwatersrand, Johannesburg
and
J. H. van der Merwe* and H. Wilsdorf
National Physical Laboratory,
Council for Scientific and Industrial Research, Pretoria†

[Received February 24, 1952]

Summary

From electron micrographs of deformed high purity aluminium numerical estimates for the spacing, length and amount of glide of the individual elementary lines have been obtained. It is found that the latter two quantities are compatible with the conception that each line is formed by dislocations emitted from one freely acting source of dislocations. The existing experimental evidence relating to the problem whether or not slip starts at the crystal surfaces is discussed. The evidence suggests that the sources of dislocations might well lie at the surfaces and therefore it is considered possible that the elementary structure is confined to a surface layer. The observed spacing of the steps, in the elementary structure as well as in the slip bands, is comparable with the theoretical critical distance below which rows of dislocations cannot pass each other. This indicates that there are many more possible sources than become active. A mechanism for the development of slip bands out of the elementary structure is proposed. This mechanism entails the annihilation of all dislocations in the immediate neighbourhood of an expanding slip line.

§1. Introduction

During an electron microscopical investigation of slip bands in aluminium of high purity a very fine surface structure was discovered (Wilsdorf and Kuhlmann–Wilsdorf (1951)). It consists of closely spaced, very fine surface steps which invariably are parallel to the acting slip planes, and the spacing of which is approximately the same as the spacing of the lamellae in slip bands,‡ (Heidenreich and Shockley (1948), Brown (1949)). As these steps appear even before the slip bands we called it the ' elementary structure '.

* Now at: Dept. of Physics, University of Pretoria, Pretoria.
† Communicated by the Authors.
‡ Measurements on the spacing and slip of the lamellae in slip bands are in progress.

While the elementary structure is described elsewhere (Wilsdorf and Kuhlmann–Wilsdorf (1952)), the origin of the elementary lines and their connection with slip bands is investigated theoretically in the present paper.

§2. Experimental Results on the Elementary Structure

It appears that slip bands are always accompanied by an elementary structure, and where two or three different slip systems are acting the corresponding two or three elementary systems are present, figs. 1, 2 and 3 (Plates XXXII and XXXIII*).

Table 1. Experimental Data on the Elementary Structure of Aluminium

1	2	3	4	5	6	7	8	9
Specimen	τ Resolved shear stress in kg/mm²	l Average length of elementary lines in μ	s Average height of el.l. in A	$s_c = \frac{\tau \cdot l}{G}$ Calculated height of el. l. in A	$\bar{d}$ Average spacing of el. l. in A	d_0 Smallest distance between two el. l. in A	$\bar{d}/d_0$	$d_0 \cdot \tau$ in A . kg/mm²
P. C.	0·56	7	20	16	530	390	1·38	220
S. C.	0·65	20	30	49	310	130	2·38	85
P. C.	0·77	3	15	9	630	480	1·31	370
S. C.	0·80	20	50	60	430	250	1·72	200
P. C.	0·82	3	10	9	590	360	1·63	300
S. C.	0·90	7	26	24	390	260	1·50	240
S. C.	1·0	17	80	66	390	250	1·60	245
S. C.	1·15	6	30	26	310	180	1·75	210
S. C.	1·25	3	15	14	420	270	1·53	330
P. C.	1·25	6	25	28	330	230	1·42	290
P. C.	1·5	3	15	17	310	200	1·56	300
S. C.	1·8	5	28	34	290	190	1·52	340
P. C.	2·0	5	45	38	250	165	1·54	330

S. C. = Single Crystal; P. C. = Polycrystalline Specimen.

The elementary lines usually have a length of a few microns, their mutual distance can be as low as 100 A and the height of the individual steps mostly lies beyond the resolving power of the technique employed, which is about 50 A, varying from specimen to specimen. Thus the line structure as such can be recognized, but the individual lines mostly are not clearly resolved. Consequently, it is impossible to measure the length of the elementary lines, their step height and spacing accurately, and not too much reliance must be put on such measurements. For this reason we hesitated to compile the following table of the main experimental data concerning the elementary structure. It is discussed in detail elsewhere (Wilsdorf and Kuhlmann–Wilsdorf (1952)). We believe the values generally to be uncertain by about 30% or perhaps even more.

* For plates see end of issue. The lines become more distinct when the photographs are viewed obliquely in the direction of the lines.

§3. The Origin of the Elementary Lines

One point in connection with the elementary structure seems to be clear and indisputable, namely that the lines are of the same nature as ordinary slip lines, only smaller. Therefore, in the light of the accepted theories on the plastic deformation of metals, they must be caused by rows of dislocations. Obviously the dislocations in any single elementary line must have originated from some source, and it is a probable assumption that there is one source to each line. Before discussing the structure in greater detail we therefore shall first investigate whether the experimental results are compatible with the idea that each elementary line is caused by one freely acting source of dislocations.

Leibfried (1951) and Eshelby, Frank and Nabarro (1951) in recent papers have for a number of cases solved the problem of how dislocations distribute behind obstacles under the influence of their mutual repulsive and attractive forces and an external shear stress. According to Leibfried the number of pairs released from one freely acting two-dimensional source of dislocations is given as $n=\tau a/\pi A$ where τ is the resolved shear stress and a is the distance between the source and the first obstacle on both sides of it against which the dislocations are piling up. As usual $A=G\lambda/2\pi=A_s$ for screw dislocations and $A=G\lambda/2\pi(1-\sigma)=A_e$ for Taylor dislocations, where G is the modulus of rigidity, λ the atomic distance in the glide plane in glide direction, and σ Poisson's ratio. As each dislocation creates a slip of λ along the distance it has travelled, the total slip near the source after n dislocation pairs have left it is $n\lambda=\tau a\lambda/\pi A$. Therefore, as $2a$ corresponds to l, the length of an individual line of the elementary structure, the step height will be expected to be $s\leqslant\tau l\lambda/2\pi A$ or $s\lesssim\tau l/G$. In the table of § 2 the observed values for s and l for different specimens are listed together with the stress τ which produced the elementary structure, and with the step depth as calculated from the above equation. Although s and l are rather inaccurate average values it is obvious that the agreement between the observed and calculated values is good. Consequently, we conclude that the conception that one freely acting source is responsible for each individual elementary line is justified. As the theoretical results for a source of dislocations of one sign and type only are very similar to those for a Frank–Read source (Frank and Read (1950)), it is not possible at this stage to decide whether the dislocations are created singly or in pairs or loops.

§4. Does Slip Start from the Crystal Surfaces ?

From the theoretical viewpoint it is obvious that the formation of a dislocation cannot be equally probable within a crystal and at its surface because different processes are involved. The close examination of the elementary lines and the single steps in slip bands reveal that the great majority of them seems to be deepest in the middle and to taper out towards both ends, fig. 4 (Plate XXXIII). This form is to be expected from

sources of the Frank–Read type, and from sources releasing single dislocations of one type only if they are situated at the surface. A source situated near the surface in the interior of the metal and releasing single dislocations of one type only should firstly create a crack and secondly, in the general case, lead to a step which is high at one end and tapers out towards the other. We therefore believe that, as far as we can see now, the latter case does not exist or is rare.

There are now two main possibilities: (1) The elementary structure is not a surface effect but is evenly distributed throughout the metal, and the sources of dislocations are of the Frank–Read type. (2) The elementary structure is confined to a surface layer and the sources all lie at the surface, and accordingly release similar single dislocations only which are curved so that they start and end at the surface. The microscopical examination of metal surfaces alone cannot distinguish between these possibilities.

Turning to the literature we find that in a recent experimental paper, Brown and Honeycombe (1951) have discovered very fine slip lines which, they said, are due to ' micro-slip ' and which probably are particularly strong elementary lines. By a very stimulating experiment they come to the conclusion that the ' micro-slip ' act uniformly throughout the metal.

On the other hand there are a number of observations recorded in the literature which suggest that slip most readily starts at the crystal surfaces. For instance, it is mentioned in several papers on strain markings—i.e. slip traces which appear on etching deformed metal surfaces—that on specimens with clear strain markings these may, with increasing distance from the original surface, get fainter until they vanish altogether (Jacquet (1945), McLean (1947), Hibbard (1948)). Further we find that they often have the form of small wisps projecting from the crystal boundaries (Jacquet (1945), McLean (1947)).

The observation that surface layers of single crystals often considerably reduce the creep rate under constant stress (Roscoe (1934, 1936), Andrade and Randall (1949), Andrade (1949), Andrade, Randall and Makin (1950), Harper and Cottrell (1950), Phillips and Thompson (1950), Menter and Hall (1950)), may be explained in two ways, namely, assuming that the surface layers impede the creation of dislocations, or alternatively that they are a powerful obstacle against the escape of dislocations through the surface (Kuhlmann (1951)), and thus these observations do not help us to decide whether the surface is a place where the generation of dislocations is particularly easy or particularly difficult. Pickus and Parker (1951) come to the same conclusion through experiments in which they copper-plated zinc crystals, thereby obtaining a surface layer which gives rise to effects analogous to natural surface layers. They, however, favour the view that it is the inhibition of the formation of dislocations in the surface which is responsible for the effect, mainly because plating has no effect in polycrystalline material. Here, they say,

the grain boundaries are places where dislocations may be formed easily and their area is so big in comparison with the free metal surface that the condition of the latter plays a small role only.

If the dislocations were released particularly easily from free metal surfaces we should expect a size effect in the sense that the resistance against creep increases with increasing size of the specimen. Andrade and Kennedy (1951) recently found such a size effect, but as the experiments were carried out with polycrystals more than only the above interpretation are possible. Another but similar size effect was discovered first by Smekal (1934) in rock salt and later by Wu and Smoluchowski (1949) in aluminium. While normally in a metal the glide combination with the highest resolved shear stress becomes active this rule breaks down when very thin specimens are used. In this case that slip system becomes active for which the resolved shear stress divided by the thickness of the specimen in slip direction is a maximum. This special size effect can be easily understood if it is assumed that slip starts at the surface.

Very strong support for the view that the dislocations are preferably formed at the surface is the effect an α-ray bombardment has on the creep of cadmium crystals as discovered by Andrade (1945), and also some recent experiments by Masing and Pfützenreuter (1951). The latter found that all metals examined by them, Pb, Zn, Ag, Au and Pt showed a faster creep in electrolytes than in air, and this effect was further increased when a current was applied, irrespective of its direction. Masing and Pfützenreuter infer that the effect cannot be caused by surface layers because it is present even with Pt, but that it is due to the reduced surface energy of the metals under the above conditions. The creation of the dislocations at the surface, they argue, becomes easier because the surface step, which must be created or the width of which must be increased by λ if a dislocation is to be formed at a surface, now has a smaller energy than normally. Thus the experiments would mean that slip starts at the surface. On the other hand there is the remote possibility that the metals' surface energy per λ^2 is appreciably bigger than the energy of a dislocation per atomic plane, and that therefore the escape of a dislocation through even a perfectly clean surface is a difficult process, which would become easier by the reduction of the surface energy. However, this appears to be highly unlikely.

Most of the observations discussed above indicate that dislocations are particularly easily formed at free surfaces and therefore it seems possible that the sources of dislocations lie at the surface and that the elementary structure is confined to a surface layer. If that should be so we might be able to understand an experiment carried out by Heidenreich and Shockley (1948). They loaded a single crystal of pure aluminium slightly below or just above its yield point for 20 minutes or more with practically no effect on the Kikuchi lines observed in electron diffraction after unloading the specimen. If, however, the loaded specimen was brought

into vibration by tapping for a short time (10 to 20 seconds), the lines were broadened or disappeared altogether, although no slip bands could be observed. The Kikuchi lines reappeared when about 0·2 to 0·4 mm of the crystal surface was polished away electrolytically. It is probable that the tapping was sufficient to produce an elementary structure on the crystal. It then was so fine that Heidenreich and Shockley could not detect it, but sufficient to extinguish the Kikuchi lines. The reason that the Kikuchi lines reappeared after removing a surface layer would then be that the elementary structure was confined to that surface layer. In this connection, however, the layer thickness of 200 to 400 μ seems rather high.

§5. Considerations on the Spacing of the Elementary Lines

When we now try to understand the rather regular spacing of the elementary lines we find that the idea with which Orowan (1941) sought to explain the spacing of the slip *bands* can be applied with success here. Orowan argued that each dislocation due to its own stress field blocks all slip planes in its immediate neighbourhood against the passage of other dislocations. With the shear stress $\tau_{xy}=[A_e x(x^2-y^2)]/(x^2+y^2)^2$ around a dislocation situated at $x=y=0$ on the slip plane $y=0$ we immediately find that under an external resolved shear stress of τ any dislocation on a glide plane at a distance of less than $A_e/4\tau$ from a glide plane containing a fixed dislocation will be arrested near that fixed dislocation.

After studying the experimental evidence and some of the theoretical aspects of the behaviour of dislocations in greater detail the following picture of the processes involved in the formation of the elementary structure and of slip bands was developed :

The generation of dislocations from sources which possibly lie in the bulk of the material, or, according to § 4, may be situated at the surfaces is an easy process. The nature of the sources is unknown. The possibility exists that they are nothing but surface steps, perhaps created accidentally by one dislocation. As for the creation of any dislocation on the plane of the surface step, the step only has to be broadened but no new edges have to be formed, this should be an easier process than the creation of a dislocation on a different plane. Moreover there may be a certain notch effect aiding the generation of a dislocation on an already existing surface step.

The sources release loops of dislocations which will be closed if emitted from a Frank–Read source and which will penetrate into the metal from the surface if the source lies at the surface. The dislocation loops grow and more follow them from the sources until the first from each source meets an obstacle which might for instance be a precipitate, a mosaic block boundary, an internal stress field or only a row of dislocations emitted by another of the sources. It was indicated above and will be discussed later in greater detail that the nearest distance at which two

rows of dislocations can pass each other is about $A_e/4\tau$. Also around each row of dislocations released from one source there is a corridor within which no new source can start to act. This corridor again extends to a distance of about $A_e/4\tau$ from the slip plane on which the dislocations lie because the dislocations which would be emitted from a source within it could not pass the row of dislocations already present. If now the number of possible sources was very high then we should expect an average spacing between the elementary lines of about 1·5 times this limiting distance. If on the other hand the number of sources would be small then the number of elementary lines should be governed by their number, and the average spacing of the elementary lines should be appreciably bigger than 1·5 times the smallest observed distance between two elementary lines.

In column 6 of the table of § 2, $\bar{d}$, the average distance between the elementary lines for a number of specimens is listed, in column 7 the smallest observed distance, d_0, and in column 8 the ratio $\bar{d}/d_0$. As will be seen the great majority of the values for $\bar{d}/d_0$ lie between 1·3 and 1·7. This means that there must be a greater number of potential sources of dislocations than there are lines in the elementary structure. Furthermore, as should be expected from the present theory, the product $d_0 \times \tau$ (column 9), does not seem to depend on the shear stress. While $d_0 = A_e/4\tau$ renders $d_0 \times \tau = 440$ A × kg mm^2 when the values of G and σ are taken for Taylor dislocations in aluminium the experimental values for $d_0 \times \tau$ vary irregularly around $d_0 \times \tau = 270$ A × kg/mm^2.

Hence it appears that

(1) Dislocations are released from sources.

(2) The creation of dislocations is an easier process than their passage through the crystal.

(3) The number of potential sources is very high (namely, at least 10^9 cm^{-2}). There are more possible sources than become active and vastly more sources than slip bands.

These results have already been predicted in a previous paper (Kuhlmann (1951)).

§ 6. Considerations on the Formation of Slip Bands

It was first shown by Heidenreich and Shockley (1948) that a slip band on aluminium which under the light microscope looks like a single line in reality usually is a group of closely spaced lines. Our own experiments showed that the spacing of these lines is about the same as that of the elementary lines. Naturally such slip bands cannot be generated by a random growth of elementary lines. To understand their formation it is assumed that accidentally an elementary line becomes longer and stronger than its neighbours, or in other words, that one of the sources emits a particularly big number of dislocation loops. If now the foremost dislocation from this ' strong ' source meets a series of smaller loops of dislocations from another ' weaker ' source on a slip plane at a distance smaller than $d_0 = A_e/4\tau$ it will be held up and then extend

around this obstacle, somewhat in the manner proposed by Frank (1948), until a closed loop or a loop starting and ending at the surface is left behind and the dislocation as a whole travels on. The next dislocation loop from the strong source will suffer the same fate, but the loops left behind will form loop pairs with the two outermost loops from the weak source because the loops left behind on the one slip plane will have the opposite sign of those on the other slip plane throughout, and therefore any two loops on the two different planes, encircling the weak source, will attract each other. Thus two dislocation loops on the two different slip planes combine to form a strongly bound unit which we call a dislocation pair. When a third dislocation loop from the strong source is left behind there will be an exchange of partners so that now three dislocation pairs encircle the weak source and so on, until all the loops from the weak source have found a partner and we are left with a series of loop pairs around the weak source. The loop pairs are neutral, i.e. they suffer no net force from the external stress, and consequently the loops will contract and vanish due to their high self-energy. If the distance between the slip planes concerned is rather smaller than $A_e/4\tau$ the process will probably be somewhat different in so far as the pair formation will cease before all dislocations from the weaker source have found a partner, because pair formation becomes more difficult as the number of pairs increases. More dislocation loops from the strong source will then form around the weak source These loops are of the type which contracts under the external stress, and when their number is sufficient they will contract, driving all the other loops before them and vanish. Moreover, a series of small loops might already contract even under the influence of a few loop pairs, or, in extreme cases, even the tendency of the oncoming dislocations to remain as straight as possible because of their elastic energy might be sufficient to annihilate them.

In any case all small elementary lines around a strong line will be annihilated, and a corridor of about $A_e/4\tau$ width on either side of the strong line will be cleared of dislocations. In or near this corridor and probably near to the first strong source another source will now start to act because many of the elementary lines in its way which would otherwise have hindered the progress of its dislocations have been removed by the first strong source. The dislocations of this second source will thereby form a strong line in turn and open a way for a third line and so on.

We thus can understand not only why the slip lines assemble to form bands but also their rather uniform spacing.

APPENDIX

Some Considerations on the Interaction of Dislocations

In this paragraph the conditions under which dislocations in parallel slip planes can block each others motion will be investigated. We begin by considering the simple case of one dislocation in each of two planes and then proceed to consider more complicated cases.

The stresses around a positive edge dislocation, and parallel to the slip plane are given by

$$\tau_e = A_e \,.\, x(x^2-y^2)/(x^2+y^2)^2$$
$$= A_e \,.\, \sin 4\theta/4y \qquad \ldots\ldots\ldots \quad (1)$$

and that around a positive screw dislocation by

$$\tau_s = A_s \,.\, x/(x^2+y^2)$$
$$= A_s \,.\, \sin 2\theta/2y, \qquad \ldots\ldots\ldots \quad (2)$$

where A_e and A_s are as defined in § 3 and $\tan\theta = y/x$. The z-axis is thereby chosen along the dislocation axis and the x-axis in the slip plane of the dislocation.

The curves of τ_e and τ_s for a slip plane parallel to the one in which the dislocation lies (at $x=0$) are shown in fig. 5. It is seen that the maximum stresses opposing the passage of a dislocation are $A_e/4y$ and $A_s/2y$ for edge and screw dislocations respectively. Hence if the resolved applied shear stress is τ the minimum distances at which two dislocations still pass each other are

$$d = A_e/4\tau \qquad \ldots\ldots\ldots \quad (3)$$

for edge dislocations and

$$d_s = A_s/2\tau \qquad \ldots\ldots\ldots \quad (4)$$

Fig. 5

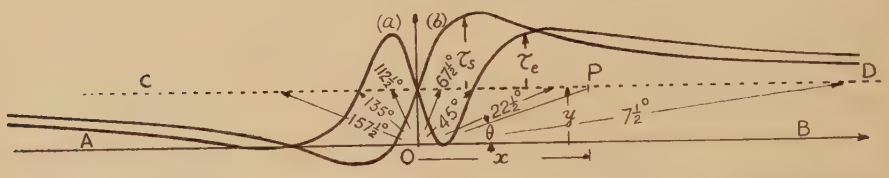

Curves of the stresses (versus θ or x) in a slip plane (I) due to a dislocation at 0 in slip plane AB.
Curve (a) : The stress τ_e due to an edge dislocation.
(b) : The stress τ_s due to a screw dislocation.

for screw dislocations. Two dislocations which block each others motion will be called a 'pair'. From (3) and (4) it follows that $d_s/d = 2\cdot(1-\sigma) = 1\cdot33$ for aluminium with $\sigma = 0\cdot33$.

The maximum opposing stresses occur at $\theta = 22\cdot5^\circ$ and $112\cdot5^\circ$ and $\theta = 67\cdot5^\circ$ and $157\cdot5^\circ$ for like and unlike edge dislocations respectively, and at $\theta = 45^\circ$ and $\theta = 135^\circ$ for like and unlike screw dislocations respectively.

From the foregoing it follows that, if two dislocations meet which are curved through at least 90° so that they are of screw type along certain portions of their whole lengths and of edge type along other portions they can only block each other provided the edge portions can do so. The reason is that once the edge portions have passed there will be at least

one crossing which easily moves towards the edge portions. Since unlike screw dislocations attract up to $\theta=90°$ it likewise follows that in a neutral pair, i.e. a pair containing two unlike dislocations the angle θ everywhere exceeds 90°.

The most common process during the growth of an elementary structure will be that a row of dislocations passes nearly midway between two rows already present.

To simplify the calculations we neglect the interaction of all more distant rows of dislocations and only consider two rows of edge dislocations between which a third row passes. Two different cases are examined, namely, that in which the dislocations in the two outer rows are of like sign (fig. 6 (*a*)) and that in which they are of unlike sign (fig. 6 (*b*)). We assume the rows not to contain too many dislocations,

Fig. 6

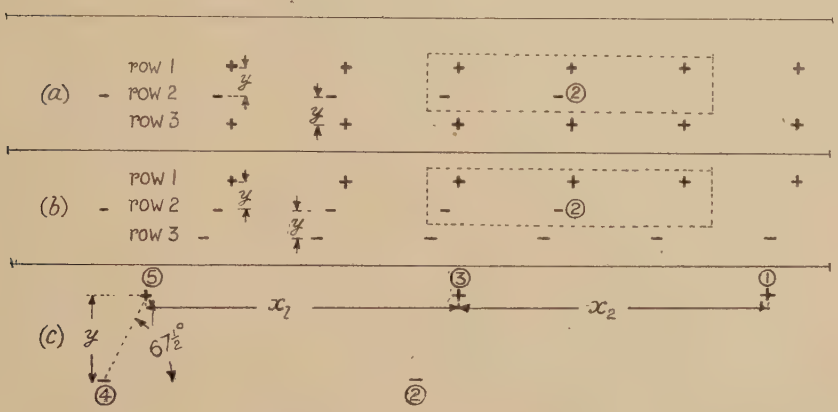

Configurations of dislocations showing a row of dislocations entering midway between two other rows. Positive and negative signs denote positive and negative dislocations respectively.

(*a*) : Outer rows of like sign.
(*b*) : Outer rows of unlike sign.
(*c*) : Configuration of the dislocations enclosed by dotted lines in fig. 6 (*a*) and 6 (*b*).

say up to 25 each. The dislocations in the outer rows shall be nearly evenly spaced and the rows as such shall be ' locked ', i.e. their dislocations cannot move as a whole. We consider now the position after the first few dislocations of the centre row have moved into the space between the outer rows. The problem is to find the external stress necessary to move the foremost dislocation (marked 2 in fig. 6) to the right. As a first step we neglect the influence of all dislocations outside the dotted lines (fig. 6 (*c*)). We assume the pair 4, 5 to be ' fixed ' and to have an inclination of 67·5°, which is the position of maximum repulsive stress between 4 and 5. We now have to find the stress for

which the inclination of the pair 2, 3 is 67·5°, i.e. the stress for which dislocation 2 will just start to pass dislocation 3. If we put $\cot 67{\cdot}5° = 0{\cdot}4$, $x_1/y = \alpha$ and $x_2/y = \beta$, where x_1 and x_2 are the distances between 1 and 3 and 3 and 5 respectively, the conditions for equilibrium of 1, 2 and 3 are :

$$\frac{1}{\alpha+\beta} - \frac{(\alpha+\beta+0{\cdot}4)[(\alpha+\beta+0{\cdot}4)^2-1]}{[(\alpha+\beta+0{\cdot}4)^2+1]^2} + \frac{1}{\beta} - \frac{(\beta+0{\cdot}4)[(\beta+0{\cdot}4)^2-1]}{[(\beta+0{\cdot}4)^2+1]^2} - \frac{\tau^y}{A_e} = 0,$$

$$\frac{1}{\alpha} - \frac{(\alpha-0{\cdot}4)[(\alpha-0{\cdot}4)^2-1]}{[(\alpha-0{\cdot}4)^2+1]^2} - \frac{1}{4} + \frac{(\beta+0{\cdot}4)[(\beta+0{\cdot}4)^2-1]}{[(\beta+0{\cdot}4)^2+1]^2} + \frac{\tau^y}{A_e} = 0,$$

$$\frac{1}{\alpha} - \frac{(\alpha+0{\cdot}4)[(\alpha+0{\cdot}4)^2-1]}{[(\alpha+0{\cdot}4)^2+1]^2} + \frac{1}{4} - \frac{1}{\beta} - \frac{\tau^y}{A_e} = 0.$$

By numerical calculation one finds that $\alpha = 4{\cdot}8(8)$, $\beta = 4{\cdot}3(6)$ and $\tau^y/A_e = 0{\cdot}053(5)$ is a solution of this set of equations. $\tau^y/A_e = 0{\cdot}053(5)$ renders $y = 0{\cdot}21\, A_e/4\tau = 0{\cdot}21d$, i.e. the smallest distance of y for which in the configuration considered 2 passes 3.

The much more simplified form of this problem in which dislocation 3 is regarded to be fixed and the influences of 4 and 5 are neglected gives the result $y = 0{\cdot}20d$. We may therefore conclude that this simpler model is a good approximation.

Next we estimate the effect which the presence of the dislocations outside the dotted lines in fig. 6 (*a*) and 6 (*b*) has and we find for both cases :

(1) The effect of the dislocation in row 3 nearest to dislocation 2 will be that of a stress to the left which at most can have the magnitude $A_e/4y$.

(2) Dislocation 2 will be attracted to the right by the dislocations of row 1 to the right of the dotted line.

(3) The effect of all the dislocation pairs formed by the dislocations of the upper two rows left from the dotted line is negligible.

(4) The effect of n dislocations left of dislocation 2 in row 3 will practically cancel that of n dislocations right from 2 in row 3.

(5) The effect of the remaining dislocations will depend on their exact configuration but will usually be small because they are far away from dislocation 2.

Depending on the exact number and configuration of the dislocations in the three rows we therefore have, under the conditions described, an extra force acting on dislocation 2. In the extreme case this force can drive dislocation 2 to the left with a magnitude of about $A_e/4y$ per atomic plane.

As was shown above the simple problem of the passage of dislocation 2 past 3 when 3 is regarded to be fixed and when the influences of all other dislocations except 1 are neglected is a good approximation to the problem of fig. 6 (*c*). Therefore the effect of the additional stress on dislocation 2 due to all dislocations outside the dotted line (fig. 6) was calculated using this model. The result is that for an extra stress of

$0{\cdot}1\,A_e/4y$, driving dislocation 2 to the left, the smallest distance at which 2 can pass 3 under the stress τ is $y=0{\cdot}27d$, and for the additional stress $A_e/4y$ which, as we saw, is about the greatest possible value we obtain $y=d$.

It can be seen easily that when dislocation 2 has moved for one interval to the right, dislocation 4 will not follow immediately because it is suffering an extra repulsion from 2. Therefore it follows that the 'vacancies' generated when the first dislocation moves on are not easily propagated and the foremost dislocations in row 2 will generally not occupy successive intervals, but there will be vacancies between them. This effect makes the passage of a row of dislocations between two other rows more difficult.

The result of the above considerations is that a row of Taylor dislocations entering midway between two rows already present, whose distance of separation is somewhat smaller than $2A_e/4\tau=2d$ will proceed for a few atomic distances. Then, as the number of dislocations before it in the two outer rows decreases and the number of those behind it increases, the progress of the row considered will become more difficult until it is stopped altogether. The centre row will be stopped the sooner the shorter it is and the smaller the distance between the two outer rows. If the distance between the two outer rows is bigger than about $2A_e/4\tau=2d$ the oncoming row will completely pass between them.

Acknowledgment

The authors would like to thank Professor G. Masing and Mr. A. Pfützenreuter for making available to them some of their results before publication. They also wish to thank the British Aluminium Company, who has supplied the high purity aluminium with which the experiments have been carried out.

This paper is published by permission of the South African Council for Scientific and Industrial Research.

References

Andrade, E. N. da C., 1945, *Nature, Lond.*, **156,** 113; 1949, *Ibid.*, **164,** 536.
Andrade, E. N. da C., Randall, R. F. Y., 1949, *Nature, Lond.*, **164,** 1127.
Andrade, E. N. da C., Randall, R. F. Y., Makin, M. J., 1950, *Proc. Phys. Soc.* B, **63,** 990.
Andrade, E. N. da C., Kennedy, A. J., 1951, *Proc. Phys. Soc.* B, **64,** 363.
Brown, A. F., 1949, *Nature, Lond.*, **163,** 961.
Brown, A. F., Honeycombe, R. W. K., 1951, *Phil. Mag.*, **42,** 1146.
Eshelby, J. D., Frank, F. C., Nabarro, F. R. N., 1951, *Phil. Mag.*, **42,** 351.
Frank, F. C., 1948, *The Strength of Solids.* (London: Physical Society), 46.
Frank, F. C., Read, W. T., 1950, *Phys. Rev.*, **79,** 722.
Harper, S., Cottrell, A. H., 1950, *Proc. Phys. Soc.* B, **63,** 331.
Heidenreich, R. D., Shockley, W., 1948, *The Strength of Solids.* (London: Physical Society), 57.
Hibbard, W. R., 1948, *Trans. A.I.M.E.*, **175,** 106.

Jacquet, P. A., 1945, *Rev. Mét.*, **42,** 133 ; 1949, *Compt. rend.*, **228,** 1439.
Kuhlmann, D., 1951, *Proc. Phys. Soc.* A, **64,** 140.
Leibfried, G., 1951, *Z. Physik*, **130,** 214.
Masing, G., Pfützenreuter, A., 1951, *Z. Metallkunde*, **42,** 361.
McLean, D. C., 1947, *J. Inst. Met.*, **74,** 95.
Menter, J. W., Hall, E. O., 1950, *Nature, Lond.*, **165,** 611.
Orowan, E., 1941, *Nature, Lond.*, **147,** 452.
Phillips, D. J., Thompson, N., 1950, *Proc. Phys. Soc.* B, **63,** 839.
Pickus, M. R., Parker, E. R., 1951, *Journal of Metals*, (Sept. 1951), *Trans. A.I.M.E.*, 792.
Roscoe, R., 1934, *Nature, Lond.*, **133,** 912 ; 1936, *Phil. Mag.*, **21,** 399.
Smekal, A., 1934, *Z. Physik*, **93,** 166.
Wilsdorf, H., Kuhlmann-Wilsdorf, D., 1951, *Naturwissenschaften*, **38,** 502 ; 1952, to be published.
Wu, T. L., Smoluchowski, R., 1949, *Phys. Rev.*, **75,** (2), 345.

LX. *The Formation of Immobile Dislocations during Slip*

By A. H. Cottrell
Department of Metallurgy, University of Birmingham*

[Received March 4, 1952]

Summary

Lomer has pointed out that certain dislocations on intersecting slip planes in the face centred cubic lattice can join to form new dislocations. It is now proposed that these new dislocations dissociate into groups of imperfect dislocations which cannot move because of the arrangement of their associated stacking faults. These immobile dislocations may be important in work hardening.

§1. Lomer's Reaction

In a recent note, Lomer (1951) has discussed the following dislocation reaction in the face centred cubic lattice. Two straight dislocations are parallel to $[1\bar{1}0]$. The first moves in a (111) plane and has a Burgers vector $\frac{1}{2}a[10\bar{1}]$ (i.e. causes a slip displacement with components $\frac{1}{2}a$, 0, $-\frac{1}{2}a$, along the crystal axes, a being the lattice constant). The second moves in $(11\bar{1})$ and has a Burgers vector $\frac{1}{2}a[011]$. They both glide towards the $[1\bar{1}0]$ line of intersection of their planes, and at this line they meet and react to form a new dislocation,

$$\frac{a}{2}[10\bar{1}]+\frac{a}{2}[011]\rightarrow\frac{a}{2}[110], \quad . \ . \ . \ . \ . \ . \quad (1)$$

thereby lowering the elastic energy of the crystal.

Lomer emphasizes that this product dislocation cannot glide in an ordinary (octahedral) slip plane. It is an edge dislocation and is restricted to glide in the (001) plane that contains its Burgers vector and its line, [110] and $[1\bar{1}0]$ respectively. This is not a common slip plane and the dislocation may be unable to move freely in it. Lomer, in fact, describes the dislocation as ' sessile '. However, it is not sessile in the sense originally used by Frank (1949 a), which refers to an imperfect dislocation (i.e. one with a Burgers vector that is not a lattice vector) that cannot glide because its Burgers vector is not in the plane of its associated stacking fault. Moreover, aluminium is believed to slip on (001) at high temperatures (Schmid and Boas (1935), Lacombe and Beaujard (1947)).

§2. A Second Reaction

Lomer's product dislocation can become very immobile, however, if it splits in the following way:

$$\frac{a}{2}[110]\rightarrow\frac{a}{6}[11\bar{2}]+\frac{a}{6}[112]+\frac{a}{6}[110]. \quad . \ . \ . \ . \quad (2)$$

* Communicated by the Author.

Frank (1949 b) has a simple rule, based on the sum of the squares of the Burgers vector lengths, for deciding whether the strain energy is lowered by a reaction; it is lowered when the sum is larger for the reacting dislocations than for the product ones. In this new reaction the sum is $\frac{a^2}{4}(1^2+1^2+0^2)=\frac{a^2}{2}$ for the reacting dislocation and

$$\frac{a^2}{36}[2(1^2+1^2+2^2)+(1^2+1^2+0^2)]=\frac{14a^2}{36}$$

for the product dislocations.

These product dislocations are imperfect and form the boundaries of stacking faults, in the planes of which they are constrained to move. The $\frac{1}{6}a[11\bar{2}]$ dislocation is one of Heidenreich and Shockley's half-dislocations (1948) and can glide in the (111) plane containing the $[1\bar{1}0]$ line of the reaction. By Frank's rule, it is repelled from the reaction site and moves back into the (111) plane to a position where the elastic repulsion on it is balanced by the surface tension of its stacking fault. This fault is a strip in the (111) plane bounded by two $[1\bar{1}0]$ lines, the line of the reaction and the line of the dislocation. The $\frac{1}{6}a[112]$ dislocation behaves in the same way in the $(11\bar{1})$ plane. The line of the reaction, where the two stacking faults join, contains the third dislocation, $\frac{1}{6}a[110]$, which can only exist at the junction of two faults.

Looking down the line of reaction the dislocations are seen as points at the corners of an isosceles triangle, two sides of which, (111) and $(11\bar{1})$, are the traces of the stacking faults. The distance between these dislocations depends on the energy of faulting and should be about the same as the distance between Heidenreich and Shockley's half-dislocations ($\simeq$5 atoms). This triangular group of dislocations cannot glide. Even for it to acquire the mobility of Lomer's dislocation one would first have to squeeze the three imperfect dislocations together, which requires very large stresses.

§3. An Alternative Reaction Sequence

If Lomer's two original dislocations are in fact pairs of half-dislocations, formed by the Heidenreich and Shockley reactions,

$$\frac{a}{2}[10\bar{1}]\rightarrow\frac{a}{6}[11\bar{2}]+\frac{a}{6}[2\bar{1}\bar{1}],$$

and

$$\frac{a}{2}[011]\rightarrow\frac{a}{6}[112]+\frac{a}{6}[\bar{1}21], \quad . \quad . \quad . \quad . \quad . \quad . \quad . \quad (3)$$

the products of reaction 2 can be obtained directly, without the aid of Lomer's reaction. Thus, when the second dislocations of each pair meet and coalesce at the line of reaction, we have

$$\frac{a}{6}[11\bar{2}]+\frac{a}{6}[2\bar{1}\bar{1}]+\frac{a}{6}[112]+\frac{a}{6}[\bar{1}21]\rightarrow\frac{a}{6}[11\bar{2}]+\frac{a}{6}[112]+\frac{a}{6}[110], \quad . \quad (4)$$

which gives the same products as reaction 2. Other combinations of half-dislocations on intersecting slip planes are possible, but most of them do not lower the elastic energy so much as this one.

§4. Work Hardening

Lomer has remarked that reactions amongst dislocations in intersecting slip planes may be important in the work hardening of face centred cubic crystals since the immobile product dislocations may obstruct slip dislocations. A feature of some worked crystals with this lattice is the *deformation band*, which is related to the work hardening process (Mott 1951). It is attractive to suppose that some of the slip dislocations already piled up against deformation bands become locked in position through reacting with other dislocations on intersecting planes, and cannot then be removed except by annealing at temperatures in the recrystallization range. It is less feasible, however, that deformation bands are nucleated by, and grow around, immobile dislocations created by such reactions; whereas deformation bands cross the active slip planes along lines at 90° to the active slip direction (Cahn 1951, Honeycombe 1951), the immobile dislocations lie along lines at 60° to it.

Acknowledgment

I am grateful to Dr. B. A. Bilby for stimulating discussions on the question of dislocation reactions.

References

Cahn, R. W., 1951, *J. Inst. Met.*, **79,** 129.
Frank, F. C., 1949 a, *Proc. Phys. Soc.* A, **62,** 202; 1949 b, *Physica*, **15,** 131.
Heidenreich, R. D., and Shockley, W., 1948, *Report on Strength of Solids*, (London: Physical Society), 57.
Honeycombe, R. W. K., 1951, *J. Inst. Met.*, **80,** 45.
Lacombe, P., and Beaujard, L., 1947, *J. Inst. Met.*, **74,** 1.
Lomer, W. M., 1951, *Phil. Mag.*, **42,** 1327.
Mott, N. F., 1951, *Proc. Phys. Soc.* B, **64,** 729.
Schmid E., and Boas, W., 1935, *Kristallplastizität*, (Verlag Julius Springer: Berlin).

LXI. *The Determination of the Internal Conversion Coefficient and Branching Ratio for the* 80 kev *γ-ray Emitted by* I^{131} *by Means of X-ray–γ-ray Coincidence Measurements*

By Patrick E. Cavanagh
Atomic Energy Research Establishment, Harwell*

[Received March 20, 1952]

Summary

The investigation of primary and secondary electron spectra as a means of determining conversion coefficients becomes difficult at low γ-ray energies. A method relying on the measurement of the x-rays emitted as a result of internal conversion does not suffer from this disadvantage. Such a method has been applied to the 80 kev γ-ray emitted by I^{131}. This is believed to be in cascade with a 283 kev γ-ray, the two forming a branch parallel to the most intense γ-ray of 363 kev. X-rays arising from the conversion of the 80 kev γ-ray should be in coincidence with 283 kev γ-rays. Such coincidences were found, and the proportion of such x-rays in the total number measured. The relative number of these x-rays and unconverted 80 kev quanta gives $1{\cdot}83 \pm 0{\cdot}16$ as the internal conversion coefficient, which places the 80 kev transition as magnetic dipole. It occurs in $(4{\cdot}3 \pm 0{\cdot}6)\%$ of the total number of disintegrations. Evidence for x-rays in coincidence with 638 kev γ-rays was also found. It is possible that these arise from the conversion of a γ-ray emitted in a transition between levels at 638 and 720 kev, of occurrence $0{\cdot}3\%$ per disintegration.

§1. Introduction

The direct determination of the conversion coefficient of the 80 kev γ-ray emitted by I^{131}, by measurement of the number of internal conversion electrons in relation to the number of primary β-particles, is difficult because of the low conversion electron energy, ~50 kev. Similarly it is difficult to investigate the branching ratio by measurements of the secondary electron spectrum. A method which relies on measurements of the x-rays emitted does not suffer from this disadvantage. X-rays from I^{131} arise solely from internal conversion of the γ-rays; there is no possibility of *K*-capture, since I^{131} is itself formed by β-decay from Te^{131}. By far the most prominent lines in the primary β-spectrum are the *K*-conversion lines of the 80 and 363 kev γ-rays. Now the 363 kev γ-ray is in cascade with no other γ-ray, hence coincidences between γ-rays and x-rays will occur principally between 283 kev γ-rays and x-rays arising from the conversion of the 80 kev γ-ray, these two γ-rays forming a cascade branch in parallel with the main γ-ray of 363 kev. Measurements of these coincidences should provide further evidence for the latter.

* Communicated by the Author.

§2. Coincidence Measurements

An anthracene-activated naphthalene crystal $1\frac{1}{2}$ in. thick was used as a γ-ray counter. The x-ray counter consisted of a 140 mg/cm^2 aluminium cylinder with a 0·01 cm diameter tungsten wire anode, and was filled with a mixture of xenon and 10% carbon dioxide to a total pressure of 44 cm mercury. This counter was operated in the high proportional region in

Fig. 1

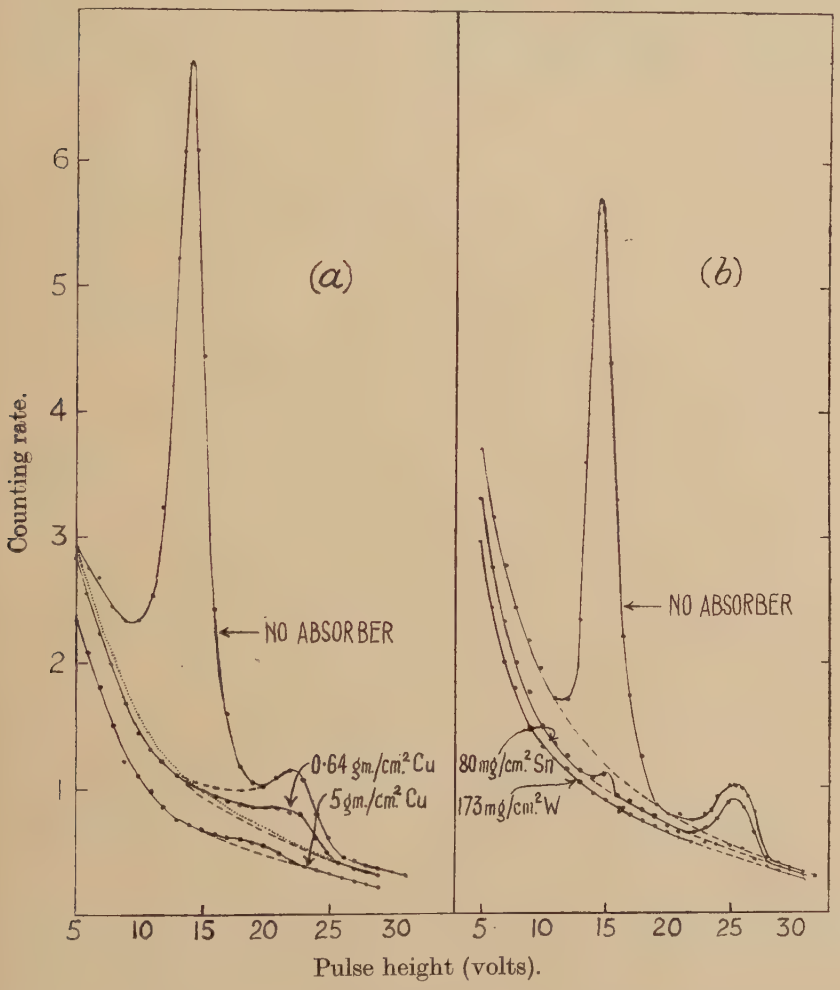

the manner described by Kirkwood *et al.* (1948), and worked into a preamplifier and 2 Mc/s amplifier with an overall gain of about 10 000. The pulse spectrum was analysed by a single channel pulse analyser of design similar to that described by Eppstein (1951) ; a typical spectrum obtained in the uncollimated conditions of the coincidence measurements is shown in fig. 1 (*a*).

The two counters were set up close together ; 5 g/cm^2 lead covered with copper was placed between them to eliminate cross-scattering. X-ray counter and source were covered with sufficient perspex to ensure that no primary β-particles or Compton electrons from the latter could be recorded.

A block diagram of the electronic apparatus is shown in fig. 2. The outputs from the amplifiers in either channel were led through discriminators into a coincidence unit. A resolving time of 0·4 μsec was found sufficient to ensure no coincidence losses. A second output from the amplifier following the x-ray counter passed to the single channel pulse analyser, the output of which was gated by the coincidences.

Fig. 2

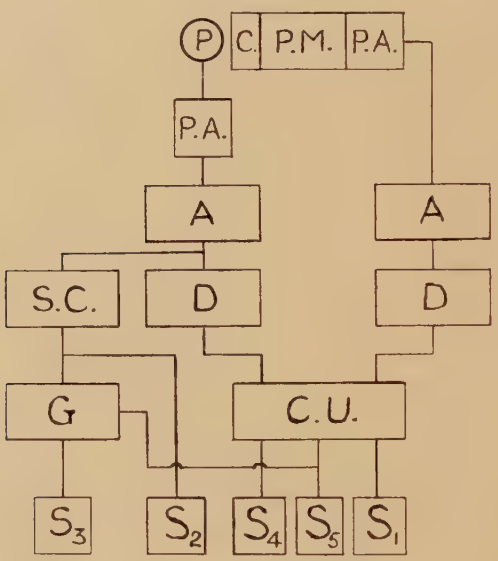

Block diagram of electronics.

C=crystal, P.M.=photomultiplier, S=scaler, P.A.=preamplifier, A=amplifier, G=gate unit, S.C.=single channel pulse analyser, C.U.=coincidence unit, D=discriminator, P=proportional counter.

The pulse analyser was set on the x-ray peak and the gated output measured as a function of the γ-ray discriminator level. Cosmic coincidences, and also those arising from the background on which the x-ray peak stood, were corrected for. The ratio of the coincidence rate to the x-ray counting rate is shown plotted in fig. 3 together with the corresponding bias curve of the single γ-ray rate. Initially it falls off faster than the single rate, as would be expected if the x-rays are in coincidence with 283 kev γ-rays. After a certain point, however, the bias curve of coincidences becomes much less steep and similar to the hard component of the single rate. The presence of coincidences between

x-rays and what we shall identify as probably the 638 kev γ-rays was at the time unexpected, but they may correspond to the coincidences between these γ-rays and low energy γ-rays found by Bell *et al.* (1951).

The bias curve of the single γ-ray rate was analysed into two components by means of lead absorption measurements in good geometry as described previously (Cavanagh 1951). The hard coincidence component was

Fig. 3

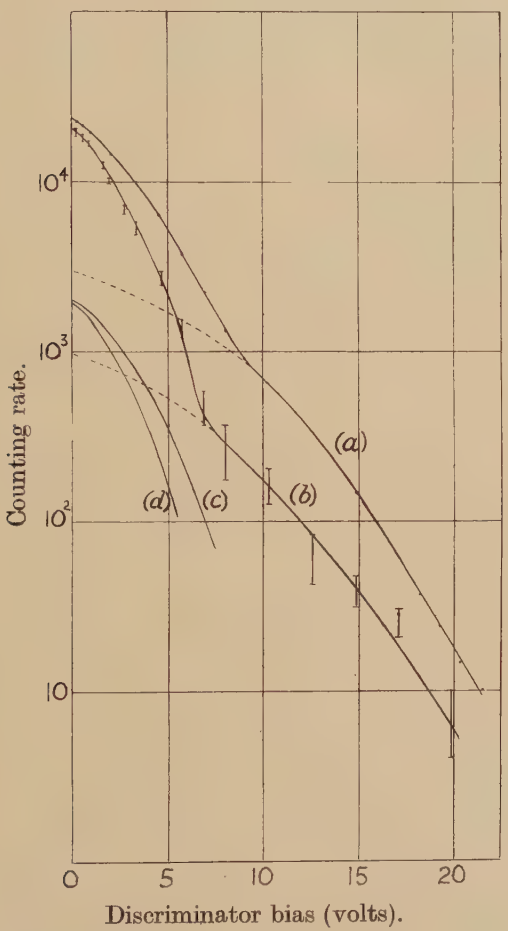

(*a*) Single γ-rate.
(*b*) Coincidence x-ray–γ-rate.
(*c*), (*d*) Soft component of (*a*), (*b*) respectively $\times 1/10$.

extrapolated to zero bias and subtracted, giving the soft component bias curve alone. For all four curves the values of bias were determined for which the initial counting rates were reduced by successive powers of two. From table 1, in which these values are set out, it is evident that all the curves are strictly similar. The average of the ratios of corresponding bias

values to those for the 363 kev γ-ray is plotted in fig. 4 against the γ-ray energy relative to 363 kev. The points lie on a straight line, though this

Table 1. Values of Bias Required to Reduce the Initial Counting Rate by Successive Powers of Two

$(\frac{1}{2})^n$ $n=$	1	2	3	4	5	6	average ratio
363 kev γ-ray	2·6	4·4	5·6	6·7	7·6		
High energy component of single rate	6·0	9·7	12·3	14·4	16·1	18·1	
Ratio to 363 kev γ-ray	2·31	2·20	2·20	2·15	2·12		2·20
283 kev γ-ray	2·1	3·45	4·55	5·40	5·90		
Ratio of 283 to 363 kev γ-ray	0·81	0·78	0·81	0·81	0·78		0·80
High energy component of coincidence rate	5·6	8·8	11·4	13·6	15·7	17·7	
Ratio to 363 kev γ-ray	2·15	2·00	2·04	2·03	2·07		2·06

Fig. 4

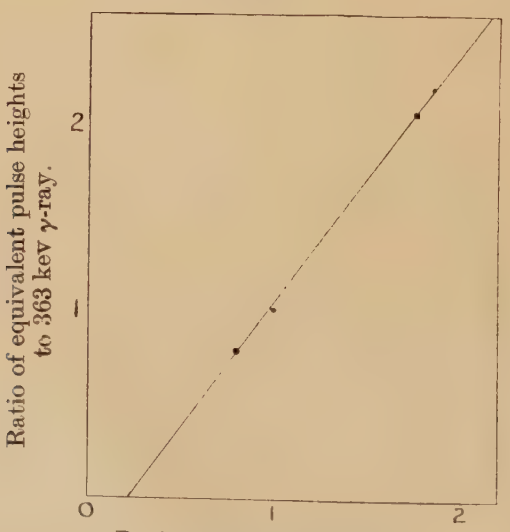

Pulse size ∨ γ-ray energy characteristic for naphthalene+1% anthracene.

does not pass through the origin. If we define the pulse height due to a γ-ray of particular energy as being that value of bias for which the initial counting rate is diminished by a certain ratio, the foregoing results may be expressed by the equation,

$$\text{Pulse height} \propto \gamma\text{-ray energy} - 45 \text{ kev.}$$

This is exactly parallel with the case for electrons.

The value of the energy of the hard coincidence component may be read off from fig. 4 and is 640 kev ; so the γ-ray involved is probably the already known one of 638 kev. From the small coincidence rate however it is evident that the γ-ray, the conversion of which gives rise to the coincident X-rays, is not in simple cascade with the relatively abundant ($\sim$8%)

Fig. 5

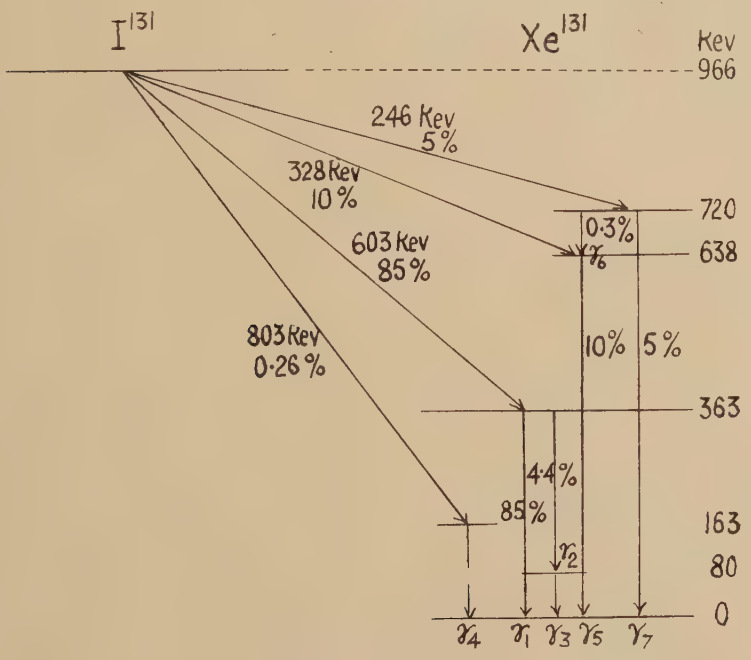

Decay scheme for I^{131}.

638 kev γ-ray, but forms only a weak cascade branch. Assuming that it corresponds to the γ-ray of about 80 kev found to be in coincidence with the 638 kev γ-ray by Bell (1951), then presumably it arises from an infrequent transition between the 720 and 638 kev levels.

§3. Analysis of X-ray—γ-ray Coincidence Measurements

In fig. 5 the 363, 283, 80, 163, 638 and 720 kev γ-rays are respectively labelled γ_1, γ_2, γ_3, γ_4, γ_5, γ_7, and the transition between the 638 and 720 kev levels γ_6. Let the branching ratios for γ_1 etc. be respectively b_1, $b_2=b_3$, b_4, b_5, b_6, b_7, where $b_1+b_2+b_4+b_5+b_7=1$, and the internal K

conversion coefficients *be* α_1, etc. Let the total efficiencies of detection of the γ-rays by the scintillation counter be ϵ_1 etc., and for the x-ray counter, ϵ_1^x, etc. Let the x-ray efficiency of the xenon counter be ϵ_x, and the fluorescent yield of xenon x-rays be f. Then the γ-ray and x-ray counting rates are respectively

$N_\gamma = N\Sigma b_i(1-\alpha_i)\epsilon_i$, $N_x = Nf\epsilon_x \Sigma b_i\alpha_i + N_\gamma{}^x$, where $N_\gamma{}^x = N\Sigma b_i(1-\alpha_i)\epsilon_i{}^x$.

The x-ray–γ-ray coincidence rate, neglecting terms of less than 1% of the total, is $G_{\gamma x} = Nf\epsilon_x[b_2(1-\alpha_2)\alpha_3\epsilon_2 + b_6(1-\alpha_5)\alpha_6\epsilon_5]$.

The two terms may be separated by means of a bias curve

$$(G_{\gamma x})_2 = Nf\epsilon_x\epsilon_2 b_2(1-\alpha_2)\alpha_3,\ (G_{\gamma x})_6 = Nf\epsilon_x\epsilon_5 b_6(1-\alpha_5)\alpha_6 .$$

The magnitude of the background below the peak in the x-ray spectrum was found by an absorption method. Copper absorbers were placed between source and counter in the actual geometry used for the coincidence measurements, and the pulse spectrum measured for each value of absorber thickness. This is shown in fig. 1 (*a*). At large thicknesses the absorption curves became characteristic of a γ-ray of energy about 360 kev. Extrapolation of these exponential portions back to zero thickness then gave the pulse distribution for the hard background below the peak. The counting rate due to x-rays alone is

$$N_x - N_\gamma{}^x = Nf\epsilon_x \Sigma b_i\alpha_i .$$

The ratio of the number of x-rays arising from conversion of the 80 kev γ-ray, γ_3, to the total number of x-rays emitted is

$$R = \frac{b_3\alpha_3}{\sum_i^7 b_i\alpha_i} = \frac{(G_{\gamma x})_2}{(N_x - N_\gamma{}^x)} \frac{N}{N_\gamma} \frac{\sum_i^7 b_i(1-\alpha_i)\epsilon_i}{\epsilon_2} \frac{1}{1-\alpha_2} .$$

A β–γ coincidence measurement was made on the source using the same γ-ray counter, and with sufficient absorber over the β-counter to exclude the low energy β-spectrum. The bias curve of $(G_{\gamma\beta}/N_\gamma N_\beta)$, corrected for backgrounds, was determined. Under these circumstances, if we neglect the branch to the isomeric level, ~1%,

$N_\beta = N(b_1+b_2)\epsilon_\beta$, where ϵ_β is the detection efficiency for β-rays.

$$G_{\gamma\beta} = N\epsilon_\beta \sum_i^3 b_i(1-\alpha_i)\epsilon_i, \text{ and } \frac{G_{\gamma\beta}}{N_\gamma N_\beta} = \frac{\sum_i^3 b_i(1-\alpha_i)\epsilon_i}{\sum_i^7 b_i(1-\alpha_i)\epsilon_i} \frac{1}{N(b_1+b_2)} .$$

Now the third term in the sum of the numerator, due to the 80 kev γ-ray, is negligibly small under the conditions of the experiment. The second term, due to the 283 kev γ-ray, is small compared with the first, and we may put $(1-\alpha_2)\epsilon_2 = (1-\alpha_1)\epsilon_1$ in it without appreciable error in the sum. Making these approximations and substituting in the expression for R we obtain

$$R = \frac{(1-\alpha_1)}{(1-\alpha_2)} \frac{\epsilon_1}{\epsilon_2} \frac{(G_{\gamma x})_2}{N_\gamma(N_x - N_\gamma{}^x)} \Big/ \frac{G_{\gamma\beta}}{N_\gamma N_\beta} .$$

The ratio ϵ_1/ϵ_2 at zero bias is given by the ratio of the Compton cross-sections, including a correction for finite absorption within the crystal. By making use of the similarity property of the bias curves for γ-rays of different energies already found, $(G_{\gamma x})_2/N_\gamma(N_x - N_\gamma{}^x)$ and $G_{\gamma\beta}/N_\gamma N_\beta$ may be compared at points for nominally equal ϵ_1/ϵ_2. The average value of R obtained in this way is $0{\cdot}58 \pm 0{\cdot}03$.

§4. The Determination of the K-Conversion Coefficient and the Branching Ratio for the 80 kev γ-ray

If the relative number of K x-ray and 80 kev γ-quanta can be measured, then knowledge of the value of R will enable us to evaluate the conversion coefficient, except for a small uncertainty due to the low intensity γ-ray in coincidence with the 638 kev γ-ray. Initially we shall ignore this and consider it later.

If the intrinsic efficiencies of the xenon counter are E_x and $E_3{}^x$ for K x-rays and 80 kev γ-rays, the corresponding absorptions under the conditions of the experiment a_x and a_3, and the counting rates A_x and A_3, then

$$\frac{A_3}{A_x} = \frac{E_3{}^x}{E_x}\frac{a_3}{a_x}\frac{(1-\alpha_3)}{\alpha_3}\frac{R}{f}.$$

The K x-ray is absorbed in the xenon gas filling by conversion in the L and M shells, but a single peak results in the pulse spectrum because the resolution is not sufficient to separate the M peak. The 80 kev γ-rays are however externally converted in the K, L and M levels. The smallest amount of energy is released in the counter when the γ-ray is converted in the K-shell and a K x-ray is emitted and escapes. In some cases an Auger electron is emitted instead and the energy released is increased by the difference in the binding energies of the K and L shells. It was the lowest energy peak for the 80 kev γ-ray which was actually measured, so that

$$E_3{}^x = (\tau_3 - \tau_3{}^L)f$$

where τ_3 and $\tau_3{}^L$ represent the total and the L-shell photoelectric absorption in xenon, and f as before, is the fluorescent yield. The value of $\tau_3{}^L/\tau_3$ is somewhat uncertain, but in the region from the K-absorption edge up to high energies it differs only slightly from 18%. From the above two expressions we obtain a value for the conversion coefficient

$$\frac{\alpha_3}{1-\alpha_3} = 0{\cdot}82\,\frac{\tau_3}{E_x}\,R\left(\frac{A_x}{A_3}\frac{a_3}{a_x}\right).$$

It is interesting to note that because the counter filling was chosen to be of the same element as emitted the x-rays and γ-rays, viz. xenon, the fluorescent yield has cancelled out in the expression for $(\alpha_3/1-\alpha_3)$.

We must now consider the effect of the γ-ray, x-rays from the conversion of which are in coincidence with 638 kev γ-rays. These coincidences, on making a correction for the different detection efficiencies for the 283 and 638 kev γ-rays, amount to about 7% of those due to x-rays and 283 kev γ-rays. Now it appears that the 638 and 720 kev γ-rays result

from electric quadrupole transitions,* hence these two levels have the same parity. If the γ-ray in question, γ_6, results from a transition between these levels it must be magnetic dipole or electric quadrupole. From the measurements reported here the 80 kev γ_3 is a magnetic dipole transition. In this region the ratio of the conversion coefficients for electric quadrupole and magnetic dipole transitions is about two, and a simple calculation shows that for an electric quadrupole transition γ_6 makes only a 2–3% contribution to the 80 kev peak. Careful measurements by Thulin (1951) on the energies of the 638 and 720 kev γ-rays give an energy difference of 85·7 kev. A γ-ray of this energy would be partially resolved from the 80·2 kev γ_3 by the xenon counter. No evidence for its presence was found, so its contribution to the 80 kev peak will be ignored.

The actual measurements of the ratio of the counting rates due to K x-rays and 80 kev γ-rays was made with a large source in a geometry well collimated with brass bricks. The source was evaporated from solution onto 7 mg/cm^2 Al and sealed in precisely the same way as those used for coincidence measurements. The actual experiment was performed at the same time after sealing (one week) as the latter to ensure that the same proportion of the 12 day xenon isomer was present. The pulse spectrum was examined with a four channel pulse analyser, type 1074A, a considerable improvement in resolution resulting from collimation, as can be seen in fig. 1 (*b*). Also shown are spectra taken with an 80 mg/cm^2 tin absorber (critical absorber for xenon K x-rays) and a tungsten absorber. The effective thickness of the counter wall was found by placing a second x-ray counter behind the first and determining the height of the x-ray peak with and without the first counter interposed.

The values of all absorption coefficients were obtained either directly or by interpolation from tables given by Compton and Allison (1947) based on the experiments of S. J. M. Allen. The value obtained for the ratio of the counting rates due to x-rays and 80 kev γ-rays, corrected for absorption, is $(A_x a_3/A_3 a_x)=9{\cdot}4$. This gives $(\alpha_3/1-\alpha_3)=1{\cdot}83\pm0{\cdot}16$, or $\alpha_3=0{\cdot}65\pm0{\cdot}03$, where the limits of uncertainty do not include possible errors in the value of τ_3/τ_x. The value of $(\alpha_3/1-\alpha_3)$ obtained falls close to the curve for magnetic dipole radiation obtained by extrapolation of the calculated results of Rose *et al.* (1949).

The ratio of the number of x-rays arising from the conversion of the 80 kev γ-ray and the total number of x-rays is $R=b_3\alpha_3/\sum_i^7 b_i\alpha_i$. Now *$b_1\alpha_1=1{\cdot}48\%$, $b_2\alpha_2+b_5\alpha_5+b_7\alpha_7\doteq 0{\cdot}15 b_1\alpha_1$, $b_6\alpha_6=0{\cdot}07 b_3\alpha_3$, and $b_4\alpha_4$ is determined by the proportion of the 12 day isomer present at the time of the measurement. If the shape of the 810 kev β-spectrum leading to the isomeric state is of the ' α ' form as suggested by Bergstrom (1950), then a measurement in this laboratory of the high energy β-spectrum gives a value for the branching ratio b_4 of 0·26%. This is consistent with

* denotes unpublished measurements from this laboratory.

measurements made of the ratio of the K x-ray and 80 kev peaks in the xenon counter over a period of a fortnight, but is in disagreement with the value obtained by Emery (1951).

Thus $\alpha_4 \sim 1$, $b_4 = 0{\cdot}26\%$, $(b_4\alpha_4)$ 7 days $= 0{\cdot}13\%$.

Substituting in the expression for R

$$b_3\alpha_3 = (2{\cdot}8 \pm 0{\cdot}4)\%$$

and

$$b_3 = (4{\cdot}3 \pm 0{\cdot}6)\%.$$

The ratio of the internal K conversion line heights of the 80 and 363 kev γ-rays is

$$\frac{b_3\alpha_3}{b_1\alpha_1} = (1{\cdot}9 \pm 0{\cdot}4)\%.$$

The value obtained for b_3, the branching ratio for the cascade 283 and 80 kev γ-rays, is in agreement with the spectrometer *measurements of $5{\cdot}8 \pm 2\%$ obtained from a consideration of the photoelectron spectrum.

The number of unconverted γ_3 (80 kev) quanta per disintegration is

$$b_3(1-\alpha_3) = (1{\cdot}5 \pm 0{\cdot}3)\%.$$

This is somewhat smaller than the value of $2{\cdot}6\%$ found by Emery (1951) by absorption measurements.

If the γ-ray in coincidence with the 638 kev γ-ray does arise in a magnetic dipole transition between the 638 and 720 kev levels its branching ratio is $b_6 = 0{\cdot}3\%$.

§ 5. Conclusions

The measurement of coincidences between γ-rays and xenon K x-rays has shown that the latter are in coincidence with 283 kev γ-rays. This provides strong evidence for the 80 and 283 kev γ-rays forming a cascade chain in parallel with the 363 kev γ-ray. There is, however, evidence for a small number of coincidences between x-rays and 638 kev γ-rays, possibly corresponding to those found between the latter and γ-rays of about 80 kev energy by Bell *et al.* (1951). However the number of coincidences makes it quite evident that only a small proportion of the 638 kev γ-rays are in cascade with other γ-rays. From this it follows that the γ-rays in coincidence with the 283 and 638 kev γ-rays cannot arise in the same transition. It is possible that the latter actually arise in a transition between the 638 and 720 kev levels.

The coincidence measurements also give a value for the proportion of x-rays in coincidence with γ-rays. A measurement of the relative number of x-rays and unconverted 80 kev quanta, using a xenon proportional counter, then made it possible to obtain a value for the internal conversion coefficient of the 80 kev γ-ray in coincidence with 283 kev γ-rays of $1{\cdot}83 \pm 0{\cdot}16$, which is consistent with a magnetic dipole transition.

A value for the branching ratio of the 80–283 kev transition is obtained of $4{\cdot}3 \pm 0{\cdot}6\%$. Also the ratio of the internal conversion line heights due

to the 80 and 363 kev γ-rays is $1{\cdot}9 \pm 0{\cdot}4$. The number of unconverted 80 kev quanta per disintegration is $(1{\cdot}5 \pm 0{\cdot}3)\%$, compared with 2·6% found by Emery (1951).

It is believed that x-ray measurements will provide a powerful method of investigating the conversion coefficients of low energy γ-rays.

Acknowledgments

Thanks are due to Mr. W. H. Taylor for many of the routine observations and calculations associated with this work, which was done at A.E.R.E. Harwell. Sources of I^{131} were supplied by the Isotope Division. Acknowledgment is made to the Director for permission to publish.

References

Bell, P. R., Cassidy, J. M., Kelley, G. G., 1951, *Phys. Rev.*, **82,** 103.
Bergstrom, I., 1950, *Phys. Rev.*, **80,** 114.
Cavanagh, P. E., 1952, *Phil. Mag.*, **43,** 221.
Compton, A. H. and Allison, S. K., 1947, *X-Rays in Theory and Experiment* (D. Van. Nostrand Co.)
Emery, E. W., 1951, *Phys. Rev.*, **83,** 679.
Eppstein, J. S., 1951, *Journ. Sci. Instrum.*, **28,** 41.
Kirkwood, D. H. W. *et al.*, 1948, *Phys. Rev.*, **74,** 497.
Rose, M. E. *et al.*, 1949, *Phys. Rev.*, **76,** 1883.
Thulin, S., 1951, *Phys. Rev.*, **83,** 860.

LXII. *A Source of Plane-polarized Gamma-rays of Variable Energy above 5·5 MeV*

By D. H. Wilkinson
Cavendish Laboratory, Cambridge*

[Received February 25, 1952]

Abstract

The reaction $^2H(p\gamma)^3He$ should constitute a source of plane-polarized gamma-rays; the reaction is one of direct radiative capture and spin-orbit coupling is not strong enough to induce changes in the z component of the intrinsic spins of the interacting particles. The gamma-ray energy may be varied from 5·5 MeV upwards by changing the energy of the bombarding protons. The polarization has been demonstrated by using the gamma-rays to disintegrate deuterons contained in a photographic plate; the photoprotons are emitted preferentially along the line of the electric vector.

§1. Introduction

When protons of about 1 MeV are captured by deuterons, gamma-rays of about 6 MeV are emitted in radiative transitions to the ground state of ^3He. The reaction is a very feeble one but the energy of the gamma-rays has been measured; it has been found that they are emitted according to a rather pure $\sin^2\theta$ law—θ is their angle of emission relative to the proton beam (Fowler, Lauritsen and Tollestrup 1949). The purity of the $\sin^2\theta$ distribution suggests strongly that $l=1$ protons are responsible for the reaction and that the radiation is electric dipole radiation. Furthermore we must suppose that this reaction does not proceed via a well-defined compound nucleus, for in this case owing to the half-integral intrinsic spin we should have to admit of radiative transitions in which $\Delta J_z=\pm 1$, characterized by a distribution proportional to $(1+\cos^2\theta)$, as well as those with $\Delta J_z=0$ which give a $\sin^2\theta$ distribution. It is probable that we are dealing with a direct radiative transition in which only $\Delta J_z=0$ appears in the absence of sufficiently strong spin-orbit coupling to induce transitions with $\Delta J_z=\pm 1$. This belief is strengthened by the fact that the observed cross section for this process is in rough agreement with that calculated by Verde (1950 a, b) for such a direct radiative transition and by Burhop and Massey (1948) for the closely-similar reaction $^2H(n\gamma)^3H$. Now the radiation field of an electric dipole transition with $\Delta J_z=0$ is everywhere plane-polarized, the electric vector lying in the plane containing the direction of propagation of the quantum and the axis of the dipole—in this case the direction of the incoming

* Communicated by the Author.

proton. The reaction $^2H(p\gamma)^3He$ should therefore constitute a source of plane-polarized gamma-rays of variable energy from the proton binding energy of 5·5 MeV upwards ; as far as is known it is unique in this respect.* In view of the interest for the study of electromagnetic interactions of having available a source of plane-polarized gamma-rays, the polarization has been verified directly using the photodisintegration of the deuteron.

§2. Experimental Method

The photodisintegration of the deuteron at gamma-ray energies of more than a few hundred kilovolts above the threshold proceeds almost entirely by electric dipole absorption. This is known from the good accord with theory of the total cross section (Carver and Wilkinson 1951) and the angular distribution of the photoprotons relative to the *direction of propagation* of the gamma-rays (e.g. Hough 1950). We may then have confidence in the prediction of theory that the angular distribution of the photo-protons relative to the *electric vector* of the gamma-rays is proportional to $\cos^2\chi$ where χ is the angle of emission of the proton relative to the *electric vector*. This property has been used in the present experiment to establish the polarization of the gamma-rays from ^3He.

The deuterium was contained in an Ilford C.2 photographic plate whose emulsion, 100 μ thick when dry, was soaked in heavy water according to the well known technique (see, for example, Gibson, Grotdal, Orlin and Trumpy 1951). This plate was placed horizontally 7 cm below a target of D_3PO_4 with excess of heavy water, which was bombarded for five hours with a horizontal beam of about 50 μA of protons of 1·1 MeV. The plate was processed and examined under a magnification of 450. No attempt was made to measure accurately the dip of the photo-proton tracks : their angular distribution projected onto the plane of the emulsion was determined† on the basis of about 120 tracks contained in a square of side 2·5 cm centred on $\theta=90°$ (about half an hour's scanning was needed to find each track). Only those tracks were accepted whose projected length was less than the maximum possible for the greatest possible energy of gamma-ray from ^3He and greater than two-thirds of this length :

* Without doubt several sources of plane-polarized gamma-rays are available in which those gamma-rays are selected which are in coincidence with a particle emitted at some angle relative to them ; the present reaction has two great advantages : it is ' static ' in that no coincidence measurements are required and so it may be used in conjunction with cloud chambers or photographic plates, and the gamma-ray energy is continuously variable. A comparable reaction is $^3H(p\gamma)^4He$ which produces gamma-rays of 20 MeV upwards and gives a strong, though not pure, $\sin^2\theta$ distribution (Argo, Gittings, Hemmendinger, Jarvis and Taschek 1950) ; these gamma-rays should also be strongly polarized.

† Owing to the thinness of the tracks produced in soaked emulsions and the rather low magnification used it was not always possible to decide on the sense of the track of a proton which had suffered an appreciable scattering ; when this was so the projected angle of the bent track was taken to be the ' weighted mean ' of the directions of its components.

tracks whose dip was greater than that of a track of minimum acceptable projected length produced by a gamma-ray of greatest possible energy were rejected. It was necessary for two reasons to impose these criteria of acceptance: firstly, the phosphorus in the D_3PO_4 gives some gamma-rays in a reaction of radiative capture whose energy release is 9·9 MEV, and rejection of long tracks (very few of which were found) eliminated the more energetic components of these transitions; secondly, neutrons of up to 4 MEV are generated in the DD reaction—the fast deuterons derive from collisions between deuterons and the bombarding protons—and these neutrons produce in the emulsion recoil protons and deuterons which were eliminated by the condition of a minimum projected length.

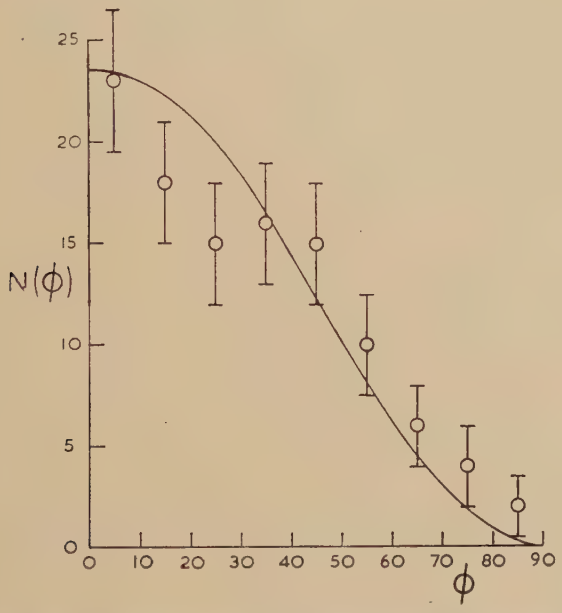

Angular distribution of photoprotons projected onto the plane of the emulsion. ϕ angle between the projected track and the supposed direction of the electric vector; $N(\phi)$ number of tracks per 10° range in ϕ. See text for meaning of error limits.

That a relatively small gamma-ray flux is due to the phosphorus had been shown by measurements with a Geiger counter using a target of H_3PO_4 with a similar excess of ordinary water. Such a 'light' target was used in an irradiation of a second plate in geometrical conditions which approximated closely to those obtaining in the earlier irradiation using a 'heavy' target. This gave a few tracks which were subtracted from the first distribution—a correction of about 10%. The corrected distribution is shown in the figure.

ϕ is the angle between the projected track and the supposed direction of the electric vector; $N(\phi)$ is the number of tracks in each 10° range

of ϕ. The error limits show $\frac{2}{3}\sqrt{n}$ where n is the combined number of tracks in each 10° range of the two distributions. The full line is the theoretical distribution expected for pure plane-polarized gamma-rays ; in computing this distribution only electric dipole transitions were assumed in the photodisintegration of the deuteron, and allowance was made for the effect of the second criterion of acceptance imposed in the experimental investigation. The agreement between theory and experiment is satisfactory in view of the rather small numbers of tracks involved, and confirms our expectation that the gamma-rays are strongly polarized.

It might appear from the figure that some evidence for lack of complete plane polarization of the gamma-rays is to be found in the tail of the experimental distribution, which rises above the theoretical curve for large values of ϕ. This discrepancy cannot be explained by our neglect of the magnetic dipole transition in the deuteron photodisintegration, as this would yield an isotropic component of only about half a track per 10° range of ϕ, nor is the departure from good geometry enough to produce this effect. The above-mentioned scattering of the photo-protons might well produce such a spurious isotropic component and, in view of the strong theoretical indications, it is probable that polarization is complete.

References

Argo, H. V., Gittings, H. T., Hemmendinger, A., Jarvis, G. A., and Taschek, R. F., 1950, *Phys. Rev.*, **78**, 691.

Burhop, E. H. S., and Massey, H. S. W., 1948, *Proc. Roy. Soc.* A, **192**, 156.

Carver, J. H., and Wilkinson, D. H., 1951, *Nature, Lond.*, **167**, 154.

Fowler, W. A., Lauritsen, C. C., and Tollestrup, A. V., 1949, *Phys. Rev.*, **76**, 1767.

Gibson, W. M., Grotdal, T., Orlin, J. J., and Trumpy, B., 1591., *Phil. Mag.*, **42**, 555.

Hough, P. V. C., 1950, *Phys. Rev.*, **80**, 1069.

Verde, M., 1950 a, *Helv. Phys. Acta*, **23**, 453 ; 1950 b, *Nuovo Cim.*, **7**, 283.

LXIII. *Some Hydrodynamical Aspects of the Swimming of Snakes and Eels*

By G. E. Gadd
National Physical Laboratory*

[Revised MS. received March 18, 1952]

Introduction and Summary

The hydrodynamical processes involved in the swimming of real fish are so complicated that analysis is probably only practicable for idealized models. We consider here a drastically idealized case for which a fairly simple mathematical solution can be found. The body is assumed to be very slender, gently tapering, and without any abruptly projecting fins, and to execute motions which are fish-like but of very small amplitude only : the flow over the body is assumed to be effectively the same as that of an inviscid ' perfect ' fluid. This idealized case has some points of resemblance to swimming snakes and eels, and it is hoped that the analysis may throw some light on the physical nature of the hydrodynamic forces propelling such creatures and on the propulsive efficiencies attained.

The first section below discusses propulsive efficiency, and the mathematical solution for the idealized case is presented in the second section. The relevance of this solution to the swimming of animals such as snakes and eels is then discussed.

§1. Ideal Efficiency

Consider a laterally symmetric body whose movements are supposed, for convenience of reference, to be confined to a horizontal plane—a convention adopted throughout this paper. Axes x, y, z moving with the forward mean velocity U of the body are chosen as in fig. 1, with the x axis pointing backwards along the direction of mean motion, the y axis horizontally to starboard, and the z axis vertically upwards. It is assumed that the centre line of the body at time t may be represented by

$$\begin{cases} y=y_0=f(x)\sin\dfrac{2\pi(x-nUt)}{l}\equiv f\sin\theta, \\ z=0. \end{cases}$$

This represents a wave motion of variable amplitude $f(x)$ which passes down the body with velocity nU. Such movements are performed by real fish in swimming. (Although for most fish the amplitude only becomes appreciable over the rear third of the body, with fish like eels and with swimming snakes the forward parts of the body share in the lateral motion.) It is assumed that the amplitude is small so that the x coordinate of any point on the centre line remains constant.

* Communicated by the Author.

The fluid pressure force on a section of the body of length dx at x will have horizontal components which can be denoted by $P_1 dx$ and $P_2 dx$ perpendicular and parallel to the centre line as in fig. 2. P_1 and P_2 will,

Fig. 1

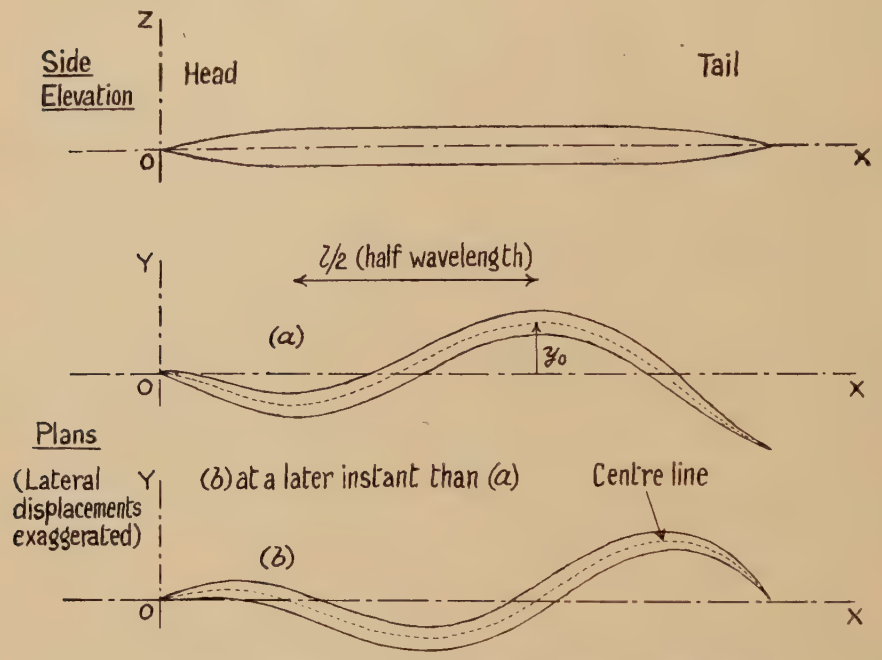

The axes of reference and the wave motion of the body.

Fig. 2

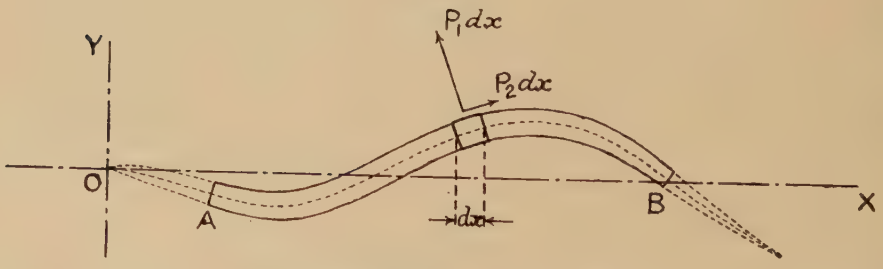

Fluid pressure forces on an element.

of course, be functions of x and t, and P_2 will be small, since it is assumed that the cross section of the body changes only gradually along the length. Hence the mean rate of doing work against the fluid pressure forces by a length AB of the body will be the mean value of

$$E \equiv - \int_A^B P_1 \frac{\partial y_0}{\partial t} dx.$$

(If any viscous forces acting on the body have negligible y-direction components, the integral E, taken over the whole length of the body, is the power which would be required of a perfect actuating mechanism. It is not, however, necessarily related to the energy which would be used up by muscles, since muscles use up energy in, for instance, sustaining a weight against gravity when no mechanical work is done.)

The usefully employed power, i.e. the forward thrust times U, will be the mean value of

$$W \equiv \left\{ \int_A^B P_1 \frac{\partial y_0}{\partial x}\, dx - \int_A^B P_2\, dx \right\} U.$$

An ' ideal efficiency ' can accordingly be defined as

$$\frac{\overline{W}}{\overline{E}} = \frac{\left\{ \int_A^B \overline{P_1 \frac{\partial y_0}{\partial x}}\, dx - \int_A^B \overline{P_2}\, dx \right\} U}{-\int_A^B \overline{P_1 \frac{\partial y_0}{\partial t}}\, dx}.$$

It is interesting to consider in passing the case of a body of constant cross section (where P_2 is zero if end effects are ignored) transmitting waves of constant small amplitude along itself. The ideal efficiency would be $1/n$, since $\partial y_0/\partial x = (2\pi f \cos\theta)/l$ and $\partial y_0/\partial t = -(2\pi n U f \cos\theta)/l$. Thus the efficiency would be independent of the particular pressure distribution over the body (save, of course, that it would cease to have meaning if the pressures were such as to give a zero or negative forward thrust).

The locomotion of such a body would be analogous to the propulsion of a boat by rowing. Here the power output of the oarsman is equal to the force on the blade of the oar times the rate at which the blade moves relative to him, whilst the useful power output is equal to the force on the blade times the forward speed of the boat. The efficiency is therefore equal to the ratio of the boat's speed to the speed of the oar blade relative to the boat. This ratio must, of course, always be less than unity for a propulsive force to exist.

§2. Slender Gently Tapering Bodies Executing Small Amplitude Fish-like Motions

The case of very slender gently tapering bodies executing very small amplitude transverse motions can be fairly easily analysed, if viscous effects are assumed to be confined to a non-separating boundary layer of negligible thickness. (This obviously requires that the hydrodynamic scale should not be too small.) It can be assumed that, just as with rigid yawed slender airship shapes (c.f. Durand, *Aerodynamic Theory*, vol. 1), the flow between any two planes close together and perpendicular to the centre line of the body is approximately dependent only on the shape and motion of the short segment of the body cut off by them.

The lateral momentum of the fluid between planes intersecting the centre line perpendicularly at x and $x+dx$ is

$$\rho s v \, dx$$

where ρ is the density of the fluid,

$$v \equiv \frac{\partial y_0}{\partial t} + U \frac{\partial y_0}{\partial x} = -\frac{2\pi U f}{l}(n-1)\cos\theta + U\frac{df}{dx}\sin\theta,$$

and s is the volume of additional apparent mass per unit length of an infinite rigid cylinder, whose every cross section has the same shape and the same direction of motion in its own plane as the cross section of the body at x. If the section were elliptical and of depth δ, as in fig. 3, s would be equal to $\pi\delta^2/4$.

Fig. 3

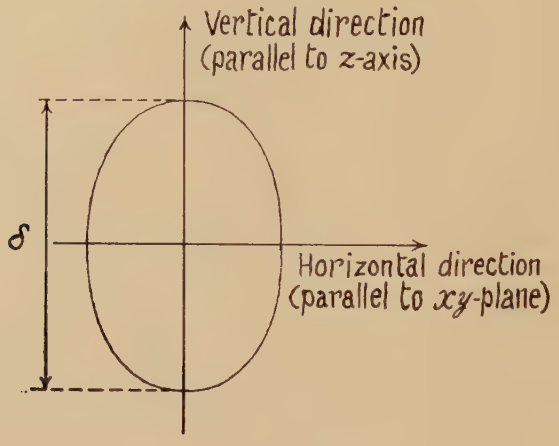

Cross section of body.

Since the induced velocities in the x direction will be very small, the fluid particles which at time t are in a plane which intersects the centre line at right angles at x, will at time $t+dt$ be in another such plane cutting the centre line at $x+Udt$. Hence the rate of change of lateral momentum of the fluid particles instantaneously between planes intersecting the centre line perpendicularly at x and $x+dx$ is equal to

$$\rho\left[\frac{\partial(sv)}{\partial t} + U\frac{\partial(sv)}{\partial x}\right]dx.$$

This must be equal and opposite to the lateral force on the length dx of the body, so that the lateral force per unit length of the body at x is

$$-\rho\left[s\frac{\partial v}{\partial t} + U\frac{\partial(sv)}{\partial x}\right],$$

(the negative sign indicating that the direction is to port). The force is perpendicular to the local centre line, as is readily apparent on consideration of the case where the cross section of the body is constant over part of the length.

It follows from the above that the instantaneous rate of doing work on the fluid, E, by the lateral movements of a length AB of the body (c.f. § 1) is equal to

$$E=\rho\int_A^B\left(s\frac{\partial v}{\partial t}+U\frac{\partial(sv)}{\partial x}\right)\frac{\partial y_0}{\partial t}\,dx$$

and it can be shewn that, irrespective of the manner in which the amplitude f varies with x, the mean value of E is always given by

$$\overline{E}=\rho U\left\{\left(s\overline{\frac{\partial y_0}{\partial t}v}\right)_B-\left(s\overline{\frac{\partial y_0}{\partial t}v}\right)_A\right\}.$$

Consider the two following special cases :—

Case (i). *Body Gently Tapering to a Point at Each End*

For such a body the assumptions underlying the above analysis might be expected to apply over the whole length, so that the points A and B can be taken as the two ends. The mean value of the ideal power required to maintain the motion is accordingly zero since s is zero at the pointed ends.

This implies, of course, that the mean forward thrust is also zero, so that according to the theory such a body could not propel itself (by small amplitude motions). The physical reason for this is as follows : The flow over any cross section of the body in a plane perpendicular to the centre line can be regarded as the resultant of a spatially uniform stream and induced vorticity within the section. The theory assumes that the algebraic total of the vorticity within any section is always zero. (In this respect it is unlike oscillating aerofoil theory, which assumes that the circulation round the aerofoil can change and imposes the condition that the flow remains smooth at the sharp trailing edge.) The induced vorticity will form a closed system, so that no vorticity can be shed to the wake. Hence the flow in the wake cannot exhibit any 'slipstream' effect, and the mean propulsive thrust must be zero.

With the same assumptions as to the nature of the flow, it would similarly follow that a slender rigid airship shape yawed at a small incidence could not experience any lateral force. (In practice there is a small lateral force on a real yawed airship, but this is because thickening and separation of the boundary layer take place on the leeward side of the tapering rear body, in violation of the assumptions of the above theory.)

Case (ii). *Body with a Portion of Constant Cross Section*

If the portion AB of the body is of constant cross section, and A and B are not too close to any sharply tapering sections where the theory would break down, the mean rate at which the lateral movements of AB do work on the fluid is

$$\rho Us\left\{\left(\overline{\frac{\partial y_0}{\partial t}v}\right)_B-\left(\overline{\frac{\partial y_0}{\partial t}v}\right)_A\right\},$$

which, with $y_0 = f \sin 2\pi(x - nUt)/l$, is equal to

$$\rho U^2 s \cdot \frac{2\pi^2}{l^2} n(n-1)(f_B^2 - f_A^2) .$$

The mean useful power output from the length AB is

$$-\rho U s \int_A^B \overline{\left(\frac{\partial v}{\partial t} + U\frac{\partial v}{\partial x}\right)\frac{\partial y_0}{\partial x}}\, dx,$$

which can be shown to equal

$$\rho U^3 s \left[\frac{\pi^2}{l^2}(n^2-1)(f_B^2 - f_A^2) - \frac{1}{4}\left[\left(\frac{df}{dx}\right)_B^2 - \left(\frac{df}{dx}\right)_A^2\right]\right].$$

If n (the ratio of the speed of the waves of lateral displacement to the mean forward speed) is sufficiently large, therefore, and if the amplitude increases towards the tail, there will be a forward thrust, and for large n the efficiency ratio approaches the form $(n+1)/2n$. For a body of constant cross section executing constant amplitude wave motions it was shown in § 1 that the efficiency is $1/n$, which $\to 0$ as $n \to \infty$, whereas $(n+1)/2n \to \frac{1}{2}$. However, the type of flow discussed here could not give rise to a forward mean thrust if the amplitude were constant, so the cases are not really comparable.

It may seem surprising that with $n=1$ the rate of doing work on the fluid would be zero, whilst the useful power output of the section would not, in general, be zero. However, this does not violate the conservation of energy law since the section AB does not, by hypothesis, form the whole of the length and end effects are ignored.

The instantaneous lateral force on the body per unit length, perpendicular to the local centre line and to starboard, is

$$\frac{\rho U^2 s}{l} g \equiv -\rho s \left(\frac{\partial v}{\partial t} + U\frac{\partial v}{\partial x}\right)$$

$$= \frac{\rho U^2 s}{l}\left[\underset{(a)}{\frac{4\pi^2 f}{l}(n-1)^2 \sin\theta} + \underset{(b)}{4\pi\frac{df}{dx}(n-1)\cos\theta} - \underset{(c)}{l\frac{d^2 f}{dx^2}\sin\theta}\right].$$

(As already mentioned, s, the volume of additional apparent mass per unit length, is equal to $\pi\delta^2/4$ if the cross section is elliptical and of depth δ.) In a particular case where f increases linearly with distance from the head, i.e. $f = \alpha x$, α constant, term (c) vanishes. If $n=2$ (a typical value for, say, an eel) and $x \simeq l$ (which for an eel means that the position is near the tail where the forces are greatest) term (a) is considerably bigger than term (b) for most of the time, although term (b) contributes twice as much to the mean forward thrust as does term (a). Figure 4 shows g/α plotted against x/l, together with the instantaneous configuration of the centre line of the body (the chain dotted curves), at two different instants of time $\frac{1}{4}$ of a period apart.

§3. Discussion of Relevance to Real Aquatic Organisms

The above solution may be relevant to the swimming of animals such as snakes and eels which are slender and have no abruptly projecting fins, although the lateral motions which they make in swimming are very far indeed from being small in amplitude.

Fig. 4

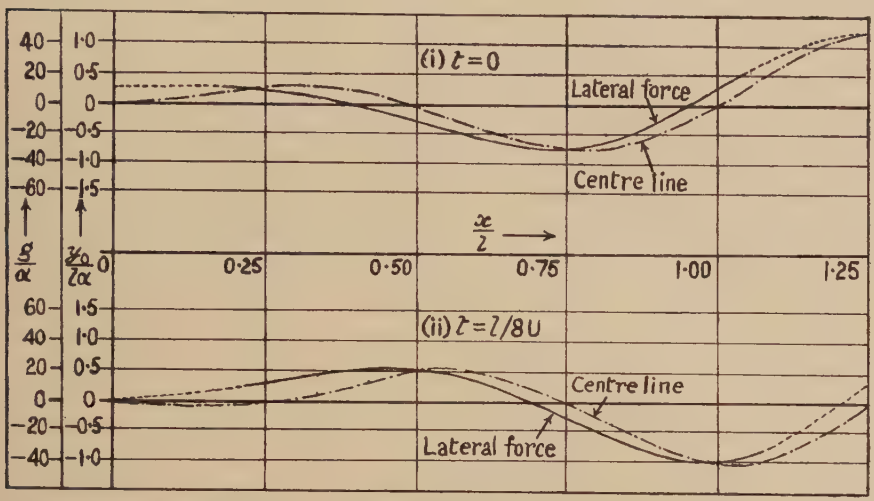

Instantaneous lateral force per unit length with $f=\alpha x$, α constant, and $n=2$.

Fig. 5

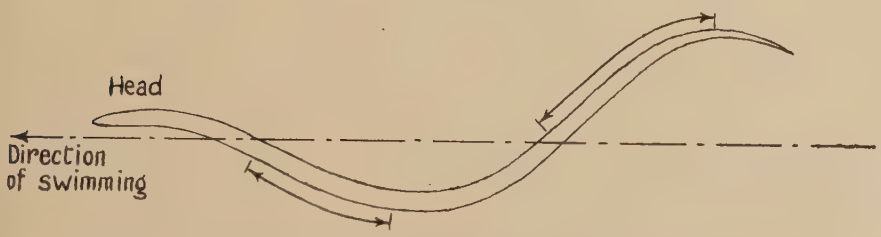

Portions of surface of swimming snake where separation may occur.

Snakes taper gently to a point at the tail, but over the central portions of the body they are of approximately constant cross section. If the forces acting were as predicted by the above solution there would be a net forward thrust over the central portions, but the total net thrust would be zero and a rearward drag would arise over the tapering rear body. In practice, however, the boundary layer probably does not remain thin everywhere as the theory assumes ; considerable thickening may take place over the forward inclined sections as indicated in fig. 5 and over the tapering rear body. The boundary layer thickening over the rear may, by reducing the effective taper, reduce the drag forces which would

theoretically be induced by the lateral accelerations, whilst the thick boundary layer over the forward inclined surfaces may modify the acceleration forces acting on the central portions of the body.

The forces on the central portions of an eel may also be somewhat as the above theory predicts, though perhaps modified by partial boundary layer separation from the forward inclined surfaces, separation which the sharp edges of the long anal and dorsal fins of the eel may help to promote. Since the side elevation of an eel appears blunt at the tail, there must also be end effects lying outside the scope of the theory.

Acknowledgments

Acknowledgments for much helpful criticism are due to Professor A. D. Young of the College of Aeronautics (where the author wrote a thesis embodying the basis of the above paper) and to H. B. Squire, Esq., and Dr. J. T. Stuart of the National Physical Laboratory.

LXIV. *The Scattering of Positrons*

By N. Cusack
Department of Physics, Birkbeck College, University of London*

[Received February 27, 1952]

Abstract

The scattering by nitrogen of positrons from copper 64 was observed with the Wilson chamber and analysed by the method of projected angles. The ratio of observed to theoretical numbers of scattering events was 0·63 for 114 nuclear scattering angles $>20°$. The results are considered together with the other relevant work and the conclusion drawn that, while the theoretical cross-sections describe correctly the large scale variations of scattering with energy, Z, and angle, the spin terms in the formulae have not been adequately tested. Positron-electron collisions were also observed, the ratio expt./theory being 1·1 for 40 events with scattering angle $>15°$.

No confirmatory evidence could be found for previous suggestions that the losses of energy accompanying positron nuclear scattering are unexpectedly frequent.

§ 1. Introduction

A recent publication by Howatson and Atkinson (1951) contains the first account of a measurement of the scattering of positrons by a light element. The purpose of the present paper is to report briefly similar observations at another energy and in another scattering gas, and to discuss the present position of this subject.

Experiments on the elastic nuclear scattering of positrons can be carried out with two objects: to test the theoretical cross-sections derived from the Dirac equation by Massey (1942), and to compare the ratio of positron to electron scattering at some given angle and energy. In either case, the ideal experiment should test closely the importance of the 'spin terms' of the theoretical formulae; it is these that make the ratio of electron to positron scattering greater than unity, and the positron cross-section always lower than the Rutherford value. That very few experiments have been performed is due no doubt to the difficulty of obtaining suitable positron sources—a difficulty which still exists. The four cloud chamber experiments on positron scattering are summarized in a table shown below. The one accurate experiment was carried out by Lipkin and White (1950), who selected their incident positrons by electron optical means and detected the scattered beam with counters. They found a ratio of electron to

* Communicated by the Author.

positron scattering some 10% higher than theory predicted, at one scattering angle of 57·6°, and at three energies in the neighbourhood of 1 MeV.

The present paper gives the results of observations on positrons from copper 64 made with a Wilson cloud chamber containing nitrogen as the scattering gas.

§2. Experimental Procedure and Results

An automatic cloud chamber was filled with nitrogen at atmospheric pressure and a pair of cameras used to photograph the tracks of positrons of mean energy 0·3 MeV. The axis of one camera was perpendicular to the plane of the chamber and the two camera axes made an angle of 25°. The photographs examined showed about 3,400 tracks of total length 361 metres. Only those tracks which had an initial length of at least 6 cm. suitable for curvature measurement (i.e. free from single scatters) were accepted and those scattering events were counted which occurred after this initial length. The total effective length in which scatters were observed was therefore 146 metres. For the good reasons given by its originators (see, for instance, O'Ceallaigh and MacCarthaigh 1944, Barker 1948) the projected angle method was used and all scattering events with projections $\phi > 20°$ were measured on the film with a goniometer microscope. Except in the latter detail, the methods used did not differ much from the normal cloud chamber technique described by Howatson and Atkinson (1951) and further account of it here is unnecessary.

The observed number of scattering events with $\phi > 20°$ was 114 and the expected number calculated from Massey's formula (1942) was 181. The latter figure was obtained by integrating the cross-section over the observed $H\rho$ distribution, which was similar to the copper 64 β^--spectrum cut off below 1 400 gauss-cm. The cross-section in question is

$$I(\theta)=\left(\frac{Ze^2}{2m_0c^2}\right)^2 \frac{1-\beta^2}{\beta^4} \operatorname{cosec}^4 \frac{\theta}{2}\left[1-\beta^2\sin^2\frac{\theta}{2}-\pi\alpha\beta\cos^2\frac{\theta}{2}\sin\frac{\theta}{2}\right].$$

The ratio N_{exp}/N_{theor} was therefore $0{\cdot}63 \pm 10\%$, the error stated being statistical only.

The observed angular distribution is given in table 1. Since the theoretical angular distribution varies little with energy in the range considered, the relative numbers in each angular range are not affected by any distortion of the energy spectrum due to multiple scattering (see below).

Table 1

Ang. range	20–30	30–40	40–60	60–90	90–180
Number	55 (66)	27 (23)	20 (15)	5 (6)	7 (4)

The numbers in brackets show how 114 scatters should be distributed theoretically.

§3. Discussion of Results

Table 2 summarizes all the cloud chamber work on positron scattering. e^-/e^+ denotes the ratio of electron to positron scattering.

Table 2

Author	Energy MeV	Scattering nucleus	No. of events (positron scatters)	Conclusions
Fowler & Oppenheimer 1938	10·5	Pb	9 ($>14\frac{1}{2}°$)	$\frac{e^-}{e^+}=1{\cdot}6\pm0{\cdot}4$
Lasich 1948	0·45 0·68 0·95	Au	30 ($>17°$)	$\frac{e^-}{e^+}$ = 1·6 1·6 1·6 Theor. values 2·3 1·8 1·7
Howatson & Atkinson 1951	0·7	A	65·5 ($>20°$)	$N_{exp}/N_{theor}=0{\cdot}92$
Present work	0·3	N	114 ($>20°$)	$N_{exp}/N_{theor}=0{\cdot}63$

The obvious comment to make about these experiments can be made of most nuclear scattering experiments with cloud chamber technique—namely, that the statistical accuracy is very low. This prevents any proper check of the angular distribution above 50°. This is unfortunate because the spin terms in the cross-section contribute about 5% of the total scattered intensity in the range 20° to 30° and about 30% at 60° to 70° (for 0·3 MeV, $\beta=0{\cdot}775$, $Z=7$). In Howatson and Atkinson's work, for instance, the spin terms contribute about 15% of the intensity in the angular region 20° to 90°, which is roughly the same as the statistical fluctuation of the observations. The more accurate method of Lipkin and White (1950) gave $e^-/e^+=3{\cdot}15\pm5\%$ at 0·7 MeV for scattering by Pt, which leaves no doubt about the excess of electron to positron scattering but is in fact about 13% higher than the theory predicts. As they point out, this may be due to neglect of screening in the theory.

The other major source of error in cloud chamber scattering experiments, especially at low energy, is multiple scattering. This leads to inaccuracy in the measurement of the energy spectrum and hence in the *expected* number of events. Multiple scattering in cloud chamber tracks has been considered by many authors, perhaps the most useful paper for workers at low energies being that of Bothe (1948). In the present experiments curvatures were measured by fitting circles through the beginning, end and middle of tracks, and the resulting errors were calculated with the help of the graph given by Bothe. It is estimated by a method similar to that of Sigrist (1943) that the expected number of events is in error by about 10% and is probably overestimated. For a given magnetic field, the multiple scattering error in $H\rho$ depends hardly at all on ρ but varies almost as $(l)^{-1/2}$, l being the length of the track. For this reason the lower limit, 6 cm, was imposed on the track length.

The other errors, arising from such things as the magnetic field measurement and the composition of the chamber filling gas, are of the order 1 or 2% and are negligible in comparison with those mentioned already. There is, however, the question of the efficiency of detection of scatters. A considerable defect of observed to expected scatters, such as found in the present work, suggests that some scatters were missed. It is, of course, impossible to prove that this was not so, but apart from the design of the scanning method itself, which involved tracing each track with a pencil and examining separately each of two photographs, the following checks on detection efficiency were applied : (i) Scatters can be to the right or left. Those on the side such that the deflected track has a cusped appearance are the easier to detect and indeed some workers count *only* these events for fear of losses. Consequently, if many scatters were missed, one would expect to observe more of the cusped variety than the other, but in fact a slight excess of the latter type was found. (ii) 100 photographs containing 40 metres of track were re-examined some months after the first examination. No more scatters were found. (iii) Losses might be expected on those photographs taken with strong sources and showing a relatively large number of tracks which might possibly obscure one another. The number of scatters per metre of track was computed for each of two groups of photographs having the length of track per picture respectively greater and less than 0·5 m. No significant difference in the number of scatters per metre was found.

From this it is reasonable to conclude that detective efficiency was high, though the possibility of a few losses particularly at low scattering angles cannot be excluded. This possibility of missed scatters at small angles, alluded to by Howatson and Atkinson and probably due to multiple scattering, must be counted one of the serious weaknesses of the cloud chamber method because it makes the apparent degree of agreement between theory and experiment depend upon a somewhat arbitrary decision as to a lower acceptance limit of ϕ.

Considering the size and probable direction of the errors involved, the cloud chamber data of table 2 lead to the following conclusion :— that the theoretical cross-sections are able to account for the large scale variations of positron scattering with energy and Z, and for angles up to about 90°, but that the finer points of the cross-sections have not been subjected to a significant test. These experiments are analogous to the earlier Wilson chamber work on electron scattering listed by Randels, Chao and Crane (1945). That such work has been superseded in such experiments as those of van de Graaf, Buechner and Feshbach (1946, 1947) and Lyman, Hanson and Scott (1951) is largely due to the intense monoenergetic beams obtainable from accelerators. Since it is unlikely that similar beams of positrons will soon be available, it is interesting to ask how comparable accuracy can be achieved. Lipkin and White's spectrometer experiment (1950) points one way and it is hoped to report in future results obtained by a combination of positron monochromator with cloud chamber.

§4. Inelastic Collisions

It has sometimes been suggested that nuclear scattering of electrons is accompanied by losses of energy much more frequently than the theory of radiative energy loss would predict. This point has been discussed recently and reasons given for rejecting the view (Davies and Shaw 1951). A similar effect, tentatively explained in terms of neutrino pair-production, was detected in a positron scattering experiment (Bothe and Ho Zah–Wei 1946). At the energies of their experiment individual losses of energy cannot be detected because of the spurious effects of multiple scattering, but they found a great preponderance of apparent increases in curvature after scattering over apparent decreases. No similar effect could be found in the present experiments. Of those 33 scattering events with $\phi > 20°$ which had more than 5 cm of track on either side of the collision, 14 showed apparent increases and 18 apparent decreases of curvature, a result easily attributable to multiple scattering alone. A small asymmetry in the direction indicated by Bothe and Ho Zah–Wei might well arise from ionization losses along the track which can amount, for tracks about 10 cm long, to several per cent at low positron energies.

§5. Positron Electron Collisions

In the experiment described above, 40 examples of positron electron collisions with $\phi > 15°$ were observed. The expected number on the basis of the Bhabha theory of the phenomenon (Bhabha 1936) was 36, giving $N_{obs}/N_{calc} = 1{\cdot}1$ with a statistical error of 16%. The relevant cross-section is

$$I(\gamma, \epsilon)\, d\epsilon = 2\pi \left(\frac{e}{m_0 c^2}\right)^2 \frac{\gamma}{(\gamma-1)^2\, \epsilon^2} F(\gamma, \epsilon)\, d\epsilon,$$

where γ=total energy of positron in units of m_0c^2; ϵ=fraction of the kinetic energy transferred to the target electron; $F(\gamma, \epsilon)$=a complicated function of γ and ϵ, of order of magnitude 1. ϵ is uniquely related to the scattering angle θ and the projected distribution of ϕ can be found with the help of Barker's tables (1948). The lower limit, 15°, of ϕ corresponds to an energy transfer from the incident positron to the target electron of about 10%. 15° was chosen here instead of the 20° used for the nuclear scatters because the nature of the positron–electron collision—a forked track—makes it much easier to detect the events even at small angles and makes more accurate the exact location of the change in positron direction.

This result confirms the more comprehensive experiment recently published by Ritter *et al.* (1951).

Acknowledgments

The author is grateful to Professor J. D. Bernal who provided facilities for the experiments, to Mr. R. E. Siday for helpful discussions, and to Mr. F. Roberts for invaluable assistance in the building of apparatus.

References

Barker, F. C., 1948, *J. Sci. Inst.*, **25,** 65.

Bhabha, H., 1936, *Proc. Roy. Soc.* A, **154,** 195.

Bothe, W., 1948, *Sitzungsber. Heidelb. Akad. Wiss. Math. Nat. Klasse Nr.* **5**.

Bothe, W., and Ho Zah–Wei, 1946, *Nachrichten d. Akad. Wiss. Göttingen, Math. Phys. Klasse,* April, 1946.

Davies, W. T., and Shaw, D. F., 1951, *Proc. Phys. Soc.*, **64,** 1006.

Fowler, W. A., and Oppenheimer, J., 1938, *Phys. Rev.*, **54,** 320.

Graaf, R. J. van de, Buechner, W. W., and Feshbach, H., 1946, *Phys. Rev.*, **69,** 452.

Howatson, A. F., and Atkinson, J. R., 1951, *Phil. Mag.*, **42,** 1136.

Lasich, W. B., 1948, *Aus. J. Sci. Res.* A, **1,** 249.

Lipkin, H. J., and White, M. G., 1950, *Phys. Rev.*, **79,** 892.

Lyman, E. M., Hanson, A. O., and Scott, M. B., 1951, *Phys. Rev.*, **84,** 626.

Massey, H. S. W., 1942., *Proc. Roy. Soc.* A, **181,** 4.

O'Ceallaigh, C., and MacCarthaigh, M. D., 1944, *Proc. Roy. Irish Acad.* A, **50,** 13.

Randels, R. B., Chao, K. T., and Crane, H. R., 1945, *Phys. Rev.*, **58,** 64.

Sigrist, W., 1943, *Helv. Phys. Acta*, **16,** 471.

Ritter, Von O., Lieseberg, C., Maier-Leibnitz, H., Papkov, A., Schmeiser, K., and Bothe, W., 1951, *Zeits. für Naturforsch.* B, **6***a*, 243.

LXV. *An Electron-Microscope Study of the Effect of Temperature and Strain-rate on the Mechanism of Deformation of Aluminium*

By R. I. Garrod
Defence Research Laboratories, Melbourne, Australia
and
J. W. Suiter and W. A. Wood
Baillieu Laboratory, University of Melbourne*

[Received February 25, 1952]

Summary

Formvar and oxide replicas have been prepared from polycrystalline specimens deformed plastically over a range of temperatures and rates of strain. Electron microscope observations support the view, put forward previously by Wood, Wilms and Rachinger (1951), that there are three basic stages in the mechanism of the deformation of metals, which have been termed the slip, cell and boundary micro-flow processes. If the temperature and rate of strain are adjusted suitably, no sign of slip is visible in the cell stage even with the high resolution available with electron microscopy. Correspondingly, in the boundary micro-flow stage, there is no evidence of any internal breakdown or disorientation of the grains. In both the cell and boundary micro-flow stages however, considerable activity occurs at the grain boundary zones, which exhibit markings similar in appearance to slip but always approximately parallel to the boundary direction.

Whilst the present paper is confined in the main to experimental observations, their interpretation in terms of structural changes and their possible relationship to the dislocation theory of deformation are discussed briefly.

§ 1. Introduction

Wood, Wilms and Rachinger (1951) have shown recently how the process of deformation of polycrystalline aluminium changes systematically with increasing temperature and diminishing strain-rate. They distinguished three stages.

The first was the familiar slip process. This held at room temperature and with the rates of strain used in normal mechanical testing. The relevant characteristics were : absence of appreciable movement at the grain boundaries, so that each individual grain changed its shape in general accordance with the external deformation of the specimen ; the production of this change in shape in effect by the sub-division of the grain into parallel lamellae which slipped relatively to each other on the intervening planes.

*Communicated by the Authors.

The second stage was termed the cell mechanism. This set in as the temperature was raised to about 200° c and the strain-rate reduced to about 0·2% per hour. As the transition occurred the slip planes became more widely spaced and irregular in direction until finally no signs of slip were visible under the optical microscope. Instead, it appeared both from microscopic and x-ray evidence that the grains had sub-divided into a coarse sub-structure of crystallographically perfect but irregularly shaped elements which formed the 'cells'. The characteristics of the deformation process at this stage were: a distinct movement of the grains relative to each other at the grain boundaries, so that there was less need for the individual grains themselves to change shape and an accommodation of such changes in shape as did occur by the coarse sub-division into cells.

The third and final stage was termed boundary micro-flow. This was favoured by further increase in temperature of deformation and further reduction in rate of strain. The cells into which the grains divided then became systematically larger until finally no sub-division at all occurred. At this stage the internal structure of the individual grains remained perfect and homogeneous, the unit of flow was the grain itself and deformation occurred entirely by micro-movements of the grains at their boundaries. This mechanism predominated as the temperature of deformation reached about 350° c and the strain-rate dropped below 0·1% per hour.

The above work was based on optical and x-ray examination. The x-ray method reveals any disorientation or distortion of the grain, but does not indicate the shape of the elements into which a grain may sub-divide. The optical microscope shows the shape and relative movement of the elements, but is subject to its limit of resolution. The present work extends the observations on the three stages by taking advantage of the higher magnification and resolution of the electron microscope.

The first stage of slip has already been studied with the electron microscope in the work of Heidenreich and Shockley (1948), and Brown (1950); the latter has also examined the slip produced by rapid deformation at sub-normal and elevated temperatures. The present observations on this stage agree generally with the results obtained by these authors. They are included here, however, since they form part of a systematic survey of the three stages as a whole.

§ 2. Replica Techniques

For aluminium the most convenient replica methods are the plastic film (e.g. Formvar) and oxide film techniques. The latter method was used by Heidenreich and Shockley, and by Brown in the work referred to above. It can provide replicas with high resolving power because of the almost structureless nature of the film. Removal of the film from the parent metal, however, involves destruction of the test specimen, so that

it is impossible to follow structural changes as one specimen is deformed progressively. On the other hand a Formvar replica can be prepared without damage to the specimen and, furthermore, after shadowing it generally gives greater contrast than a corresponding oxide replica. There is some difference of opinion about the resolution obtainable by the Formvar methods ; estimates vary from about 100 to 400 A (Nutting and Cosslett 1950). If the higher limit applied, this technique would not reveal some of the finer structural changes that might accompany deformation. However, much of the background structure of the replica, in particular the ' orange peel ' appearance, depends on the prior electropolishing and etching treatment of the aluminium. It has been found that with the perchloric acid and acetic anhydride solution recommended for polishing by Jacquet (1937), Formvar replicas can be obtained which show adequately the fine-structure within the slip-zones. It is interesting to note that the structure in a replica from a specimen polished in this solution is much finer than that in a replica obtained from a surface polished with the Windsor-Brown (1944) orthophosphoric-acid type of solution (compare figs. 2 and 9, Plates XXXIV and XXXV*). Moreover, it has been generally observed in the present work that whereas a shadowed Formvar replica, from a specimen deformed at room temperature, will indicate slip and fine structure in the slip process in a large proportion of the grains, a corresponding oxide replica will only show up slip zones clearly in a much smaller number of regions, and fine structure in these zones only in isolated areas. This difference is attributed to the different manner in which the Formvar and oxide films follow the contour of the surface. The oxide film appears to have approximately the same thickness normal to the metal surface and to any steps produced in the surface by the slip movements. The contrast between the slip and inter-slip regions is therefore large when the electron beam is parallel to the rise of a step, but drops quite sharply as the beam departs from that direction. On the other hand, the thickness of the Formvar film is less uniform and the contrast therefore less sensitive to the angle between the electron beam and the slip direction. Hence, although oxide replicas may show up finer details under favourable conditions, it is necessary to explore carefully a number of replicas in order to obtain a representative picture of the whole slip process. It is hoped to treat this latter aspect more fully in a separate paper.

For these reasons, in the work to be described the Formvar replica method has been mainly employed after preliminary development of polishing techniques to provide suitable surfaces. At the same time oxide replicas were also prepared for comparison where confirmation of particular features of interest by an independent technique appeared desirable. All the micrographs illustrated here are from Formvar replicas, since the corresponding oxide replicas provided no additional information.

---

*For plates see end of issue.

§ 3. Experimental

The material used was aluminium of 99·98% purity, from which flat tensile specimens were prepared with a parallel gauge length of 1 in. and a cross-section 0·25 × 0·06 in.

The specimens were annealed to give a grain size of approximately 0·02 cm and then electropolished in either a Jacquet or a Windsor-Brown solution. In the latter case it was necessary to etch the specimen after polishing to remove the anodic film (Wilms 1950).

The test-pieces were subjected to appropriate deformation to provide examples of the three stages of deformation already referred to, after which surface replicas were prepared for examination in an R.C.A. (type E.M.U.) electron microscope. Negative Formvar replicas were obtained by the dry-stripping technique described by Schwartz, Austin, and Weber (1949), and shadow-cast with chromium before examination. If a specimen was used also for the oxide replica, it was first washed and then the replica obtained by the method of Keller and Geisler (1944) with a potential in the anodizing bath of 30 v.

In some cases, after a specimen had been elongated a few per cent at elevated temperature the surface became too rumpled to give satisfactory Formvar replicas. This difficulty was overcome by repolishing and etching the specimen and then subjecting it to a small further strain under the same conditions as previously, before preparing a replica. In this way it was possible to follow the structural condition produced at a given temperature and strain rate at progressive stages from the annealed to the highly deformed state.

§ 4. Results

(1) *Slip Stage at Room Temperature*

Typical slip lines shown by the optical microscope are illustrated by fig. 1 (Plate XXXIV). These lines, which appear single under the optical examination, are resolved into zones of finer parallel lines by the electron microscope as indicated by figs. 3 and 4 (Plate XXXIV). This confirms previous observations (Heidenreich and Shockley 1948, Brown 1950, Cahn 1951). In the present case, which refers to a specimen elongated rapidly by 12% at room temperature, the inhomogeneity of the deformation from grain to grain is also shown. In the more deformed areas (fig. 4) the fine sub-structure in the immediate neighbourhood of the slip zones spreads to the regions between the zones. The average width of the fine slip lamellae as projected on the free surface of the specimen was estimated to be approximately 350 A. (The true width will depend on the angle between the slip direction and the free surface.)

One point of importance, specially relevant to the present work, is the absence of apparent deformation at the grain boundaries. As far as can be seen from inspection of many replicas, the slip traces continue sharply up to a boundary and then change direction quite abruptly when a grain of different orientation is encountered.

(2) *Cell Stage*

As already mentioned, the slip lines shown by the ordinary microscope become more widely spaced and finally disappear as the temperature of deformation is raised and the rate of strain is lowered. It was of particular interest to know whether the disappearance was due to the limitation of the optical method, and whether deformation still proceeded by slip but on a sub-microscopic scale.

The evidence now supplied by the electron microscope shows that the slip process does in fact disappear entirely, at least within the limits of resolution of the method. When the cell mechanism predominated, no signs of slip could be detected on any scale, either in Formvar or in oxide replicas. Instead sub-boundaries corresponding to the cells within the grains were found. A typical cell boundary, for a specimen extended at 300° c at the rate of 0·17% per hour, is shown in fig. 5 (Plate XXXIV). This photograph illustrates the further point that *cell boundaries appear to be at least as sharp as the grain boundaries in the initial material*; there is no sign of disordered transitional zones. Also the difference in orientation between neighbouring cells is small; this is shown by the direction of the markings left by the polishing. (In the illustration shown here, polishing by orthophosphoric acid was used deliberately to bring out this point because it leaves more pronounced markings than does the Jacquet polish.)

In contrast with the first stage, however, the structure shows evidence in this second stage of abnormal deformation at the grain boundaries themselves. This activity is described more fully in the next stage where it is still more emphasized.

(3) *Boundary Micro-flow Stage*

For this stage, previous optical and x-ray work had suggested that there was little internal dissociation of the grains, either by breakdown into cells or into slip lamellae. Instead, the grains appeared rather to behave as entities except for the active boundary zone where neighbouring grains would develop differences in level relative to the initial surface. The freedom from internal breakdown was confirmed in the present investigation by the electron-microscope observations, which showed no sign of internal sub-boundaries at the higher magnification and resolution. A typical micrograph, from a specimen strained at 0·11% per hour at 390° c, is shown in fig. 6 (Plate XXXIV); this merely indicates surface irregularities due to the polish.

The electron microscope, however, threw new light on the active zone at the grain boundaries. In most cases, the zone was traversed by roughly parallel steps as shown in fig. 7 (Plate XXXV). In others, these steps were irregular as indicated by fig. 8 (Plate XXXV). In both cases, however, the markings bore a close resemblance to ordinary slip markings as found in the first stage. They are not identical with slip, for in the first place they are confined to the boundary zone. In the second place they are not limited to a specific crystallographic direction as in ordinary slip, for they are always roughly parallel to the grain boundaries which,

it is known, can take any crystallographic direction. They strongly suggest, however, that the relative displacement of the grains can occur in the boundary zone by a movement analogous to slip, that is, by the local disorientation of the structure into lamellae and by a micro-shear on the intervening planes.

In some cases, the transitional zone appeared continuous as in fig. 10 (Plate XXXV). An apparent difference in orientation in this zone is then suggested by the changes in direction of the surface markings, purposely emphasized in this particular instance by the use of the orthophosphoric acid type of polish. However, the difference is primarily due to the slope of the region between the grains ; for if the surface is re-polished flat and re-etched, it is found that the grain boundary is at one extremity or the other of the zone and that the orientation in each grain is uniform up to the common boundary. It is possible of course that the difference in level in these cases might include discrete steps as before, but on too fine a scale to be resolved when this type of polish is used.

(4) *Slip at Elevated Temperature*

The dual influence of strain rate and temperature may be emphasized by examination of the way in which the deformation changes as the temperature is raised, for specimens which are elongated at rapid rates of strain. Figures 11 and 12 (Plate XXXV), refer to a specimen which had been strained 12% in 20 seconds at 390° c. Compared with the slip at room temperature, it will be observed that the deformation is a combination of the slip mechanism and considerable movement at the grain boundaries. The slip that occurs, however, is coarser and more irregularly spaced than that occurring at room temperature. It also loses the regularity of crystallographic direction (fig. 12) characteristic of the normal slip process. These results are in general agreement with previous observations (Brown 1950, Cahn 1951). In addition, however, it has been found that the ridges at the boundary zone parallel to the boundary direction, which have been described previously for the cell and boundary micro-flow stages, are also present in this type of deformation. Figure 11, for example, exhibits steps in the slip lines as they reach an active boundary zone.

§ 5. Conclusions

The suggested interpretation of the three basic stages on the basis of the previous optical and x-ray work and the present electron microscope examination, may be summarized by the diagrams in fig. 13. These indicate the section of a grain in a specimen which is strained by shear in the direction of the arrows. The first stage, shown by fig. 13 (*a*), shows the slip process at room temperature. The grain shears by dissociation along slip bands, each containing a fine structure ; but there is no movement at the grain boundaries themselves, except of course to conform with the changed shape of the grain as a result of deformation. The second stage,

Fig. 13

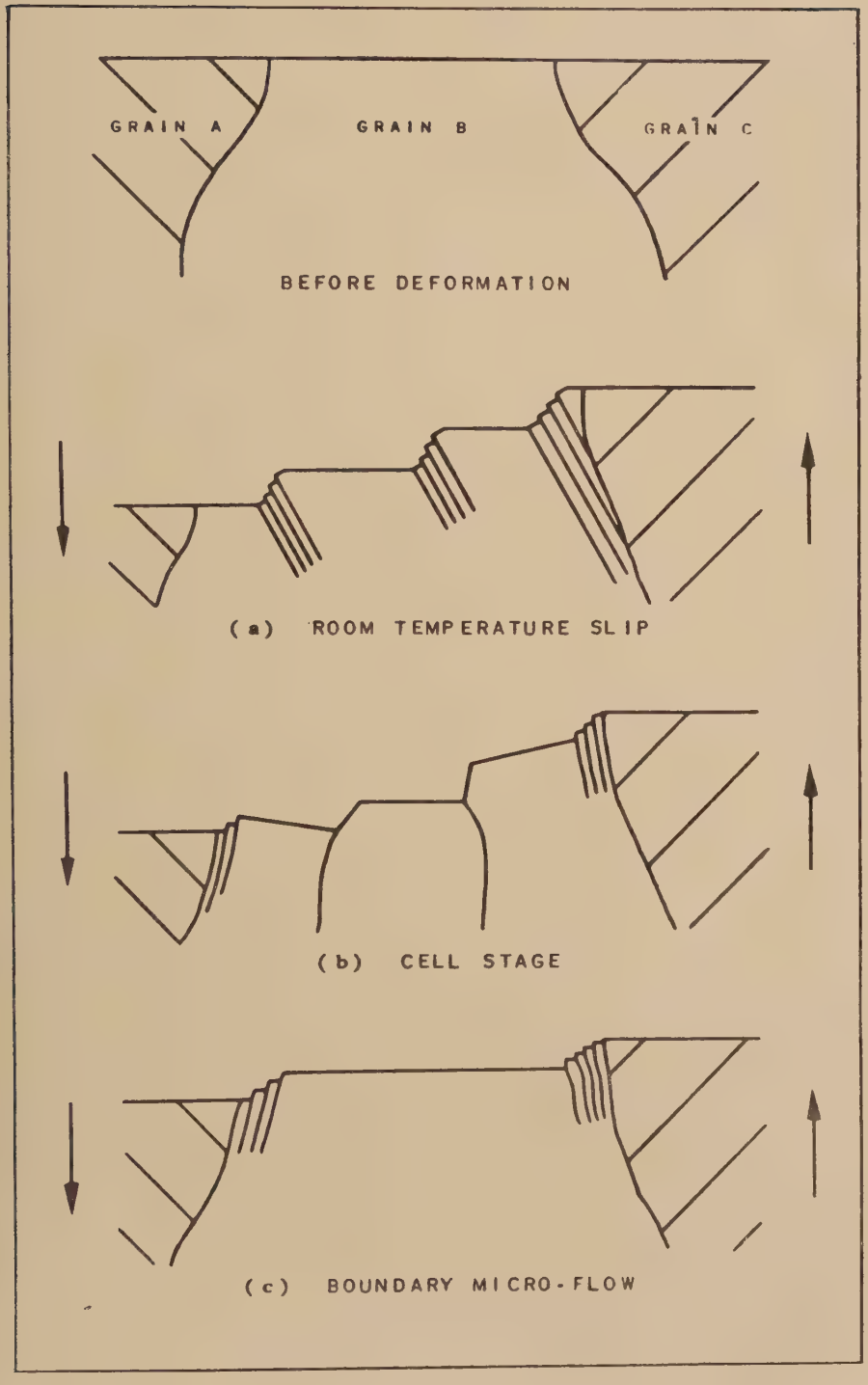
GRAIN A
GRAIN B
GRAIN C
BEFORE DEFORMATION
(a) ROOM TEMPERATURE SLIP
(b) CELL STAGE
(c) BOUNDARY MICRO-FLOW

i.e. the cell mechanism, is given by fig. 13 (*b*). Some contribution is made at the grain boundary, but the internal movement is on a much coarser scale. (In fig. 13 (*b*) the steps at the grain boundary have been exaggerated for clarity and are actually on a much smaller scale than the total changes in elevation occurring over the grain boundary zone.) The final stage when all the movement is at the grain boundary and no movement occurs within the grain is then indicated by fig. 13 (*c*).

The major factor determining the nature of the deformation process on this view is the degree of activity at the boundary. There are two extreme cases. One extreme occurs when the temperature is high enough to activate the misfitting atoms at the boundaries. If also the applied rate of strain is sufficiently low, then apparently the external deformation of the specimen can be accommodated entirely by flow at the boundary. This is the third stage referred to above. If the rate of strain is too high, however, the grains themselves must break down internally despite the boundary activity. The other extreme is when the temperature is too low to activate the boundary atoms. Then disruption and relative movements must occur within the grains whatever the rate of strain ; this constitutes the first stage of slip. The second, or cell mechanism, is then an intermediate stage ; it may be expected that the extent of the breakdown in this stage will depend on the degree of boundary activity and therefore in turn on the temperature and rate of strain, as in fact is found.

The present work is confined in the main to experimental observations and their direct interpretation in terms of structural changes. It is not desired at this stage to discuss in detail the atomic movements underlying these changes. But it is of interest to note briefly here their relation to the theory of deformation by the movements of dislocations. In the slip process, to which the theory is normally applied, it is postulated that the relative movement results from the motion of dislocations predominantly in the glide planes. Even when dislocations are deflected locally by some disturbance to a different plane, as in some types of cross-slip (Cahn 1951), the normal glide planes are also operative. The present results however, suggest that this characteristic is lost when deformation occurs at elevated temperatures and low rates of strain. The cell boundaries form *in the absence of slip movements* and without any relation to specific crystallographic planes. Also the steps formed at the main grain boundaries have no specific crystallographic direction. Under these conditions therefore, the movements at the boundaries and sub-boundaries result presumably from a concentration and irregular passage of dislocations in a manner which is determined by the conditions of deformation.

Acknowledgment

The authors desire to thank Professor J. Neill Greenwood for his interest and encouragement in the work and one of them (R.I.G.), the Chief Scientist, Department of Supply, Australia, for permission to publish this paper.

References

Brown, A. F., 1950, *Inst. Metals : Metallurgical Applications of the Electron Microscope*, p. 103 (Monograph and Report Series, No. 8).
Cahn, R. W., 1951, *J. Inst. Metals*, **79,** 129.
Heidenreich, R. D., and Shockley, W., 1948, *Phys. Soc.: Report of a Conference on the Strength of Solids*, p. 57.
Jacquet, P. A., 1937, *Compt. Rend.*, **205,** 1232.
Keller, F., and Geisler, A. H., 1944, *J. Appl. Physics*, **15,** 696.
Nutting, J., and Cosslett, V. E., 1950, *Inst. Metals : Metallurgical Applications of the Electron Microscope*, p. 65 (Monograph and Report Series, No. 8).
Schwartz, C. M., Austin, E. A., and Weber, P. M., 1949, *J. Appl. Physics*, **20,** 202.
Windsor-Brown, E., 1944, *Brit. Pat. No.* 558, 925.
Wilms, G. R., 1950, *J. Inst. Metals*, **76,** 629.
Wood, W. A., Wilms, G. R., and Rachinger, W. A., 1951, *J. Inst. Metals*, **79,** 159.

LXVI. CORRESPONDENCE

The Self-Perpetuating Step in Crystal Growth from the Melt

By Bruce Chalmers and Ursula M. Martius
Department of Metallurgical Engineering, University of Toronto*

[Received April 9, 1952]

Considerable attention has been given recently to the problem of the nucleation of new layers on a growing crystal surface; Frank (1949) has shown that a suitably oriented screw dislocation can serve as a self-perpetuating step, so that growth can always take place by the extension of existing planes rather than by the initiation of new layers. The corresponding problem does not appear to have been studied in relation to the growth of a crystal from the melt. In this case the thermal conditions are an important factor and a self-perpetuating step may occur in the following manner, which does not require lattice imperfections.

Fig. 1

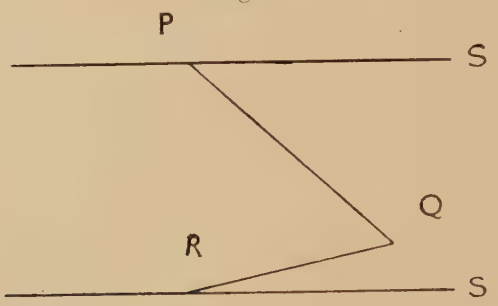

Solid-liquid interface Zero temperature gradient.

The general theory of crystal growth shows that the addition of atoms to the growing solid takes place most readily on to the least closely packed faces of the crystal. Consequently, all non-close packed faces will receive atoms until they have disappeared, the surface then consisting only of the most closely packed faces. If growth were taking place under 'ideal' conditions, i.e., in a liquid in which there is no temperature gradient, this process would result in a crystal of equilibrium form, i.e., of octahedral shape, if the structure is face centred cubic. This may be represented as in fig. 1, in which S S are plane walls bounding the substance under consideration. The interface between the solid and the liquid consists of the close-packed planes PQ and QR (in this two-dimensional representation). Further growth could only take place by the formation and growth of new close packed layers. This requires two-dimensional nucleation. However, in real cases there is always a temperature gradient, and this changes the situation as follows. Consider

* Communicated by the Authors.

fig. 2 in which the liquid is again bounded by the two plane surfaces S. It is assumed that the temperature gradient is maintained by the flow of heat from right to left, and that all the isothermal surfaces are plane, such as AA. In such circumstances, a zone of limited width BBB′B′, which is below the equilibrium freezing temperature, will exist in the liquid near the interface, while the rest of the liquid is above this temperature. This thermal condition does not permit the existence of solid beyond B′B′. The solid-liquid interface will then consist of components CD/DC, etc., which are close-packed planes, crystallographically equivalent to PQ, QR in fig. 1. Re-entrant corners, such as C, form preferential sites for solidification, since an atom joining onto the crystal at such a point will have five nearest neighbours, exactly as it would if two dimensional nucleations had already taken place on a close-packed surface. Forming a row along the *line* of intersection of CD and DC it will find six nearest neighbours. Further solidification will be on planes parallel to CD and DC, starting from the newly formed row. Each atom will find at least

Fig. 2

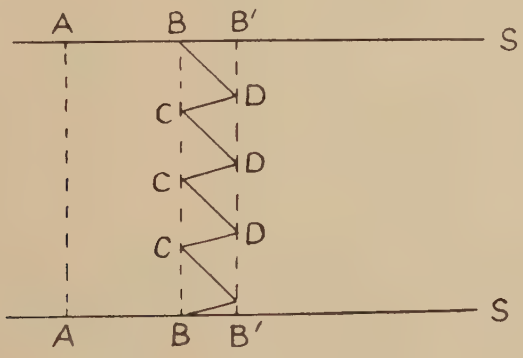

Solid-liquid interface Finite temperature gradient.

five nearest neighbours. Thus, neither two-dimensional nucleation nor a dislocation step are necessary for continuous solidification, since the stepped interface is perpetuated by the forward movement of the supercooled zone.

It is evident that the step structure of the growing surface may be unsymmetrical with respect to the growing interface. This may be associated with the difference that has been observed (Chalmers and Rutter, to be published) between the real direction of growth and the normal to the mean or macroscopic interface. There are indications that symmetry or asymmetry of close packed planes with respect to the direction of heat flow provides the explanation for the observed preferred directions of crystal growth.

References

Chalmers B., and Rutter, J., to be published.
Frank, C. F., 1949, *Proc. Faraday Soc., Discussion on Crystal Growth.*

A Parabolic Law for Metal Oxidation which is Not Controlled by Diffusion

By W. J. Moore*
Catholic University of America, Washington, D.C.†

[Received April 25, 1952]

The high temperature oxidation of many metals follows a rate law $dy/dt=k/y$, where y is the thickness of oxide film and t is the time. The parabolic rate constant has been related (Wagner 1933) to the diffusion coefficient for defects in the oxide, D_i, by $k=2D_i(f_1-f_2)$, where f_1 and f_2 are the defect fractions at the interfaces. Most of the observed parabolic rate constants can be interpreted satisfactorily on the basis of the diffusion mechanism. There are a number of cases, in which n-type oxides are formed, which have rate constants with low activation energies and large negative activation entropies. Examples are :

Metal	Oxide	ΔH^* (kcal)	ΔS^* (cal deg^{-1})	Reference
Zn	ZnO	28·5	−22·6	(Moore and Lee 1951)
Ti	TiO_2	24·3	−22·8	(Gulbransen and Andrew 1949 a)
Zr	ZrO_2	16·8	−27·3	(Gulbransen and Andrew 1949 b)
Al	Al_2O_3	21·4	−28·6	(Gulbransen and Wysong 1947)

Below a limiting pressure, some of these rate constants become dependent on the oxygen pressure. It is difficult to explain the large negative ΔS^* by any diffusion mechanism, except possibly grain-boundary diffusion of oxygen. An alternative mechanism can be suggested, however, which does not involve diffusion control, but nevertheless leads to a parabolic rate law.

Let us consider the typical case of ZnO. The ZnO film will contain a certain small fraction of interstitial zinc atoms. Let us suppose that at the surface of the ZnO film there are s adsorption sites per cm^2, which are covered at sufficiently high oxygen pressure by adsorbed oxygen atoms. These atoms can act as electron traps (Bevan, Shelton and Anderson 1948), abstracting electrons from the interstitial zinc atoms to form interstitial zinc ions,

$$Zn_i+O\ (ads)=Zn_i^{+}+O^{-}\ (ads).$$

Since the number of surface sites may be small, and since the reaction is considerably exothermic, the equilibrium concentration of Zn_i^+ ions in the oxide film will be s/y.

---

* Communicated by the Author.
† Temporarily at H. H. Wills Physical Laboratory, University of Bristol.

The difficult step in the growth of the oxide film will be that in which the $(O^-)_{ads}$ accepts a second electron to become $O^=$. For free ions, this step is endothermic by about 6·5 ev, and the only likely source of this energy is the Madelung energy of the completed ZnO structure. Thus the O^- accepts the second electron only as the Zn_i^+ moves next to it at the interface. The rate determining reaction is, accordingly,

$$Zn_i^+ + O^- \text{ (ads)} = ZnO \text{ (crystal)}.$$

The rate of film growth is therefore $dy/dt = k_2 s(s/y)V$ and the observed parabolic rate constant is $k = k_2 V s^2$, where V is the volume of oxide per ion, and k_2 is the specific rate of the second-order interface reaction. The proposed mechanism serves to explain the large negative ΔS^*, the low ΔH^*, the dependence on oxygen pressure in accord with a Langmuir isotherm in P_{O_2} as observed for zinc oxidation, and the marked acceleration of the reaction by ozone.

To consider whether a volume concentration of interstitial ions can be determined by a surface concentration of adsorbed ions of opposite sign, let us take an extreme example in which the interface reaction rate is negligibly small, and let us also neglect any effect from the underlying metal. If a is the charge density of O^- ions at the surface, and n is the concentration of Zn_i^+ ions in the oxide, $n/n_0 = \exp(-4\pi aex/kTD) = \exp(-z)$, where D is the dielectric constant and x is the distance from the surface. Now $a = se$, where s is the number of active surface sites per cm^2, which may be taken to be, say, 10^{-5} times the total surface sites, or about 10^{10} per cm^2. Then, at 700° K, $z = 5 \times 10^4 x$. If x is 10^3 Å, about the maximum thickness involved, $z = 0{\cdot}5$ and $n/n_0 = 0{\cdot}61$. This would seem to be the maximum deviation to be expected from uniform concentration, for if the screening of the surface due to positive ions was included, by properly solving the Poisson-Boltzmann equation, the effect would be to further reduce z.

The author wishes to thank Professor N. F. Mott for interesting discussions of this subject.

References

Bevan, D. J. M., Shelton, J. P., and Anderson, J. S., 1948, *J. Chem. Soc.*, 1729.

Gulbransen, E. A., and Andrew, K. F., 1949 a, *Metals Trans.*, **185,** 741 ; 1949 b, *Ibid.*, 515.

Gulbransen, E. A., and Wysong, W. S., 1947, *J. Phys. Chem.*, **51,** 1087.

Moore, W. J., and Lee, J. K., 1951, *Trans. Faraday Soc.*, **47,** 501.

Wagner, C., 1933, *Zeits. f. physikal. Chem.*, **21,** 25.

Gamma-Ray Angular Correlation for Proton Bombardment of Boron

By G. M. Lewis
Department of Natural Philosophy, The University, Glasgow*

[Received May 7, 1952]

The $^{11}B(p, \gamma)^{12}C$ reaction yields cascading γ-rays of 4 and 12 Mev, also a 16 Mev γ-ray (cf. Hornyak, Lauritsen, Morrison and Fowler 1950). The angular correlation of the cascading γ-rays emitted approximately at right angles to the incident proton direction has been investigated. Figure 1 illustrates the experimental arrangement. The protons after magnetic resolution travelled down a long straight copper tube, through an aperture in a copper plate to the target. The aperture diameter in preliminary work was $\frac{3}{8}$ in., later it was $\frac{1}{4}$ in. The $\frac{1}{32}$ in. thick copper target backing subjected to currents $\sim 50\,\mu$amps was cooled by water beneath. The γ-rays were observed by two scintillation counters consisting of sodium iodide blocks ($\frac{3}{4}$ in. diam. $\times 1\frac{1}{2}$ in.) on E.M.I. multipliers. The counters travelled on a circular track situated in the cross-sectional plane of the

Fig. 1

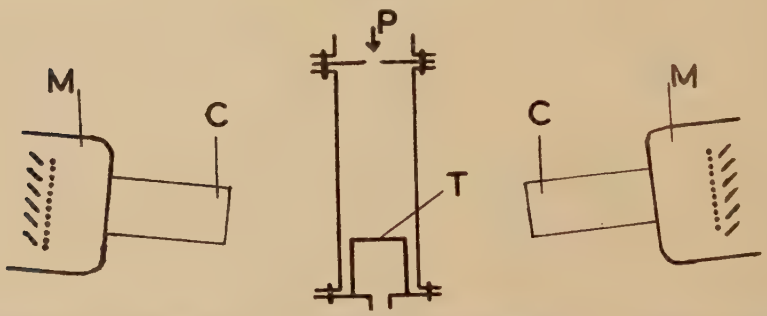

Experimental arrangement. C: NaI(Tl) crystal. M: photo-multiplier; P: proton-beam; T: target.

aligned $\frac{1}{32}$ in. thick, 1 in. diam., copper beam tube, with the crystal block centres $\sim 2\frac{3}{4}$ in. from the target. The counters were tilted, at about 5° to this plane, so that the γ-rays observed did not travel through the target backing. Energies less than 1·2 Mev were discriminated against to avoid annihilation quanta and Compton γ-rays, and to reduce effects from electrons and positrons in flight. A monitor counter of similar type was placed some 10 in. from the target to check on the number of disintegrations.

The two main counters fed pulses into a coincidence unit of resolving time 0·7 μsecs: the pulses after suitable delay were also fed into a similar unit measuring random coincidences; and the true coincidences C were

* Communicated by Professor P. I. Dee, C.B.E., F.R.S.

determined. If C_1, C_2 denote the counts in the main counters and N that in the monitor, the variation in the quantity (NC/C_1C_2) with azimuthal angle θ between the two counters gave the angular correlation. In any given run one counter was fixed, and the ratio (N/C_1) found experimentally to be constant, so that the ratio (C/C_2) gave the correlation.

The correlation determined for a thick boron target for 220 kev protons is shown in fig. 2, and may be represented by : $1+(0{\cdot}365\pm0{\cdot}06)\cos^2\theta$. From separate measurement of the excitation curve it was established that $\sim$94% of the radiation responsible for this anisotropy must be associated with the lowest resonance. Similar measuring apparatus had given $(18{\cdot}5\pm3)$% anisotropy with ^{60}Co in accord with the result of Brady

Fig. 2.

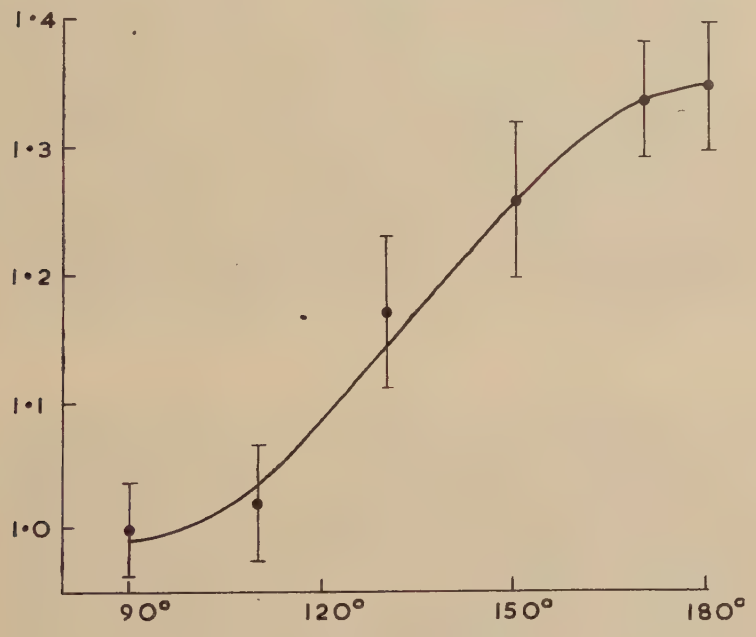

γ–γ angular correlation using 220 kev protons.

and Deutsch (1950). As no known anisotropy seemed available as a check at high γ energies, it was necessary to assess the spurious coincidences arising from any one γ-ray alone. LiOH was bombarded by protons and only small effects obtained, involving a coincidence rise near 90°. An overall correction of $\sim1\frac{1}{2}$% anisotropy was indicated from this cause, giving finally : $1+(0{\cdot}38\pm0{\cdot}06)\cos^2\theta$ for the boron case, above.

The theory of triple cascade processes has been developed by Biedenharn, Arfken and Rose (1951). They give reasons for believing that the ^{12}C nucleus, formed in the capture of a proton of orbital momentum 1 by ^{11}B, undergoes transitions of type 2–Dipole–2–Quadrupole–0. If the fractional

contributions to capture of the channel spins 1 and 2, of the colliding particles, be close to equality, the correlation $\sim 1+(3/7)\cos^2\theta$ follows, which is near the experimental results above. The final choice of reaction variables must take into account other anisotropies of the emission (Kern, Moak, Good, Robinson 1951).

Experiments of a preliminary type, using mostly the $\frac{3}{8}$ in. aperture, for 400 kev protons on a thick boron target seemed to indicate a decrease in anisotropy. This radiation contains less than 50% of the lowest resonance radiation. The results led to a possible correlation $1+(0{\cdot}24\pm 0{\cdot}06)\cos^2\theta$.

I am particularly indebted to Dr. J. G. Rutherglen and Dr. R. D. Smith for the use of the high tension set, and for helpful suggestions, and to Prof. P. I. Dee for promoting my work on reaction γ-rays.

References

Biedenharn, L. C., Arfken, G. B., and Rose, M. E., 1951, *Phys. Rev.*, **83,** 586.
Brady, E. L., and Deutsch, M., 1950, *Phys. Rev.*, **78,** 558.
Hornyak, W. F., Lauritsen, T., Morrison, P., and Fowler, W. A., 1950, *Rev. Mod. Phys.*, **22,** 291.
Kern, B. D., Moak, C. D., Good, W. M., and Robinson, G. P., 1951, *Phys. Rev.*, **83,** 211 (A).

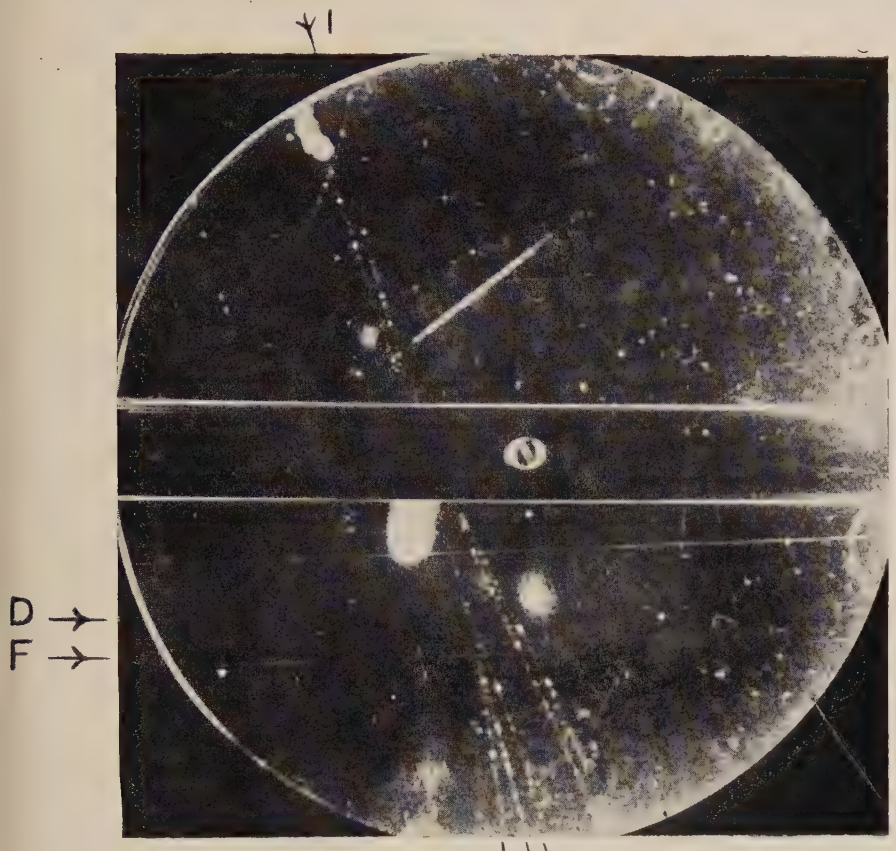

PLATE XXVIII

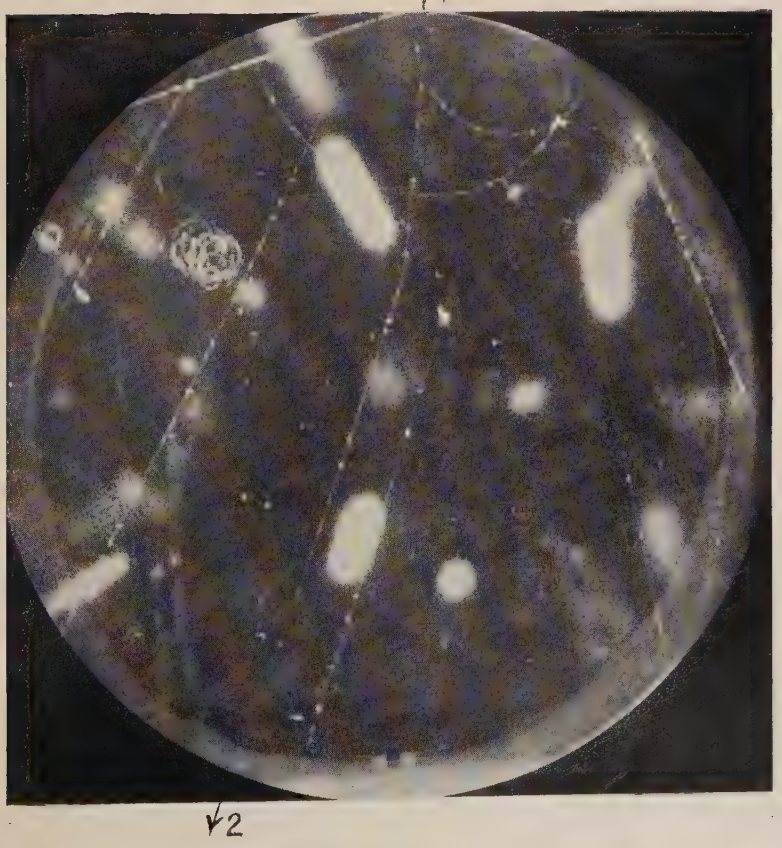

PLATE XXIX

PLATE XXX

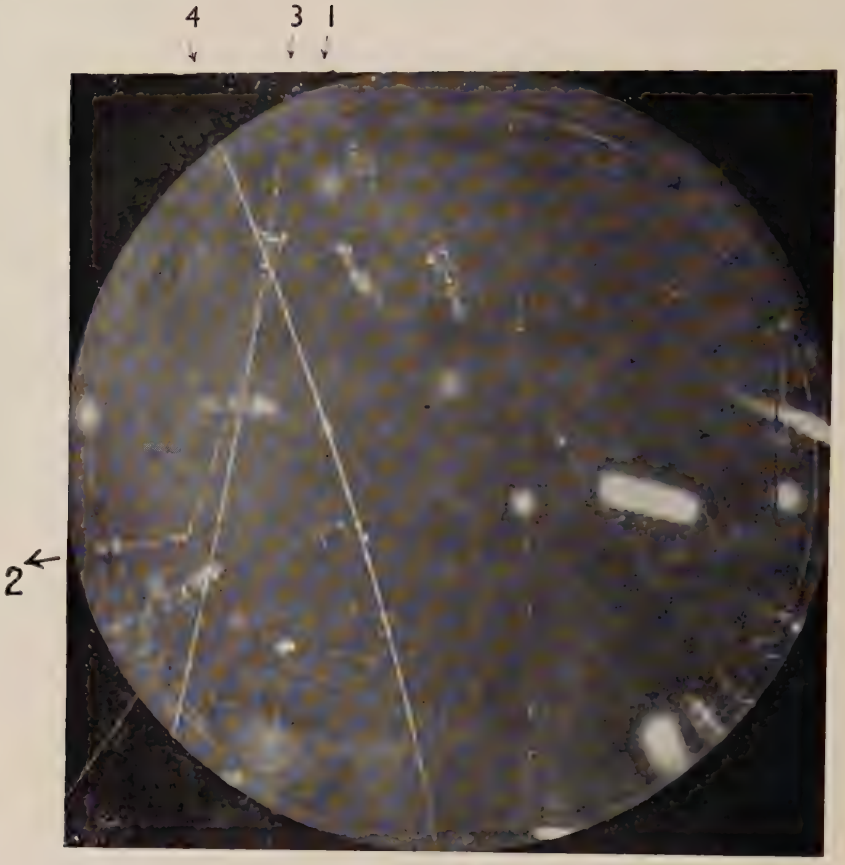

PLATE XXXI

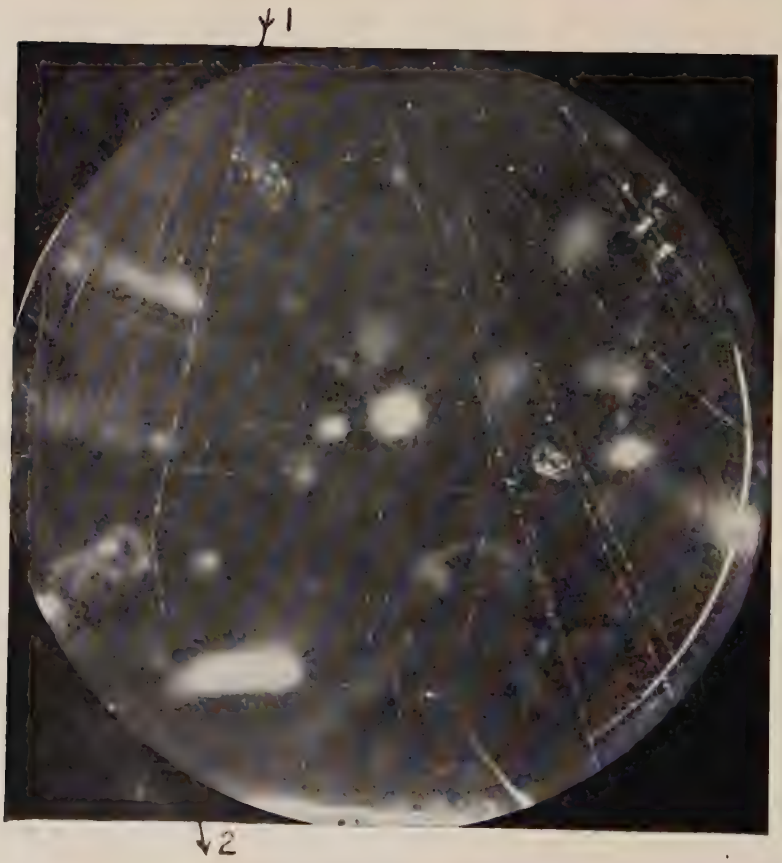

Fig. 1

Slip lines and elementary structure on a single crystal, extended to 18%. Negative SiO-replica shadowed with tungsten oxide. 30 500 : 1.

Fig. 2

Elementary structure and slip band crossed by elementary lines of a second system. Single crystal after 16% extension. Replica as above. 14 800 : 1.

Fig. 3

Three systems of elementary lines on a polycrystalline specimen after 41% extension. Replica as in fig. 1. 15 000 : 1.

Fig. 4

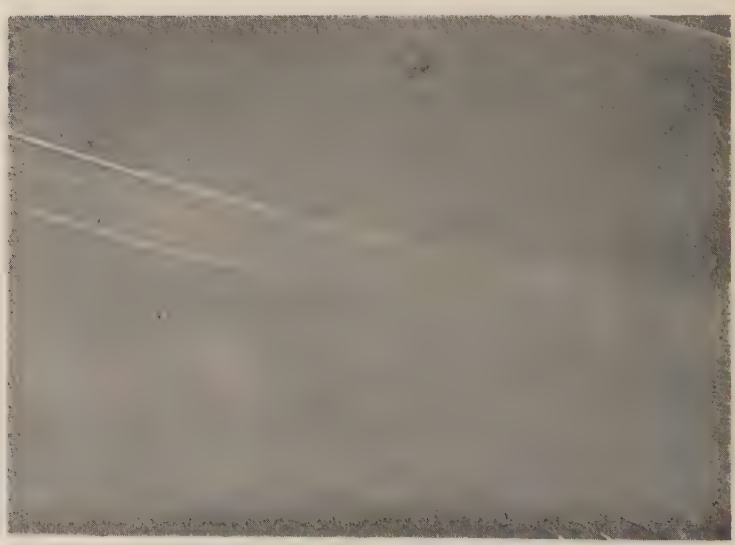

Slip lines on a polycrystalline specimen. Extension 17%. Note the lines' gradual fading-out. Replica as in fig. 1. 10 300 : 1.

Fig. 1

Extension at Room Temperature (Optical). ×100

Fig. 2

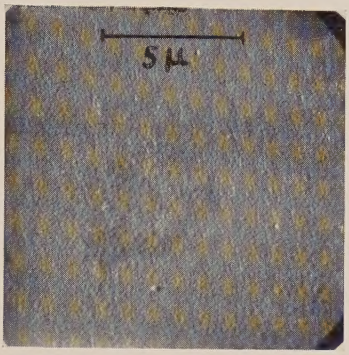

Annealed Specimen, showing Interior of a Grain (Jacquet Polish). ×3730

Fig. 3

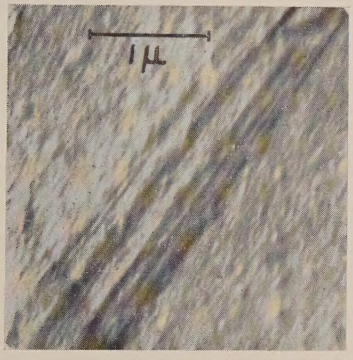

12% Extension at Room Temperature (Rapid Strain). ×15 300

Fig. 4

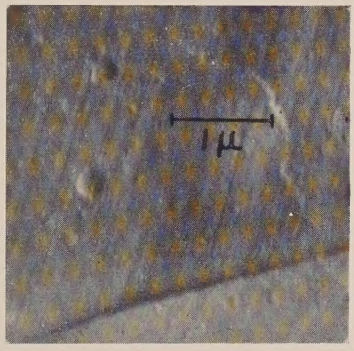

12% Extension at Room Temperature (Rapid Strain). ×13 300

Fig. 5

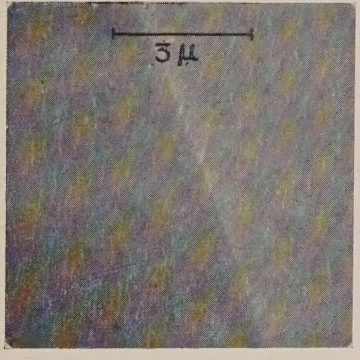

Cell Boundary after 8·5% Extension in 50 hours at 300° c (Windsor-Brown Polish). ×5920

Fig. 6

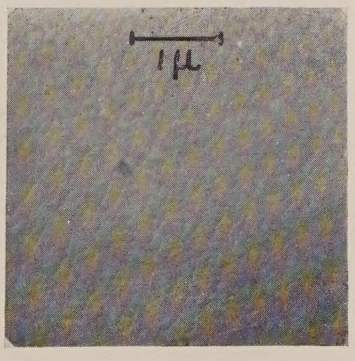

Interior of a Grain after 8% Extension in 72 hours at 390° c (Jacquet Polish). ×11 850

Fig. 7

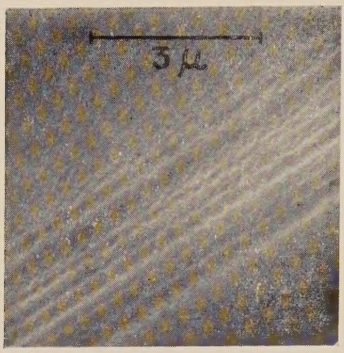

Same Specimen as for fig. 6, but showing Deformation at the Grain Boundary Zones.
×7600

Fig. 8

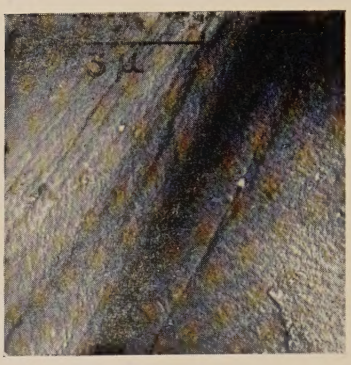

Same Specimen as for fig. 6, but showing Deformation at the Grain Boundary Zones.
×7600

Fig. 9

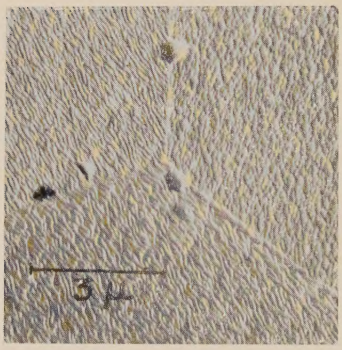

Annealed Specimen (Windsor-Brown Polish).
×5920

Fig. 10

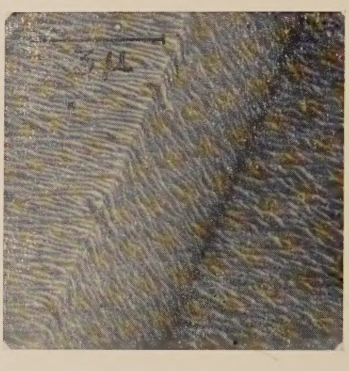

After 0·9% Extension in 73 hours at 250° c showing Boundary Zone between 2 Grains (Windsor-Brown Polish).
×5920

Fig. 11

After 12% Extension in 20 seconds at 390° c showing Intersection of Slip System with Active Boundary Zone.
×3730

Fig. 12

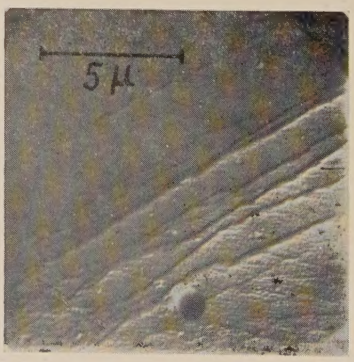

Same Specimen as for fig. 11, showing Coarse, Irregular Slip.
×3730

LXVII. *Notices of New Books and Periodicals received*

Properties of Matter. By F. C. Champion and N. Davy. (Blackie & Sons.) Second Edition. [Pp. 328.] Price 27*s.* 6*d.*

Those familiar with the first edition of this book will find that the essential character of the work has remained unchanged. The second edition is some 30 pages longer than the first, the more important additions being concerned with gravimeters, seismic prospecting, the measurement of osmatic pressure, and non-Newtonian fluids. There are a number of other minor additions, and the paragraph on the measurement of diffusivity has been replaced by an account of a more recent method. The main body of the original text, however, is unaltered, and even the few minor errors which occurred in the first edition have remained uncorrected. N. T.

Tensor Analysis. By I. S. Sokolnikoff. [Pp. 335.] (John Wiley & Sons.) Price 48*s.* net.

This new work is in the clear style of previous publications of the author. It is addressed to ' graduate students interested in applications of mathematics ', and goes far enough to give those interested, possession of a powerful tool of analysis.

The initial two chapters present general theory of tensors and matrices. The remaining four chapters deal with applications to geometry, analytical mechanics (both Newtonian and relativistic) and the mechanics of deformable media. All are treated in reasonable detail except perhaps this last chapter on elasticity and fluid mechanics. However, part of this is fully covered in the authors previous book on linear elasticity.

A pleasing feature is that the theory is developed in a general manner thus avoiding ' the erroneous impression that the formulation of tensor analysis depends somehow on geometry or relativity '. A. K. H.

Diffusion in Solids, Liquids and Gases. By W. Jost, Professor of Physical Chemistry in the Technical High School of Darmstadt. [Pp. 551.] Price 12$.

Professor Jost's earlier book ' Diffusion und chemische Reaktion in festen Stoffen ' appeared in 1937. To the present reviewer, as to many other research workers in this field, this book served as a most valuable introduction to that German work on reactions in solids which laid the basis for so many recent developments. A further book by the same author is, therefore, most welcome. The scope is, however, rather different. It is about diffusion, and reactions in solids are brought in rather as an illustration of this than in their own right. Thus oxidation reactions are discussed, particularly as giving rates of flow through oxides; but there is little, if any, discussion of nucleation in solid reactions. In contradistinction to the earlier book, there is a discussion of diffusion in liquids and gases, of which the former is particularly useful. The book is excellent on the general mathematical formulation of diffusion problems and on oxidation at high temperatures; it does not attempt to cover fully some of the most recent developments, such as the role of grain boundaries in diffusion, Kirkendall effect, the role of vacancies or the relation between self-diffusion and creep. N. F. M.

The Science of Flames and Furnaces. By M. W. Thring. [Pp. 416+xiv.] (Chapman and Hall.) Price 42*s*.

This book should be read by every user of fuel who is concerned to economize—from the open-hearth steel maker making his thousand tons a day to the householder charging 0·005 tons of anthracite into his domestic boiler to put it to bed, and wondering if anything could be done to make it eat a little less. It is a systematic exposition of the physical and chemical processes occurring in flames and furnaces ; of the way in which they influence furnace design, and of the thermodynamic limitations which they impose on the performance of the furnace, considered as a device for transferring virtue (energy in principle convertible into work under the given conditions) from fuel to product.

Quantitative prediction and analysis is always Mr. Thring's aim, and the book is packed with formulae, together with references to original papers. Mr. Thring steers clear of the pitfall of glossing over the possible non-existence (in the strict sense) of the thing that one is trying to measure : so, for example, he gives six methods of measuring flame temperature, so as to separate the ' gas ' and ' radiant ' temperature of the flame.

The householder who during a shortage of coal burns wood in a domestic boiler should study this part of the book particularly, and (whatever his fuel) the chapters on the liberation of heat by combustion, heat transfer, and the aerodynamics of hot systems.

Prediction of furnace performance has been fraught with uncertainty from the earliest times—ever since Nebuchadnezzar's inaccurate estimation of virtue in the heat-treatment of Shadrach, Meshach and Abednego. And Mr. Thring is keenly aware of the desirability of experimental checks of all practicable kinds. These are discussed at some length, together with the study of models where a principle of similitude applies.

In his closing chapter, Mr. Thring discusses the limitations of the scientific method. And here it is that I simultaneously applaud and cavil. He compares the activities of the furnace student with those of the general practitioner or veterinary surgeon ; the statistical biologist, and the medical research worker. This is excellent : we should at all times encourage links between our specialist activity and almost every other form of human endeavour. For the scientific habit of mind is not—in my belief—fundamentally an approach to ' science ' : it is an attitude to life, and the more we integrate it with other activities, the better creative research we shall do. I am puzzled, however, when he discusses the ' interaction of the *artistic* side of the furnace problem with the scientific side '. I would applaud the introduction of the artistic side were this possible on paper : open-hearth operations are, in fact, of striking beauty which famous artists have tried (and failed) to commit to canvas. And is not the essence of artistic activity properly so-called that in it functional and emotional activity are indissolubly blended ? And is not emotion the driving force in our research ? But this is not what his context implies. Should not the phrase read ' interaction of furnace craft with furnace science ' ?

I am surprised, too, that he should compare the furnaceman studying the fundamental laws governing furnace types with the medical research worker experimenting *to find out how the species can be improved.* ' I do not seek to cure my patients ', said Freud, ' only to understand them '. ' And here ', Mr. Thring could retort with some force ' is the only schizophrenia or dichotomy that we would be wise to cultivate deliberately : if you want to improve a furnace, it may be wise to forget that awhile, and seek only to understand it '.

C. R. Burch.

[*The Editors do not hold themselves responsible for the views expressed by their correspondents.*]